Alma Mater Studiorum – Università di Bologna

DOTTORATO DI RICERCA IN

BIOLOGIA CELLULARE E MOLECOLARE

Ciclo 33

Settore Concorsuale: 05/E1 - BIOCHIMICA GENERALE

Settore Scientifico Disciplinare: BIO10 - BIOCHIMICA

INDENTIFICATION OF AN α-KETOGLUTARATE ANALOGUE AS AN ANTICANCER AGENT

Presentata da: Houda Abla

Coordinatore Dottorato

Prof. Giovanni Capranico

Supervisore

Prof.ssa Anna Maria Porcelli

Correlatore

Dott.ssa Luisa Iommarini

Esame finale anno 2021

TABLE OF CONTENTS

TABLE OF CONTENTS

ABSTRACT…….…….1

ABBREVIATIONS……..3

INTRODUCTION……6

Hallmarks of cancer……...7

Mitochondria: cellular hub for metabolic and bioenergetic reactions……8

Mitochondria and metabolic reprogramming in cancer…….9

HIF signalling and hypoxic adaptation in cancer…….10

Oncometabolites contribution to cancer progression……...14

αKG: a metabolite with pleiotropic activity……..16

αKG at the heart of physiological reactions…….16

αKG as a limiting substrate for dioxygenases……..19

Targeting hypoxia and HIF signalling in cancer……...24

HIF inhibitors……...25

Targeting mitochondrial CI in cancer……..26

αKG as an anticancer agent……..29

AIMS……...33

EXPERIMENTAL PROCEDURES…….……34

Chemical synthesis and stability analyses on αKGlogues……..35

Cell culture……..38

HIF-TM transduction……38

SDS-PAGE & western-blotting…….38

Cell viability……39

Colony forming assay (clonogenic assay)…….40

Cell migration (wound-healing assay)……..…40

LC-MS metabolomics analyses…….41

Nuclear morphology assessment……...41

Flow cytometric analysis of apoptotic cell death……..…42

β-galactosidase-associated senescence assay……..…..42

Multicellular tumor-derived spheroids……..…..42

***Drosophila* imaginal wing discs as tumor model…….……43**

Fly manipulation and volume analysis…….……44

Statistical analysis……..45

RESULTS……....…46

Selected αKGlogues are able to prevent HIF-1α stabilization in hypoxia……47

αKGlogues specifically alter cancer cells growth and *in vitro* tumorigenic properties……51

Long-term effect on cancer cell viability is partially related to HIF pathway alteration…….62

αKGlogue PP provokes αKG intracellular accumulation and imbalanced αKG/SA ratio……..66

The molecular mechanisms underlying αKG-PP effect imply the block of mTORC1 pathway…….69

αKG-PP displays anti-proliferative properties in cancer-derived spheroids and *in vivo*……...72

DISCUSSION…….…75

REFERENCES……...82

ABSTRACT

Often correlated to a poor prognosis and increased mortality in cancer patients, hypoxic adaptation in tumors is mainly endorsed by Hypoxia Inducible Factor (HIF-1α). Under conditions of oxygen scarcity, this transcription factor triggers the expression of specific target genes implicated in glycolysis, neoangiogenesis and survival. Although hypoxia signalling constitutes an interesting target, the development of therapeutics has been limited by the high rate of drug resistance.

We previously showed the lack of a respiratory Complex I causes the accumulation of αKG associated to destabilization of HIF-1α that render cancer cells unable to adapt to hypoxia as a result of PHDs stimulation by their substrate αKG, ultimately resulting in a blocked tumor growth *in vivo.* This project aims to propose a selective metabolic approach based on the supplementation of αKG as an anticancer agent. To counter αKG limited permeability, the ketoacid was coupled to distinct hydrophobic carriers giving 7 ester analogues of αKG (αKGlogues) generated for the purpose of this study. The analogues were screened for their capacity to oppose to HIF-1α stabilisation under hypoxic conditions and to selectively hamper cancer cells growth without marked toxicity on non-cancer counterparts. This approach allowed us to select αKG-PP as a potent and safe αKGlogue since it limits HIF-1α stabilisation at long term, selectively impairs cancer cells proliferation and their *in vitro* tumorigenic properties while being well tolerated by the non-cancer counterparts. Further, a synergistic effect of the hydrophobic carrier, independent of HIF-1α, was also unveiled. Metabolomics analysis revealed an intracellular peak in αKG upon treatment coupled to a rearrangement in other TCA cycle intermediates. αKG accumulation correlated with Raptor hyperphosphorylation at short-term, suggesting the αKGlogue mediates its effect through the block of mTORC1 signalling and protein synthesis. Finally, in the perspective of an αKG-based anticancer therapy, the selected analogue displayed anti-proliferative properties on 3D cancer spheroids and a *Drosophila melanogaster* cancer model. The present data highlight the safety and potency of the selected molecule both *in vitro* and *in vivo*, as well as the potential of αKG-based treatment to consider for future combinatory therapies to tackle cancer progression.

ABBREVIATIONS

2-HG: 2-hydroxyglutarate
5-hmC: 5-hydroxymethylcytosine
5fC: 5-formylcytosine
5caC : 5-carboxylcytosine
Ac-CoA : Acetyl-CoA
ALDA/ALDC: aldolase A and C
AML: Acute myeloide leukemias
AMPK: AMP activated kinase
Asn: Asparagine
ATP: Adenosine triphosphate
ARNT: Aryl Hydrocarbon Receptor nuclear translocator
BHD: Birt-Hogg-Dubé syndrome
bHLH-PAS: helix–loop–helix - per-arnt-sim
CI: Complex I
CA9: Carbonic anhydrase
CBP: CREB binding protein
ccRCC: Clear cell renal cell carcinoma
CH: Cysteine/histidine rich domain
CTAD: C-transactivation domain
DMSO: Dimethyl sulfoxide
EDTA: Ethylenediaminetetraacetic acid
EMT: Epithelial-to-mesenchymal transition
ETC: Electron transport chain
FA: Fumarate
FADH2: Flavine adenine dinucleotide
FAO: Fatty acids β-oxidation
FH: Fumarate hydratase
FIH1: Factor inhibiting HIF
GAPDH: Glyceraldehyde 3-phosphate dehydrogenase
GBBH: ɤ-butyrobetain hydroxylase
GDH : Glutamate dehydrogenase
GLS: Glutaminase
GT: Glutamine transaminase
GOT: Glutamate oxaloacetate transaminases
GPT: Glutamate pyruvate transaminases
GLUT: Glucose transporter
GS: Glutamine synthase
HAPs: Hypoxia-activated-prodrugs
HDAC: Histone deacetylase
LC-MS: Liquid chromatography-Mass spectrometry
KMV: 3-methyl, 2-oxovaleric acid
HIF: Hypoxia inducible factor
His: Histidine
HK: Hexokinase
HRE: Hypoxia responsive element
IDH: isocitrate dehydrogenase

IGF: Insulin-like growth factor
IMM: Inner mitochondrial membrane
IMS: Inter-membrane mitochondrial space
JmjC: Jumonji-containing domain
JHDM: JmjC histone demethylases
KDM: Lysine Demethylase
LDHA: Lactate dehydrogenase A
LZIP: Leucine-zipper domain
MCT: Mono-lactate transporter
MDH: Malate dehydrogenase
MDM2: Mouse double minute 2
mtDNA: Mitochondrial DNA
MMPs: Metallo-proteinases
mTOR: Mammalian/Mechanistic Target of rapamycin
MTT: 3-(4,5-dimethylthiazol-2-yl)-2,5-diphenyltetrazolium bromide
nDNA: nuclear DNA
NADH: Nicotinamide adenine dinucleotide
NMLH: N-methyllysine hydroxylase
NADPH: Nicotinamide adenine dinucleotide phosphate
NTAD: N-transactivation domain
OAA: Oxaloacetate
ODDDs: Oxygen-degradation dependent domain
OMM: Outer mitochondrial membrane
OXPHOS: Oxidative phosphorylation
P5C: Pyrroline-5-Carboxylate
P4H: Proline 4(*R*)-hydroxylase
PBS: Phosphate Buffer Saline
PFK: Phosphofructokinase
PKM2: Pyruvate Kinase M2
PDK: Pyruvate dehydrogenase kinase
PDH: Pyruvate dehydrogenase
PHD: Prolyl hydroxylase
Pro: Proline
PVDF: Polyvinylidene floride
pVHL: Von Hippel Lindau protein
ROS: Reactive oxygen species
SDS-PAGE : Sodium dodecyl sulfate polyacrylamide gel electrophoresis
SA: Succinate
SDH: succinate dehydrogenase
SRB: Sulforhodamine B
TBS: Tris Buffered Saline
TCA: Trichloroacetic acid
TCA cycle: Tricarboxylic acids cycle
TETs: Ten Eleven Translocases
TDG: Thymine-DNA glycosylase
TLC: Thin Layer Chromatography
TM-HIF: Triple-mutant HIF1A
VDAC: Voltage-dependant anion channel
VEGF: vascular endothelial growth factor
WT: wild-type

αKG: α-ketoglutarate
αKGDDs: αKG-dependent dioxygenases
αKGDHC: α-ketoglutarate dehydrogenase complex
αKG-G: α-ketoglutarate geraniol
αKG-N: α-ketoglutarate nerol
αKG-L: α-ketoglutarate linelol
αKG-Cl: α-ketoglutarate 2, 4-dichloride
αKG-tB: α-ketoglutarate terbutyl
αKG-P: α-ketoglutarate phenyl
αKG-PP: α-ketoglutarate diphenyl

INTRODUCTION

Hallmarks of cancer

Long thought to be a genetic disease, constant progress in understanding cancer biology now provide more insight into the multifactorial character of this burden. Malignant transformation occurs in a subset of neoplastic precursors as a result of genetic and epigenetic insults leading to uncontrolled expansion, to ultimately form complex tissues with a deranged architecture. A consistent body of evidence sustain that cancer onset happens as a succession of multiple processes (Hanahan and Weinberg 2000). Additionally, tumors are characterised by their high heterogeneity in terms of cellular population. Cancer cells were shown to actively cooperate with their recruited associated stromal cells and *vice versa* to foster tumor formation, progression and response to therapy. In this context, the diverse and complex characteristics that govern tumorigenesis have been elegantly stratified by Hanahan and Weinberg who defined 6 main capabilities as cancer cells hallmarks (Hanahan and Weinberg 2011). Through their progression towards malignancy cancer cells acquire the capacity to sustain proliferative signalling, to resist growth regulators and evade growth suppressors, they gain replicative immortality and resist cell death, and the whole culminates in cancer cells hyperproliferation. Further, to sustain this growth rate and the subsequent needs in nutrients and oxygen supply, cancer cells trigger continuous angiogenesis (angiogenic switch) leading to their characteristic anarchic vasculature. Lastly, malignancies gain invasive and migratory abilities following the loss of cell-cell and cell-ECM junctions or overexpression of pro-EMT transcription factors.

Moreover, recent knowledge permitted to index additional “enabling traits” represented by genomic instability and inflammation highlighting the contribution of the microenvironment to tumor progression (Hanahan and Weinberg 2011). Finally, two emerging hallmark capabilities further underline cancer cells ability to evade immune destruction and reprogram their metabolism. In this regard, cancer metabolism has gained tremendous interest in the past two decades allowing considerable progress in understanding the complexity of malignancies and amongst all to consider new approaches to better tackle them.

Mitochondria: cellular hub for metabolic and bioenergetic reactions

Far from their bacterial origins, mitochondria constitute important organelles that occupy a central role in many cellular processes. Next to cellular respiration, they are also involved in programmed cell death, calcium-homeostasis and stress response. As semi-independent organelles, mitochondria carry their own genetic material and translation machinery contained in the mitochondrial matrix (MM) (Friedman and Nunnari 2014). Mitochondrial DNA (mtDNA) is a double stranded circular molecule of 16,569 base pair that encodes for 13 proteins of the total proteins the organelle counts, the rest being encoded by nuclear DNA (nDNA), synthetised in the cytoplasm then imported to the mitochondria. mtDNA displays some peculiarities that distinguish it from genomic DNA: in addition to being deprived of protective histones or a DNA repair system, mitochondrial DNA is maternally inherited and can exist in multiple copies in a single organelle (polyploidy). Hence, a condition of homoplasmy (wild-type or mutant) thus exists when all mtDNA copies are identical. By opposition, the co-existence of two mitogenomes (wild-type and mutant) in a single cell defines a heteroplasmic state. In a general manner, a heteroplasmic mutation translates at the phenotypic level beyond a defined threshold (usually between 70-90% mutation load). In addition, the homo/heteroplasmy (mutation load) levels is also influenced by mitotic segregation as mitochondria and thus mtDNA molecules are randomly segregated during mitosis.

The countenance of the MM is englobed by the inner mitochondrial membrane (IMM), known for its highly restricted permeability. A second, more permeable membrane wraps up the inner mitochondrial membrane thereby creating a space in between: the intermembrane mitochondrial space (IMS) (Frey and Mannella 2000). The IMM forms invaginations or "cristae" within the mitochondrial matrix which density directly reflects tissue energetic needs. At the functional level, mitochondria are important players involved in a plethora of reactions both in cellular bioenergetic and metabolism. Following glycolysis-derived pyruvate conversion to Acetyl Co-A (Ac-CoA) in the mitochondrial matrix, the latter is coupled to oxaloacetate and engages in the tricarboxylic acids (TCA) cycle reactions. Deeply anchored into the inner mitochondrial membrane IMM, reside the respiratory chain complexes or electron transport chain (ETC) (Khulbrandt et al., 2015). From complex I to complex IV, the enzymatic giants insure oxidative phosphorylation of reducing equivalents (NADH, $FADH_2$) produced by the TCA cycle, electron transport and proton pumping to the IMS space thus creating an electrochemical gradient necessary for ATP synthesis by F_0 F_1-

ATP-synthase or complex V that together with other 4 complexes of ETC formed the oxidative phosphorylation (OXPHOS). Besides glucose metabolism, mitochondria are at the heart of many other catabolic processes (Fatty acids β-oxidation, glutamine and branched-amino acids) as well as biosynthetic reactions including nucleotides, amino acids, fatty acids and heme synthesis. Finally, the organelles are also indispensable for metabolic by-products elimination (urea cycle, ROS) (Spinelli and Haigis 2018).

Mitochondria and metabolic reprogramming in cancer

Because of their central position in cellular metabolism and energy production, since the mid-90s mitochondria have gained growing interest for their contribution to key steps of tumorigenesis (initiation, progression and metastasis). Indeed, numerous studies demonstrate the active implication of the organelles as modulators of metabolic and hypoxic adaptations characterising cancer cells thereby sustaining their uncontrolled proliferation and growth into tumors (Porporato et al., 2018).

In cancer cells, glycolysis and TCA cycle intermediates are deviated from their initial purposes. Instead of energy production, they are mainly used to provide the necessary precursors for biosynthesis of macromolecules (proteins, lipids, nucleic acids) in order to support proliferation. In this frame, Otto Warburg was the first to note that cancer cells preferably use glucose as an energy source to release lactate thereby concluding to a possible mitochondrial aberration. Later, further studies demonstrated that cancer cells rewire their metabolism from oxidative to glycolytic independently from their mitochondrial efficiency (Smolková et al., 2011). Indeed, despite the low energy yield glycolysis allows (2 ATP molecules vs. 36 from oxidative phosphorylation), it seems to rather constitute a more favourable alternative for fastly proliferating cancer cells (Lunt and Vander Heiden 2011). In this regard, glucose being the most abundant nutrient in the extracellular space, cancer cells augment their glucose consumption rate by upregulating the expression of glucose transporters and glycolytic enzymes as a result of oncogenes-mediated stimulation (DeBerardinis et al., 2008) (Lunt and Vander Heiden 2011). Another advantage of the glycolytic pathway is that it provides cancer cells with the precursors necessary for macromolecules biosynthesis such as pyruvate and citrate for *de novo* lipid synthesis, NADPH and ribose sugars for nucleotide synthesis (DeBerardinis et al., 2008).

On the other hand, glutamine is the most abundant amino acid available to cancer cells. It therefore plays an important role in carbon and nitrogen metabolism. In this frame, glutaminolysis constitutes an anaplerotic pathway that refills the TCA cycle with α-ketoglutarate (αKG). In fast proliferating cells, it constitutes a new entry point to the cycle as a result of glucose shifting from oxidative phosphorylation (DeBerardinis et al., 2007). Moreover, several studies demonstrate that glutamine-derived αKG, undergo mitochondrial reductive carboxylation as the main carbon source to support the growth of cancer cells bearing mitochondrial defects or submitted to low oxygen conditions (Fendt et al. 2013) (Mullen et al., 2012) (Wise et al., 2011) (Metallo et al., 2012). The ketoacid is converted to citrate through an isocitrate dehydrogenases IDH1/IDH2-dependent reaction (Wise et al., 2011) (Metallo et al., 2012). Part of the citrate generated is used to sustain lipogenesis through Ac-CoA, on the one hand, and to replenish the pool of TCA cycle with oxaloacetate (OAA) and other intermediates. Paradoxically, a portion of the glutamine-derived αKG still engages in the oxidative TCA cycle pathway in order to generate reducing equivalents (Mullen et al., 2014). Therefore, even though the main energy sources are rearranged in cancer cells, it is now clear that the co-existence of both glycolytic and oxidative/reductive metabolisms all of which are complimentary to sustain cancer cells high growth rate (Zheng et al., 2012).

HIFs signalling and hypoxic adaptation in cancer

Hypoxia Inducible Factors (HIFs) are heterodimeric transcription factors of the basic-helix-loop-helix-PER-ARNT-SIM (bHLH-PAS) family (Wang et al., 1995). At the structural level, the transcription factors include a constitutively expressed nuclear-subunit β (Aryl Hydrocarbon Receptor nuclear translocator, ARNT) and an oxygen-labile subunit α which expression is tightly regulated by oxygen availability. In mammals, subunit β counts two described isoforms, respectively ARNT (or HIF-1β) and ARNT2, while three paralogues of the α subunit have been described so far, HIF-1α, HIF-2α and HIF-3α. HIF-1α and HIF-2α are the best characterised and structurally similar. HIF-3α presents distinct structural features (Yang et al., 2015) (Figure 1) and can exist as different spliced variants some of which were reported to negatively regulate HIF-1α and HIF-2α activity (Makino et al., 2001). In addition to their bHLHL and PAS domains, HIFs structures encompass N- and C-transactivation domains (N-TAD, C-TAD). In addition, subunits alpha specifically harbours an overlapping oxygen-dependent degradation domain (ODDD) (Figure 1). HIF-1α is ubiquitously expressed in mammalian cells whereas HIF-2α and HIF-3α expression is selectively restricted to some

tissues (Ema et al., 1997) (Yang et al., 2015). HIF-1α paralogs were also identified in other lower organisms, for instance in *C. elegans* as well as in *Drosophila Similar* is the corresponding paralogue thus suggesting the conservation of HIF system in all organisms (Semenza 2012).

Under low oxygen tension (0.1-5% O_2), subunits α escape oxygen-dependent degradation, translocate to the nucleus where their heterodimerization with subunit β occurs through a complex interaction involving the proteins respective bHLH and PAS-A domains (Jiang et al., 1996). The complex formation allows further interaction with a core DNA sequence (G/ACGTG) located in the Hypoxia Response Element (HRE) in the promoter region of HIF target genes, thereby triggering their transcription. Conversely, in high oxygen tension (5-21% O_2) subunits α are rapidly degraded (half-life <5minutes) through a complex oxygen-dependent enzymatic cascade. HIF sensing is mediated by post-translational modifications at the level of two proline residues located within the ODDD of subunits α (Figure 1). Prolines 402 and Pro564 for HIF-1α or Pro405 and Pro531 for HIF-2α undergo a 4-*trans*-hydroxylation catalysed by Fe(II)/αKG-dependent dioxygenases (αKGDDs), namely prolyl hydroxylases containing domain (PHDs) (Jaakkola et al., 2001) (Ivan et al., 2001). As members of the αKGDDs family, the activity of the dioxygenases is allosterically regulated by the levels of TCA cycle intermediate α-ketoglutarate (αKG). Conversely, HIF-3α possesses one single proline hydroxylation site in its ODDD. This step is necessary for further recognition and binding by von Hippel-Lindau (pVHL) tumor suppressor protein of the E3 ubiquin ligase complex (Yu et al., 2001). HIF α subunits are subsequently polyubiquitinated and targeted to proteasomal degradation. HIF signalling is further controlled by another post-translational modification catalysed by a distinct enzyme of the αKGDDs family, namely Factor Inhibiting HIF (FIH1) which interferes with its transcriptional activity. In this regard, FIH1 catalyses a β-hydroxylation of an asparagine (Asn) residue located in the hypoxia protein C-TAD domain (Asn803 for HIF-1α and Asn851 for HIF-2α) thereby impeding its interaction and subsequent binding to cysteine/histidine-rich domain (CH1) domain of p300/CBP transcriptional co-activator (Mahon et al., 2001) (Lando 2002) (McNeill et al., 2002) (Figure 1). This mechanism thus constitutes an additional O_2-dependent checkpoint to control HIF pathway. Next to the canonical oxygen-dependent regulation, HIF-1α stability, transcriptional and translational expression can be modulated by different effectors following non-canonical mechanisms especially in the context of cancer

(Iommarini et al., 2017). Amongst these non-canonical effectors are oncometabolites, which will be described in detail in the next section.

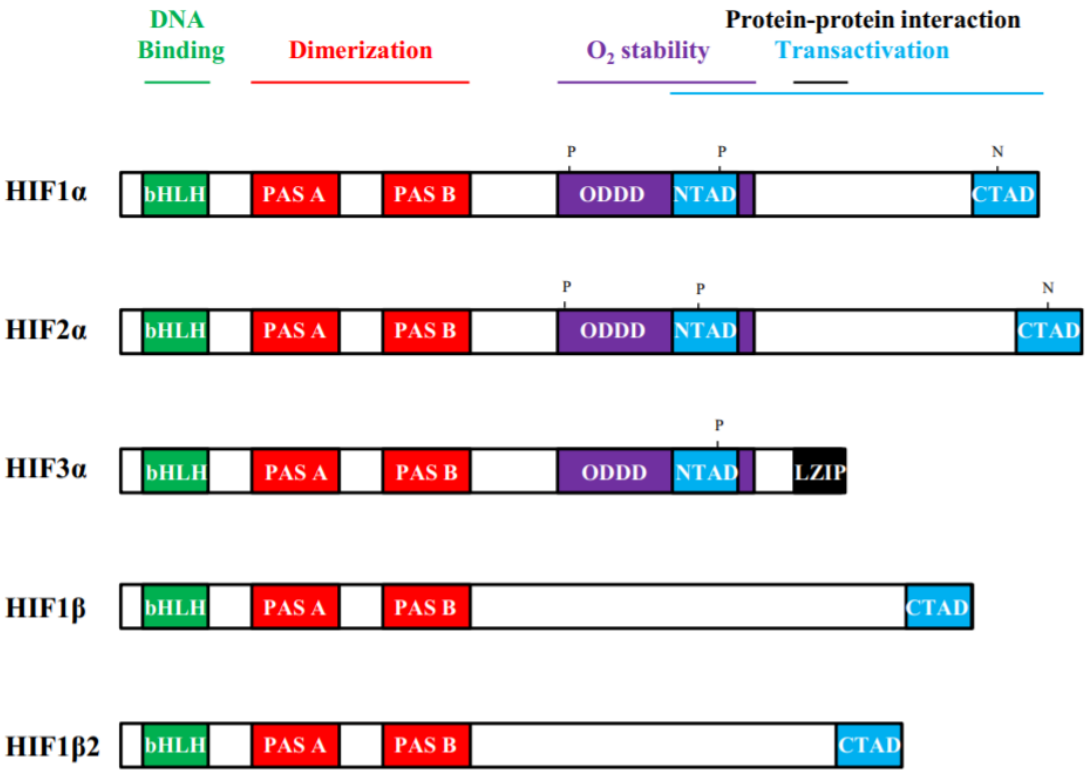

Figure 1: Schematic representation of HIFs structural domains and their corresponding roles (Ravenna et al., 2015). Each motif is represented in a different colour. All HIF isoforms bear a basic-Helix-Loop-Helix (bHLH) and a tandem PER-ARNT-SIM (PAS-A, PAS-B) domain necessary for DNA binding and subunits heterodimerization, respectively. HIF α subunits harbour an N-Transactivation Domain (NTAD) located within the oxygen-dependent-degradation domain (ODDD). This latter is site for oxygen-dependent post-translational hydroxylation of two proline residues (for HIF-1α and HIF-2α) by prolyl hydroxylases ultimately targeting the subunits for proteasomal degradation. By contrast, HIF-3α includes a single proline residue for hydroxylation. HIF-1α and HIF-2α structures also comprise a C-transactivation domain (CTAD) determining for the protein transcriptional activity. In this domain resides an asparagine residue site for FIH1-catalysed hydroxylation. Instead, HIF-3α possesses a Leucine-zipper domain (LZIP) involved in protein-protein interaction. Oxygen-insensitive HIF β subunits are deprived of ODDD and bear a single CTAD. P: Proline residue, N: Asparagine residue. *Permission to reuse allowed*

As described earlier, cancer cells preferably rewire their metabolism towards aerobic glycolysis even in high oxygen conditions. However, tumor organisation due to uncontrolled growth and microenvironment pressure all result in chronic HIF signalling especially in the

tumors innermost parts. HIF activation orchestrates cell adaptation to low oxygen availability in order to sustain cell survival in such extreme conditions. In this frame, the transcription factor counts amongst its numerous targets many pro-glycolytic genes. It mediates an increase in glucose consumption rates by upregulating glucose transporters GLUT1, GLUT3 (Semenza et al., 2012). Similarly, it stimulates the expression of different glycolytic enzymes including hexokinases 1 and 2 (HK1, HK2), phosphofructokinase (PFK1, PFK2), aldolase A and C (ALDA, ALDC), Pyruvate Kinase M2 (PKM2). Pyruvate dehydrogenase kinases (PDK1, PDK3) (Kim et al., 2006) are also upregulated by hypoxia resulting in pyruvate dehydrogenase (PDH) inactivation thereby opposing to pyruvate engaging into the TCA cycle and favouring its conversion to lactate. Consequently, lactate dehydrogenase A (LDHA) as well as mono-lactate transporters (MCT1, MCT4) expression is upregulated in hypoxia along with carbonic anhydrase (CA9). The latter enzyme contributes in concert with MCT transporters to insure H^+ efflux thereby inducing intracellular alkalinisation and extracellular acidification reported to promote invasion (Figure 2) (Semenza et al., 2012). In line with this, HIF stimulates the expression of metallo-proteinases (MMP-2, -9, -14) and extracellular matrix remodelling further enhancing cancer cells metastatic potential (Semenza et al., 2012). As an adaptative factor for oxygen restriction, HIFs stimulates angiogenesis through the increased transcription of angiogenic growth factors including VEGF to enhance vessel formation thereby sustaining one of cancer hallmarks (Figure 2) (Semenza et al., 2012). Further, hypoxia was reported to downregulate oxygen consumption along with ETC activity (Papandreou et al., 2006) (Masson and Ratcliffe 2014) while promoting the expression of glutamine dehydrogenase (GDH) likely to stimulate glutamine-dependent anaplerosis (Jiang et al., 2017). In these conditions glutamine reductive carboxylation is preferably used by cancer cells to sustain fatty acid and lipids synthesis as a consequence of pyruvate rewiring from the mitochondria (Wise et al., 2011) (Metallo et al. 2012). Finally, by eliciting the activation of repressor genes *SNAI1*, *SNAI2*, *ZEB1*, *ZEB2*, HIF is also involved in epithelial-to-mesenchymal transition (EMT) (Unwith et al., 2015) (Semenza et al., 2012) and regulates several genes involved in stemness, cell immortalisation, genomic instability and therapy resistance (Unwith et al., 2015).

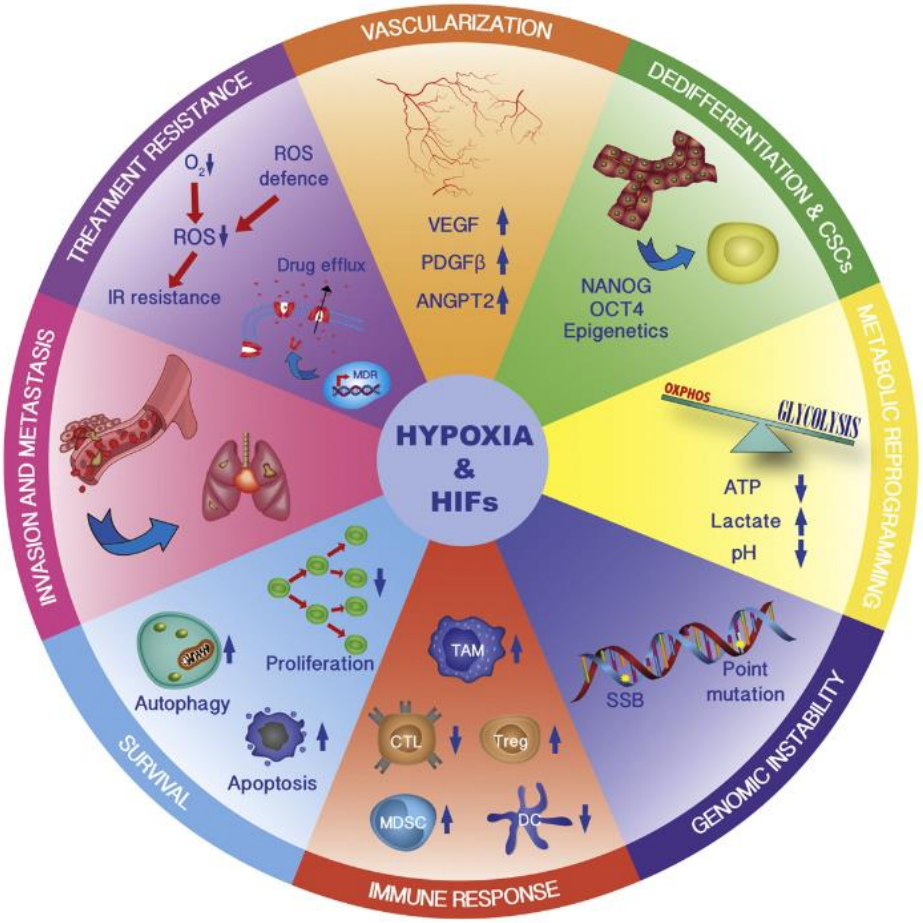

Figure 2: HIF signalling and cancer hallmarks: beyond metabolic adaptation (Wigerup et al., 2016). Through a wide range of targets, the activation of chronic hypoxic signalling promotes multiple processes that ultimately contribute to sustain cancer progression, metastasis and resistance to therapy. *Permission to reuse allowed*

Oncometabolites contribution to cancer progression

Succinate dehydrogenase (SDH), fumarate hydratase (FH) and isocitrate dehydrogenases (IDH1 and IDH2) are considered as tumor suppressors since loss of function mutations affecting these TCA cycle enzymes were reported in different types of cancers. The subsequent accumulation of substrate metabolites, namely succinate (SA), fumarate (FA) and 2-hydroxyglutrate (2-HG) was demonstrated to play an active role in oncogenic signaling, thereby classifying them as oncometabolites (Sciacovelli and Frezza 2016). Loss of function mutations in SDH genes have been reported in hereditary paraganglioma and pheochromocytoma, renal cell carcinoma, gastrointestinal stromal tumors and T-cell leukemia (Niemann and Müller, 2000) (Vanharanta et al., 2004) (Stratakis et al., 2009) (Baysal et al., 2007). On the other hand, FH was found mutated in hereditary leyomatosis and

renal cell carcinoma, paraganglioma and pheochromocytoma, clear cell carcinoma and neuroblastoma (Tomlinson et al., 2002) (Castro-Vega et al., 2014), whereas heterozygous somatic mutations affecting IDH1 and IDH2 were reported in gliomas and acute myeloide leukemias (AML) (Yan et al., 2009)(Mardis et al., 2009). In the latter case, the resulting arginine replacement (R132 in IDH1 and R172 or 140 in IDH2), provokes a shift in the enzyme's substrate affinity (Yang et al., 2010) and the gain of an NADPH-dependent neomorphic function leading to αKG reduction to (*R*)-2-hydrxyglutarate (D-2-HG) (Dang et al., 2009) (Ward et al., 2010). Notably, 2-HG generation by wild-type IDH2 was also reported during glutamine reductive carboxylation in cancer cells submitted to hypoxia (<1% O_2) (Wise et al., 2011). Since 2-HG is a chiral molecule, the existence of an L-2-HG isomer has also been reported in human cancer cells bearing defects in mitochondrial respiratory chain (Mullen et al., 2012) or as a result of promiscuous activity of LDHA and malate dehydrogenase (MDH) under hypoxic conditions (Intlekofer et al., 2015) (Intlekofer et al., 2017). At the structural level, SA, FA, D-2-HG and L-2-HG are very close to αKG. Such structure analogy allows oncometabolites to competitively inhibit the activity of αKG-dependent dioxygenases by occupying the enzyme's catalytic site, with different levels of potency (Koivunen et al., 2007) (Xu et al., 2011). As members of the αKG-dependent dioxygenases family (αKGDDs), PHDs and FIH1 constitute privileged targets for the oncometabolites. In this regard, inhibition of PHDs following SA and FA accumulation was shown to block HIF-1α degradation in normal oxygen conditions, thereby inducing a state of pseudohypoxia *in vitro* and *in vivo* cancer models (Pollard et al., 2005) (Selak et al., 2005) (Isaacs et al. 2005). Although their effect on PHDs is still debated, both D- and L-2-HG markedly reduced FIH-dependent hydroxylation of HIF-1α, explaining in part the high levels of the hypoxia protein observed in IDH-mutated cancers (Zhao et al., 2009) (Chowdhury et al., 2011).

Genetic instability is a hallmark of cancer (Hanahan and Weinberg 2011). In line with this, epigenetic aberrations have also been widely described in cancers (Esteller et al., 2008). They are even thought to precede classical transforming events as in the case of tumor suppressors genes. Indeed, cancer cells show genome wide hypomethylation, CpG islands promoter hypermethylation, as well as histone modification, all converging to genomic instability (Esteller et al., 2008). The dynamic character of epigenetic modifications and the tight interplay with cellular metabolism altogether play a part in malignant transformation. In this regard, the implication of oncometabolites in the modulation of this aspect has been widely

studied, most likely by altering the activity of Ten Eleven Translocases (TETs) family of DNA 5-methylcytosine hydroxylases and Histone Lysine demethylases (KDMs) both members of the αKGDDs superfamily. In this frame, several studies linked supra-physiological levels of SA, FA or 2-HG with repressed activity of TET hydroxylases and KDMs in various cancer subtypes (Xiao et al., 2012) (Xu et al., 2011) (Shim et al., 2014) (Laukka et al., 2016) (Chowdhury et al., 2011). A further illustration of this detrimental effect was the hypermethylated phenotype displayed by SDH and FH-deficient tumors (Letouzé et al., 2013) (Loriot et al., 2015) (Sciacovelli et al., 2016) as well as in IDH-mutated models (Figueroa et al., 2010) (Turcan et al., 2012) (Xu et al., 2011). Accordingly, pathological levels of SA, FA and 2-HG promoted EMT activation in cancer cell models (Loriot et al., 2015) (Sciacovelli et al., 2016) (Grassian et al., 2012) (Colvin et al., 2016) strongly confirming their pro-tumorigenic activity. In particular, 2-HG was also reported to block cell differentiation in hematopoietic cells (Figueroa et al., 2010) (Losman et al., 2013) (Lu et al., 2012), thereby supporting the pro-leukemogenic role of this oncometabolite.

However, the inhibition exerted by oncometabolites on αKGDDs family members was shown to be reversible considering its competitive nature. This can be achieved by modulating αKG/oncometabolite ratio through αKG supplementation (Xu et al., 2011) (MacKenzie et al., 2007) (Tennant et al., 2009).

αKG: a metabolite with pleiotropic activity

αKG at the heart of physiological reactions

αKG, or 2-oxoglutarate (2OG) is a tricarboxylic acid composed of 5 carbons with two weak carboxylic functions and a ketone group in the α position. Within the TCA cycle, IDH3 produces αKG through an irreversible reaction taking place in the mitochondria and where NAD^+ is limiting (Plaut et al., 1983). Wild-type IDH1 and IDH2 normally catalyse the reversible $NADP^+$-dependent oxidative decarboxylation of isocitrate to either in the cytosol (IDH1) or in the mitochondria (IDH2). As a precursor of glutamine, the ketoacid can also originate from glutaminase (GLS)-mediated glutaminolysis and subsequent glutamate deamination by glutamate dehydrogenase (GDH) (Figure 3). Conversely, the reaction catalysed by GDH being reversible, transamination of αKG by GDH forms glutamate, which further amination by glutamine synthase (GS) gives glutamine. Furthermore, an additional reaction mediated by cytosolic or mitochondrial ω-amidase, particularly reported in

mammalian liver and kindey, can also generate αKG as follows: glutamine transamination by glutamine transaminase (GT) first produces an intermediate ketoacid: a-ketoglutaramate, which subsequent hydrolysis by ω-amidase releases αKG and ammonia (Cooper et al., 2016). Hence, through the glutamine-αKG axis, the ketoacid is tightly involved in amino acids metabolism, an anabolic pathway of particular importance especially in cancer cells (Xiao et al., 2016). Likewise, glutamate pyruvate transaminases (GPT1/2) and glutamate oxaloacetate transaminases (GOT1/2 cytoplasmic and mitochondrial respectively) respectively produce αKG from glutamate and pyruvate or oxaloacetate transamination reactions (Figure 3). (Sookoian et al., 2015). Like most of the TCA cycle intermediates, αKG diffuses from the mitochondrial matrix to the cytoplasm and vice-versa. It crosses the inner mitochondrial membrane through a 2-oxoglutarate-malate antiporter and the outer mitochondrial membrane through voltage-dependant anion channel (VDAC) (Monné et al., 2013).

Owing to its metabolic origin and structure, αKG is found at the centre of a wide range of physiological processes qualifying it as pleiotropic molecule (Abla et al., 2020). First of all, both glutamine and αKG have an anabolic role on protein synthesis since glutaminolysis increases intracellular glutamate pools which will be used together with αKG as precursors in transamination reactions for proline, arginine, ornithine amino acids synthesis. The two latter amino acids are known to stimulate growth factors release such as growth hormone (GH) and Insulin-like growth factor (IGF) (Harrison and Pierzynowski, 2008). Clinical studies also reported benefits of αKG alone or in combination (with ornithine or arginine) both in animals and in humans on protein synthesis, muscle mass and body weight gain in post-operative, -trauma patients or those suffering from extensive burns, but also in malnourished aging patients (Zdzisińska et al., 2017). Further, many studies related positives effects of αKG on bone tissue formation suggesting the metabolite to have an anabolic effect and inhibit bone resorption *in vivo* (Zdzisińska et al., 2017). Secondly, αKG structure confers the metabolite a high reactivity. Indeed, with its two carboxylic and ketone groups, αKG is capable of neutralising hydrogen peroxide (H_2O_2) through non-enzymatic oxidative decarboxylation thus preventing oxidative stress damage in mammalian and *Drosphila melanogaster* models (Long et al., 2011) (Bayliak et al., 2015). αKG was also described to neutralise ammonia and ethanol-induced oxidative stress as well as for its antidote effect in case of cyanide poisoning (Abla et al., 2020).

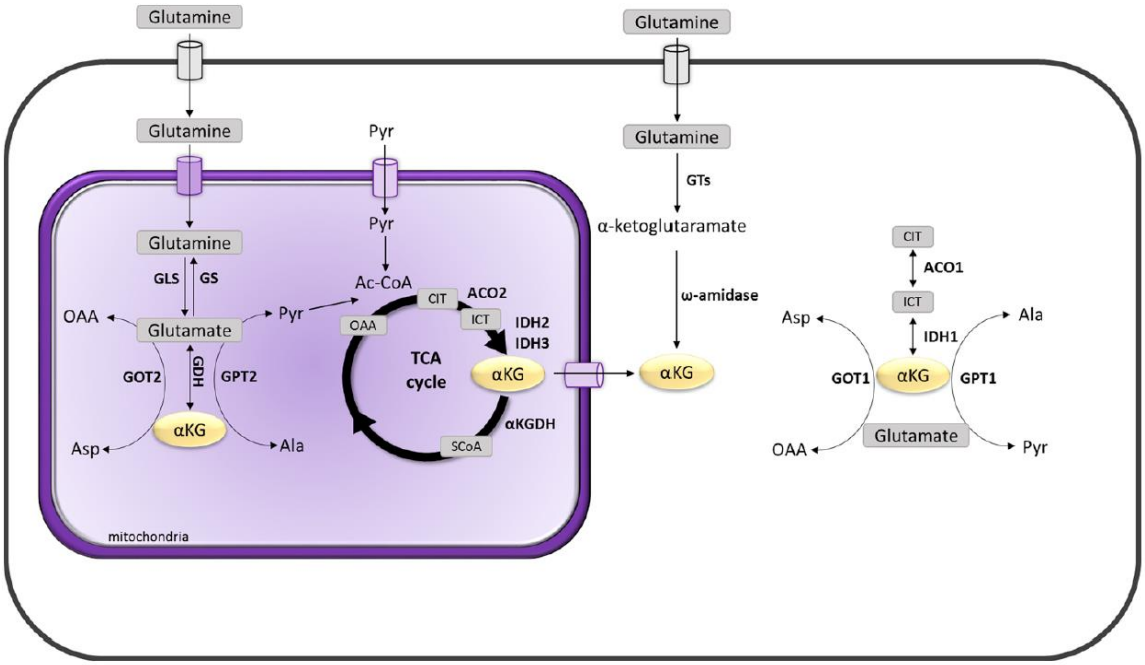

Figure 3: αKG biosynthetic pathways (Abla et al., 2020). αKG derives from glutamine and glutamate deamination in the mitochondria, mediated by glutaminase (GLS) and glutamate dehydrogenase (GDH), respectively. In the cytosol, glutamine transamination by glutamine transaminases (GTs), generates α-ketoglutaramate that is subsequently converted into αKG by an ω-amidase. Moreover, αKG can originate from transamination of glutamine by GTs or glutamate by GPT1/GOT1, in the presence of Pyr/OAA respectively. Inside the mitochondria, GPT2 and GOT2 isoforms catalyze the same reactions. Lastly, the conversion of TCA cycle intermediate isocitrate catalyzed by isocitrate dehydrogenases IDH2 and IDH3 in the mitochondria or IDH1 in the cytosol constitutes another source of αKG

The processes of metabolism and aging being tightly related, dietary restrictions and pharmacological modulation of energy metabolism were previously described to benefit longevity although the underlying molecular mechanisms are still not clearly defined. As aging is often coupled to events like genomic instability, telomere shortening, epigenetic alterations, through its metabolic properties αKG seems to display a beneficial effect in reversing or delaying such alterations. In this frame, Chin and colleagues showed that αKG was able to inhibit ATP synthase β-subunit in *C. elegans*, resulting in increased lifespan and autophagy induction through the inhibition of TOR signalling (Chin et al., 2014). In continuity with this, the metabolite delivered as calcium salt similarly increased lifespan, survival and age-related morbidities reducing different negative factors such as inflammation in female mice (Shahmirzadi et al., 2019). Interestingly, αKG was also correlated to

pluripotency maintenance in mice embryonic stem cells by promoting histone and DNA demethylation (Carey et al., 2015).

αKG as a limiting substrate for dioxygenases

In addition to bridging energy and amino acid metabolisms, the ketoacid is at the crossroads of biological events orchestrated by the super-family of αKGDDs enzymes. Being the dioxygenases obligate substrate, the enzymes use αKG along with iron and ascorbate to catalyse hydroxylation reactions on specific residues of their target proteins while releasing succinate as in the regulation of HIF levels by PHDs or during the early phases of nucleic acids *N*-demethylation endorsed by TET family enzymes.

αKGDDs constitute a widespread family of phylogenetically conserved enzymes harbouring the same fold and requiring αKG as well as a non-haem iron for their catalytic activity. In humans, these enzymes display affinity for various types of substrates ranging from amino acid residues, nucleic acids to metabolic intermediates (Markolovic et al., 2015). At the structural level, *bona fide* αKGDDs share the same double-stranded β-helix (DSBH) fold, also commun to the Jumonji C (JmjC) chromatin-associated proteins. The DSBH core is made of 8 antiparallel β-strands (I–VIII), that fold two by two in a helical manner (β-helix) to form two distorted β-sheets conferring to the enzymes a characteristic distorted barrel structure at the end of which reside the active site with iron/metal and αKG binding pockets (Islam et al., 2018). αKG dioxygenases catalyse a two-electron oxidation hydroxylation reaction of their respective substrates through the sequential binding of ferrous iron, αKG followed by O_2 and substrate. Binding of each respective substrate implies interactions with specific amino-acid residues and coordination sites occupied by 6 water molecules (Schofield and Ratcliffe 2004). First, iron binding to the active site is enabled by interaction with a highly conserved amino-acid triad (facial triad) that constitute the iron Fe(II)-binding motif (Figure 4). Facial triad typically presents as a *HX(D/E)…H* motif and include a proximal and a distal histidine residues (respectively located in the β-II and β-VII strands), while the third residue was mainly reported to be an aspartate (Hegg and Jr 1997). Then, two coordination sites occupied by two water molecules are subsequently displaced to allow αKG binding. The ketoacid chelates Fe^{2+} in a bidentate manner via its C-1 carboxylate and ketone oxygen, thereby forming an octahedral complex (Figure 4). Further electrostatic interactions between its C-5 carboxylate and a basic residue as well as a neutral side chain residue allow binding stabilisation (Markolovic et al., 2015). This step is followed by substrate binding and

subsequent uncovering of the final coordination site favouring oxygen binding. αKG oxidative decarboxylation produces succinate, carbon dioxide and a water molecule along with a ferryl intermediate (FeIV_O) (Figure 4) which reacts with substrate C-H to form the hydroxylated product, while Fe(IV) is reduced to Fe(II). At the term of the reaction, the hydroxylated product is first released followed by succinate (Islam et al., 2018). Of note that some, but not all αKGDDs also necessitate the presence of ascorbate which seems to mainly stand an antioxidant role protecting the iron metal from oxidation.

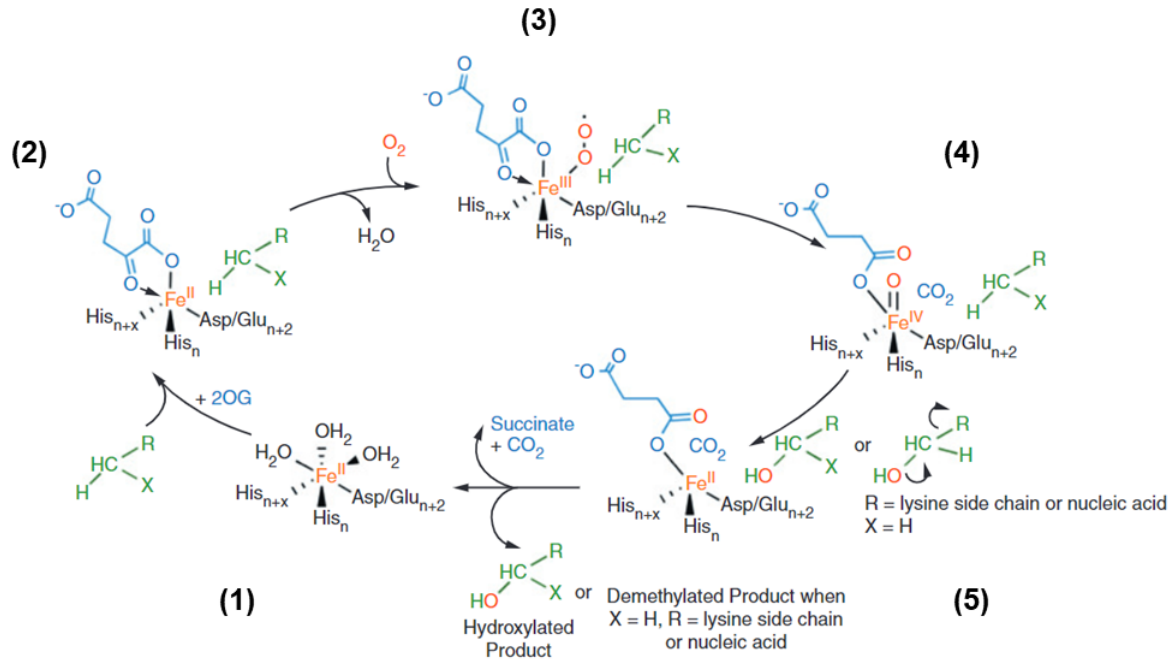

Figure 4: Mechanism of αKG-dependent dioxygenases catalysed hydroxylation (Adapted from (Aik et al., 2012). First, iron binds to the active site following interaction with the amino-acids facial triad **(1)**. Then, two coordination sites occupied by two water molecules are displaced to allow αKG binding. The ketoacid chelates Fe^{2+} in a bidentate manner thereby forming an octahedral complex **(2)**. This step is followed by substrate binding **(2)** and subsequent uncovering of the final coordination site favouring oxygen binding **(3)**. αKG oxidative decarboxylation produces succinate, carbon dioxide and a water molecule along with a ferryl intermediate (FeIV_O) **(4)** which reacts with the substrate to form the hydroxylated product, while Fe(IV) is reduced to Fe(II) **(5)**. The hydroxylated product is first released followed by succinate **(5)**. *Permission to reuse allowed*

Amongst the αKGDDs super-family, prolyl hydroxylases (PHDs) are the most important and the best described members, because of their role in hypoxia sensing. Displaying very high affinity for molecular oxygen with K_m values in the range of 100-250μM, these enzymes thus constitute notable oxygen sensors (Kaelin and Ratcliffe 2008). To date, three PHD paralogues

have been described so far: PHD1, PHD2 and PHD3 (also known as EglN2, EglN1 and EglN3 respectively, the orthologues of Egl-9 in *C. elegans*) (Epstein et al., 2001) (Ivan et al., 2002) although a fourth isoform has also been reported (Kaelin and Ratcliffe 2008). At the cellular level, PHD1 was shown to exclusively locate in the nucleus while PHD2 is cytoplasmic and PHD3 was found in both sub-cellular compartments (Metzen et al., 2003). In addition to oxygen sensing and HIF regulation, some PHDs were reported to be involved in additional cellular processes. For instance, PHD1 and PHD3 have been reported to have growth suppressive effects (Erez et al., 2003) (Fong and Takeda, 2008). Presenting with the lowest K_m for O_2, studies in mammalian cells have shown that HIF-1α levels are mainly regulated by PHD2 in normoxia and PHD1 to a lesser extent (Berra et al., 2003). By contrast, PHD1 preferably acts on HIF-2α, while PHD3 displays affinity only for HIF-2α C-TAD (Appelhoff et al., 2004) (Ivan and Kaelin 2017). Although altogether, the process of HIF regulation seems to be more intricate and mainly dependent on the cellular context as well as expression levels of each respective isoform (Ivan and Kaelin 2017). Interestingly, PHD2 and PHD3 but not PHD1 expression was described to be stimulated by hypoxia suggesting the existence of a negative feedback control on HIF signalling (Berra et al., 2003). FIH1, for which a single isoform has been described so far, presents a different sequence to PHDs and further structural and computational studies identified the enzyme with a Jumonji homology region thereby classifying it in a distinct subfamily of αKGDDs (Hewitson et al., 2002) (Lando et al., 2002). FIH1 displays a K_m value of 90μM for O_2 (Koivunen et al., 2004). Likewise, to carry on their catalytic activity, PHDs and FIH1 are strictly dependent on αKG intracellular amounts with K_m values of 50μM and 25μM, respectively, suggesting the enzymes activity can be influenced by the slightest fluctuations in the ketoacid levels (Table 1) (Koivunen et al., 2004). As a matter of fact, it can also be modulated by the levels αKG of structural analogues, namely succinate which constitutes the product of the HIF-hydroxylating enzymes along with other oncometabolites (FA and 2-HG) (Table 1). In this frame, fumarate was described to be the most potent in negatively modulating PHDs dioxygenase activity (Koivunen et al., 2007) followed by succinate, thereby giving more insights into their role as oncometabolites. Citrate, oxaloacetate and pyruvate also displayed the ability to interfere with PHDs and FIH1 with different levels of potency. The latter seems to be more sensitive to citrate and oxaloacetate competitive binding (Koivunen et al., 2007). It is important to note that the reported values are calculated on recombinant enzymes. Thus, the situation *in vivo* is more dynamic and directly depends on multiple additional factors.

K_m (µM)				IC50 (µM)			
2OGGDs	**Fe^{2+}**	**2OG**	**O_2**	**Succinate**	**Fumarate**	***R*-2HG**	***S*-2HG**
EGLN1	0.05	1-270	65-250	510	80	300	240-1,150
EGLN2	0.05	2	230	830	120	210	630
EGLN3	0.1	10	230	570	60	-	90
FIH1	0.5	25-150	90-240	>10,000	>10,000	1,100-1,500	190-300
P4HA1	2	20	40	190	400	1800	310
TET1	5	55	0.3-30	390	540	4000	1,000
TET2	4	60	0.5-30	400	570	5000	1,600

Table 1: K_m and IC50 values of αKGDDs for their co-substrates and αKG structural analogues (Adapted from (Losman et al., 2020).

Eukaryotic chromatin is organised in basic units, namely nucleosomes. Nucleosome structure comprises an octamer of core histones (H2A, H2B, H3 and H4) around which is wrapped a 147 bp DNA segment. Chromatin core histones can undergo numerous post-translational modifications (methylation, acetylation, phosphorylation, ubiquitylation and SUMOylation) at the level of their free tails. In particular, methylation span at lysine and arginine residues. Histone modifications directly reflect the state of chromatin folding (euchromatin vs. heterochromatin) hence giving insight on transcriptional activation or repression. Long considered as static, histone methylation landscape seems to define a histone code that is read and interpreted by adapted proteins (Pedersen and Helin 2010). DNA and histone tails epigenetic modifications play and important role in the regulation of transcription regulation, genome integrity and cell fate.

Enzymes of the Ten Elven Translocase family are dioxygenases known to catalyse active DNA-demethylation by oxidising 5-methylcytosine (5mC) in CpG rich islands of genes promoters (Tahiliani et al., 2009). This process takes place in a multiple step reaction that successively gives rise to 5-hydroxymethylcytosine (5-hmC), 5-formylcytosine (5fC) then 5-carboxylcytosine (5caC) ultimately leading to base-excision by Thymine-DNA glycosylase (TDG) (Ito et al., 2011) (He et al., 2011). There are known 3 TET isoforms, TET1-TET3 all of which display the typical double-stranded β-helix fold characterising αKGDDs (Wu and Zhang 2017). As a member of Fe(II)/αKG-dependent dioxygenases, TETs-catalysed reaction on DNA requires the presence of both substrates for optimal activity. Likewise, the activity of the enzymes is also sensitive to oxygen availability (Table 1).

In parallel, chromatin-associated Jumonji-containing domain proteins (JmjC) represent the largest class of demethylases and belong to the αKGDDs family thanks to structural similarities with other members of the super-family. These proteins, also known as JmjC histone demethylases (JHDM) or Lysine Demethylases (KMDs) thus harbour a JumonjiC (JmjC) domain and are capable of catalysing histone demethylation through oxidative decarboxylation of αKG in the presence of O_2 and Fe(II) (Tsukada et al., 2006). As stated in previous sections, both TETs and KDMs are sensitive to competitive inhibition by oncometabolite 2-HG (Xu et al., 2011), both 2-HG enantiomers acting as weak competitive inhibitors and reversibly occupying the enzymes catalytic site (Laukka et al., 2016) (Xu et al., 2011).

Next to its role in oxygen-dependent HIF degradation and epigenetic regulation of gene expression, αKG is also involved in the synthesis and crosslinking of collagen fibers, the major component of connective tissues (Figure 5). Collagen strains are composed of amino acids triplet Xaa-Yaa-Gly, where Xaa is usually (*2S*)-proline, Yaa, (*2S,4R*)-hydroxyproline and Glycine residues. Collagen fibers are stabilised under the effect of two types of αKG-dependent dioxygenases: proline 4(*R*)-hydroxylase (P4H), which catalyse stereospecific *trans* prolyl 4-hydroxylation of the proline residue in the Yaa position (Gorres and Raines 2010), and proline 3(*S*)-hydroxylases which catalyse prolyl-3-hydroxylation, at Xaa position. By its chemical properties *trans* 4-hydroxyproline stabilizes collagen polypeptides. This step is necessary for subsequent folding of collagen triple helixes thus setting the pavement to other post-translational modifications. Like other OGDDs, P4H requires substrates αKG and O_2, Fe(II) and ascorbic acid as a cofactor to reduce iron. The lack of ascorbate causes the development of scurvy disease secondary to prolyl hydroxylase inactivity and thus collagen instability.

Moreover, αKG pleiotropic position also involves it in L-carnitine biosynthesis thereby in lipid metabolism, by serving as a substrate for N-methyllysine hydroxylase (NMLH) and ɤ-butyrobetain hydroxylase (GBBH). Both enzymes of αKGDDs family respectively catalyse the first and last step of L-carnitine synthesis, a cofactor that insures the import of long chain fatty acids into the mitochondria for β-oxidation (Vaz and Wanders 2002). On the other hand, αKG and PHD1 were reported to modulate NF-κB signalling cascade implicated in inflammatory response to cytokines, cell survival and proliferation observed in tumorigenesis. Cummins and colleagues (Cummins et al., 2006) demonstrated that inactivation of IKKβ kinase following an oxygen-dependent hydroxylation of a proline

residue (P191) is mediated by PHD1 (Figure 5). IKKβ is known to activate NF-κB after phosphorylating Inhibitory κB-α (IκB-α), thus uncovering the transcription factor's Nuclear Localisation Sequences in hypoxic conditions.

In conclusion, shedding light on the multiple implications of αKG in all the above-mentioned metabolic, epigenetic and regulatory processes gives a general view of multiple virtues the ketoacid can offer in the scope of developing potential therapeutic applications.

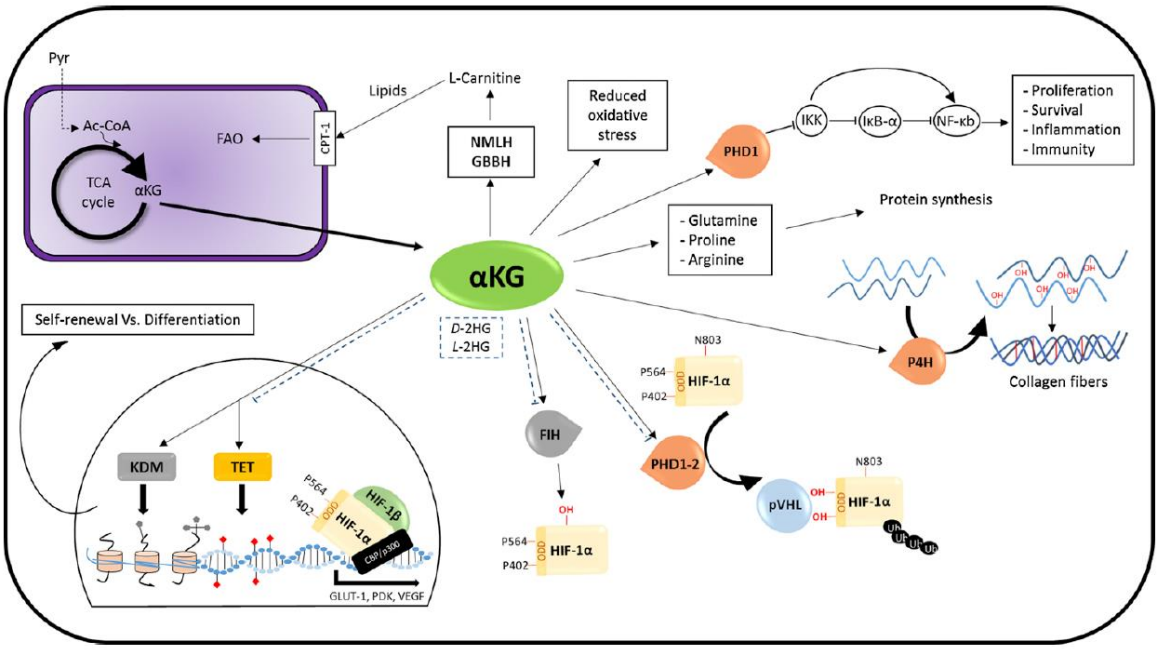

Figure 5: Pleiotropic implication of αKG in cell homeostasis (Abla et al., 2020). αKG is involved in multiple cellular processes both in physiological and pathological contexts. It protects against oxidative stress, modulates protein and lipid biosynthesis, and is involved in fatty acids β-oxidation (FAO). As substrate of αKG dependent dioxygenases, it activates hydroxylases (PHDs and FIH1) to limit HIF-1α signalling, leading to pVHL-mediated protein poly-ubiquitination and proteasomal degradation in normoxia. The metabolite also affects gene expression and cell stemness by promoting epigenetic DNA and histone demethylation by TETs and KDMs enzymes. Finally, αKG stimulates PHD1 to inactivate NF-κB signalling and is likewise determining in the process of collagen monomers stabilization.

Targeting hypoxic adaption as a therapeutic strategy in cancer

Tumor hypoxia in solid tumors often correlates with a poor prognosis and increased mortality in cancer patients (Vaupel et al., 2001) (Bertout et al., 2008). The activation of HIF

signalling, or hypoxic adaptation is well documented to confer an aggressive phenotype coupled to chemo- and radiotherapy resistance as a result of an uncontrolled tumor growth and aberrant vascular architecture (Vaupel et al., 2001) (Bertout et al., 2008). Consequently, a great interest had arisen to tackle HIF pathway in neoplasms through direct or indirect approaches.

HIF inhibitors

One class of compounds developed to target hypoxia signalling are Hypoxia-activated-prodrugs (HAPs). These inactive compounds engineered to be converted into their active pharmacological forms in a hypoxic environment following enzymatic activation present thus the advantage of target specificity. Often designed to target DNA replication, many of these prodrugs are being presently tested in clinical trials (Phillips et al., 2016). Next to that, a wide range of molecules have been reported in literature for their ability to antagonise HIFs heterodimerisation, DNA-binding and transcriptional activity or mRNA expression. In this frame, acriflavine binds PAS domains of HIF-a1 and HIF-2α subunits and was shown to potently reduce tumor growth and vascularization in xenograft models (Lee et al., 2009). Similarly, PT2385 which displays a higher affinity for HIF-2α subunit is being investigated in clinical trials in patients with ccRCC renal cell carcinomas (Chen et al., 2016). In the class of compounds blocking HIF-a transcriptional activity, Bortezomib, a proteasome inhibitor already approved for the treatment of multiple myeloma, reportedly stimulated FIH-dependent repression of HIF-1α transcriptional activity. However, when used as a single therapy the drug lacked potency in colorectal cancer patients cohorts (Mackay et al., 2005). In the same class, molecules of the chetomin family were not pursued because of toxicity issues despite their ability to repress HIF-p300 interaction. In the category of candidates opposing to HIF-DNA binding, despite showing interesting effects on VEGF expression *in vitro*, both polyamides and echinomycin were not as potent in clinical trials and were thus not pursued. Finally, the largest part of compounds described so far are those blocking HIF mRNA translation or protein expression and potentially the most promising. In this scope, an interesting candidate is EZN-2698. An RNA antagonist reported for its ability to specifically inhibit the expression of HIF-1α mRNA levels and its target genes correlating with reduced tumor growth *in vitro* and *in vivo* (Greenberger et al., 2008). In clinical trials this compound showed promising effects in patients with renal cell carcinoma (Wigerup et al., 2016). Within the class of topoisomerase inhibitors, camptothecin analogue, namely topotecan was able to downmodulate HIF-1α translation and protein levels resulting in reduced tumor growth in

xenograft models (Rapisarda et al., 2009). Further, irinotecan as well as its active metabolite (SN38) displayed low toxicity levels and encouraging results in Phase I clinical trials in patients with brain tumors (Norris et al., 2014). In addition, compounds opposing to HIF stabilisation which have been approved or are currently investigated in clinical studies, include histone deacetylase (HDAC) inhibitors (Romidepsin and trichostatin) as well as Heat-shock protein 90 (Hsp90) inhibitors (Masoud and Li, 2015). In the frame of an indirect approach, drugs targeting signalling pathways upstream of HIF are also under investigation. Indeed, it is well known that HIF-1α mRNA levels are upregulated by PI3K/AKT/mTOR pathway, hence molecules modulating with this pathway can constitute an interesting alternative. Amongst mTOR inhibitors, Temsirolimus stands out as the most promising as it passed phase II clinical trial and is now approved by the FDA for the treatment of metastatic renal cell carcinoma (Revaud et al., 2010) (Batelli and Cho, 2011).

Although considerable efforts have been invested in developing HIF-targeted therapies, the high rate of therapy resistance hints to the necessity of combining approaches in order to enhance treatment success chances. In this frame, it is important to note that the severe alteration of mitochondrial CI activity has been correlated to chronic HIF-1α destabilisation subsequently blocking tumor growth *in vitro* and *in vivo* (Kurelac et al., 2019).

Targeting mitochondrial CI in cancer

Respiratory complex I (CI) or NADH:ubiquinone oxidoreductase is the largest protein of the ETC with its 44 subunits, 7 of which (ND1-6 and ND4L) are encoded by mtDNA. The remaining 37 subunits are encoded by nDNA then imported into the mitochondria where they assemble into a functional enzyme. This finely tuned process involves different chaperone proteins (Guerrero Castillo et al., 2017). Mitochondrial CI plays a key role in energy homeostasis and is similarly involved in the maintenance of redox balance as well as in cellular processes like apoptosis. The protein heads the ETC to catalyse the oxidation of TCA cycle-derived NADH thereby transferring 2 electrons to ubiquinone while pumping two protons into the mitochondrial intermembrane space thereby generating an electrochemical gradient and contributing to the ATP production by F_0-F_1 ATP-synthase.

Despite the great deal of studies reporting mitochondrial mutations spanning in CI subunits in many cancers, such mutations are unlikely able to trigger oncogenic transformation *per se*. Nonetheless, the contribution of the mtDNA mutations in CI genes in the process of oncogenesis, cancer progression, metastasis and therapy resistance has been widely debated

(Leone et al. 2018), and lately further investigations allowed to stratify the pathogenicity of such defects depending on: i. the mutation type, ii. the mutation load or threshold (Giuseppe Gasparre et al. 2011) (Iommarini et al. 2014) and iii. the functional vs. structural severity these mutations induce on the activity of the complex. Consequently, mutations affecting mtDNA-encoded subunits are sub-divided in 3 groups: those mildly affecting CI function/activity, severe shifts altering the enzyme activity but not its overall stability and finally disruptive mutations which totally impair the complex assembly (Iommarini et al. 2013).

To further illustrate this concept, heteroplasmic missense or frameshift mutations in mtDNA genes encoding for CI subunits were reported to play a pro-tumorigenic role. Consistent with a mild functional alteration of the complex enzymatic activity, such mutations were shown to enhance cancer cells tumorigenic potential *in vitro* through mechanisms involving reactive oxygen species (ROS), HIF-1a or Akt kinase signallings (Leone et al. 2018). In the same time, growing evidence is emerging to support the contribution of mitochondrial mutations in CI encoding genes in metastasis and resistance to chemotherapy (Ishikawa et al. 2008) (Girolimetti et al. 2017) (Guerra et al. 2012). By contrast, at homoplasmic loads some mutations in CI mtDNA-encoded genes correlated with a reduced tumor growth *in vitro* and *in vivo* (Park et al. 2009), while studies on indolent oncocytomas carried by our group and others unveiled the high occurrence rate of mutations affecting CI genes in this tumor subtype (Gasparre et al. 2007). Further modulation of the hetero/homoplasmy levels highlighted the *oncojanus* role of mitochondrial-encoded complex I genes in affecting tumor fate, either by impinging tumor progression or on the contrary favouring it. One good example is homoplasmic 3571insC/*MT-ND1*, defined as a disruptive or disassembling mutation as it impeaches CI assembly. A homoplasmic but not heteroplasmic load of the mutation, translated at a metabolic level with imbalanced αKG over SA ratio in favour of αKG, a feature that was similarly recapitulated by genetically CI-deprived cells (Kurelac et al., 2019). The two metabolites tightly regulating the activity of prolyl hydroxylases and HIF sensing, such a metabolic context resulted in chronic HIF-1α destabilisation ultimately blocking tumor growth both *in vitro* and *in vivo* (Porcelli et al., 2010) (Calabrese et al., 2013) (Iommarini et al., 2014) (Kurelac et al., 2019).

Hence, this knowledge gives further insight into the double-edged implication of mitochondrial CI in tumor progression, metastasis and resistance to therapy modulated by the

oncojanus role of mtDNA-encoded genes progression. Although further investigation is warranted, evidence is also emerging in favour of an *oncojnaus* implication of CI nDNA-encoded genes (Leone et al., 2018).

In continuity with this, pharmacological targeting of the complex activity could thus constitute an appealing approach for the development of new cancer therapies. In this frame, molecules have been reported thus far. Although classical compounds (alkaloids, rotenone, piericidin A and capsaicin) displayed strong anti-proliferative properties *in vitro*, their effect is coupled to considerable ROS generation thereby compromising their use for safety issues. Many other molecules are emerging and gaining substantial interest. Amongst these, BAY 87-2243 and AG311 were described to block CI activity leading to reduced oxygen consumption and induce cancer cell death *in vitro* and *in vivo* in glucose-deprived conditions (Bastian et al., 2017). In particular, treatment with BAY87-2243 induced ROS accumulation, reduced ATP levels which correlated with AMPK activation in melanoma cells (Ellinghaus et al., 2013) (Schockel et al., 2015). More recently, biguanides, drugs approved for the treatment of type II diabetes mellitus have gained growing attention for their ability to inhibit mitochondrial CI through a non-competitive inhibition of ubiquinone reduction (Bridges 2014). From this class, a number of studies have been dedicated to studying the anti-neoplastic effect of metformin, especially after epidemiological studies revealed the drug to have protective properties on cancer onset and to ameliorate prognosis. *in vitro* the drug was reported to display an anti-proliferative effect through a specific inhibition of CI. In this context, metformin determined a bioenergetic crisis, reduced glucose oxidation in the mitochondria and increased cancer cells dependency on glutamine reductive carboxylation (Fendt et al., 2013). Like other CI inhibitors, metformin's anti-neoplastic effect was more marked under glucose starvation conditions, suggesting that cancer cells mainly use glycolysis for survival following CI inhibition (Birsoy et al., 2014) (Andrzejewski et al., 2014). Similarly, in our cell models we confirm metformin's ability to block HIF-1α stabilisation (unpublished data) and its capacity to alter cancer cells viability and *in vitro* clonogenic abilities. However, this effect seems to be partly independent from CI activity inhibition (off-target effect) and is more important as treatment doses increase. Remarkably, metformin, BAY87-2243 and AG311 were all able to induce HIF-1α destabilisation in hypoxic conditions in the tested models (Wheaton et al., 2014) (Ellinghaus et al., 2013) (Schockel et al., 2015). A direct consequence of CI inhibitors effect could be a stimulated activity of prolyl hydroxylases. Indeed, it is possible that reduced oxygen consumption would

increase oxygen availability thereby stimulating prolyl hydroxylases to target HIF-1α for degradation even in low oxygen condition (*pseudonormoxia*). On the other hand, and as previously demonstrated in our CI-deprived models, NADH accumulation following the abolition of CI-dependent NADH dehydrogenase activity induces an imbalanced NAD^+/NADH ratio that downmodulates the activity of αKG dehydrogenase complex (αKGDHC) causing αKG levels to increase ultimately boosting PHD activity (Calabrese et al., 2013) (Iommarini et al., 2014) (Kurelac et al., 2019). Other molecules interfering with the complex activity include antidiabetic canagliflozin which was able to inhibit the proliferation of prostate and lung cancer cells, reduced glucose uptake and ATP levels leading to AMPK phosphorylation (Villani et al., 2016). Similarly, antilipemic agent fenofibrate also showed the potency to reversibly inhibit the mitochondrial complex thereby inducing cancer cells apoptotic cell death *in vitro* or autophagy as a mechanism to sustain proliferation (Brunmair et al., 2004). The list of CI inhibitors still goes on with compounds from the isoflavonoids family (ME-344) or JCI-20679 all of which were reported for their repressive potential on the complex activity and on cancer cell growth (Lim et al., 2015) (Akatsuka et al., 2016). However, before future therapeutic applications on clinical patients, the mechanism and specificity of action as well as safety of each respective candidate still need to be clearly assessed.

αKG as an anticancer agent

In light of *in vitro* affinity studies on different αKGDDs (Koivunen et al., 2007), further studies demonstrated the reversible nature of αKGDDs inhibition exerted by αKG analogues highlighting the importance of the ratio oncometabolite/αKG in such a context. As first demonstrated by MacKenzie and colleagues, concomitant increase of αKG levels was able to overcome PHD inhibition mediated by SA and FA in an *in vitro* assay (MacKenzie et al., 2007). Likewise, 2-HG inhibition of histone demethylases, was also reversed by increasing amounts of αKG (Xu et al., 2011).

This knowledge opened new perspectives for novel therapeutic strategies, amongst which the possibility of using αKG as an anticancer agent to counteract oncogenic progression has emerged. About a decade ago, the first studies started investigating the ability of αKG to oppose to HIF signalling in cancer models, through a provoked intracellular accumulation of the metabolite via a genetic or pharmacologic modulation. In this frame, numerous studies set the tone, describing antitumorigenic effects of the ketoacid. Our group demonstrated that the

increased αKG/succinate and NADH/NAD^+ ratio in cells lacking a functional mitochondrial complex I. Overall, this condition prevented HIF-1α stabilisation and delayed tumor growth both *in vitro* and *in vivo* (Porcelli et al., 2010) (Calabrese et al., 2013) (Iommarini et al., 2014) (Kurelac et al., 2019). We demonstrated that αKG intracellular accumulation is able to enhance PHDs activity resulting in chronic HIF degradation even under low oxygen tension, a condition we termed *pseudonormoxia*. By contrast, other works used exogenous supplementation of free or conjugated αKG. Indeed, because the hydrophilic character of the molecule limits its membrane permeability, some groups opted for cell-permeable αKG ester analogues. Such compounds were shown to efficiently permeate through the plasma membrane thereby enhancing the metabolite intracellular levels to finally reverse PHD inhibition exerted by fumarate and succinate in SDH-deficient cells (MacKenzie et al., 2007) (Tennant et al., 2009). Similarly, treating Hep3B and LLC cancer cells models with exogenous αKG induced a dose-dependent HIF-1α destabilisation in hypoxia (Matsumoto et al., 2006) (Matsumoto et al., 2009) and counterbalanced HIF-1α-nuclear accumulation in SDH-mutant fibroblasts (Brière et al. 2005). Further, HIF-1α targeting for proteasomal degradation subsequently to αKG-analogues exposure was mediated by PHD2 reactivation and independently of oxygen tension *in vitro* and *in vivo* (Tennant et al., 2009) (Tseng et al., 2018) further confirming the role of this isoform in HIF-1α regulation. In continuity with this, αKG supplementation correlated with a dose-dependent downregulation of HIF downstream targets at transcriptional and post-transcriptional levels (Matsumoto et al. ,2006) (Matsumoto et al., 2009) likely suggesting the ketocid also stimulates FIH1 activity. At the metabolic level, αKG severely reduced ATP levels, glucose consumption and lactate levels, finally leading to a PHD3-dependent apoptotic cell death (Tennant et al., 2009) (Tennant and Gottlieb, 2010). Moreover, in combination with respiratory chain complex I inhibitor BAY-87 2243, dimethyl-αKG was able to block glycolysis through an MDM2-dependent transcriptional reprogramming ultimately triggering parthanatos in cancer cells (Sica et al., 2019). In a metastatic breast cancer cell model αKG-based treatment enhanced oxidative phosphorylation, impaired cancer cell clonogenic properties *in vitro* and tumor growth *in vivo* (Tseng et al., 2018). Interestingly, Rzeski and colleagues reported an anti-proliferative effect of αKG on a set of colon adenocarcinomas cells in normoxia (Rzeski et al., 2012). The effect was mediated via a blockade in DNA synthesis followed by cell cycle arrest. These reports infer multiple implication of the metabolite in distinct signalling pathways that overall converge towards a single outcome that is reduced proliferation. Notably, following αKG-analogues structure optimisation, the ketoacid was able to permeate within complex 3D

structures and exhibited a high potency in blocking hypoxic signalling in colon cancer-derived tumor spheroids (Tennant et al., 2009) while tumor xenografts exposed to those analogues were significantly smaller in size and less dependent on glucose consumption (Tennant et al., 2009). Intriguingly, despite the block in tumor growth secondary to CI ablation, we showed that our CI-deficient models are able to recruit pro-tumorigenic M2 macrophages in what seems to constitute an adaptative mechanisms aiming to maintain tumor subsistence (Kurelac et al., 2019). Of note that αKG was previously reported to favour M2 macrophages polarisation (Liu et al., 2017), however in our case further investigations are necessary to determine if αKG accumulated secondary to CI ablation may result in M2 macrophages activation as a side-effect.

More recently, a bulk of studies rather highlighted the implication of αKG in the epigenetic regulation of gene expression by modulating histone and DNA demethylation, considering its role as a limiting substrate during TETs and KDMs catalysed reactions. In this frame, pharmacological or genetic inactivation of a-ketoglutarate dehydrogenase (αKGDH) induced an accumulation of intracellular αKG and translated with increased TET1 and TET3 enzymatic activity both *in vitro* and *in vivo*. Such an approach reversed DNA hypermethylation and reactivated miR-200 family pathway thereby blocking cell migration and EMT in breast cancer models (Atlante et al., 2016). To further emphasize the beneficial effect of the metabolite in opposing to the accumulation of repressive epigenetic markers, treatment with αKG counterbalanced succinate-mediated inhibition of TETs by increasing 5-hmC and reducing 5-mC in paraganglioma SDH-deficient cells (Letouzé et al., 2013). Moreover, in a pancreas ductal adenocarcinoma (PDAC) model, dimethyl-αKG administration reactivated TET-mediated DNA demethylation favouring tumor cell differentiation through a mechanism that recapitulates p53 anti-tumorigenic response (Morris et al., 2019), while it was shown to counteract Wnt hyperactivation in patients-derived intestinal organoid model (Tran et al., 2020). In addition to stimulating histone demethylation in breast cancer cells, dimethyl-αKG induced senescence and reversed resistance to genotoxic stress secondary to ionized radiation (Efimova et al., 2016).

AIMS

Solid tumors sustain their high growth rate through a metabolic and hypoxic adaptation mainly orchestrated by HIF-1α, which controls the transcription of target genes implicated in glycolysis, neoangiogenesis and metastasis. At the clinical level, these tumors are associated with a higher risk of therapy resistance, relapse and poor prognosis in cancer patients even more that few molecules directly targeting hypoxia/HIF-1α axis have been approved so far due to safety issues or limited therapeutic efficacy. We previously showed the lack of respiratory Complex I causes the accumulation of αKG associated with the destabilization of HIF-1α that renders cancer cells unable to adapt to hypoxia, a condition we termed *pseudonormoxia*, and ultimately blocks tumor growth *in vivo.*

This project thus aims to propose a metabolic-based approach to tackle cancer cell proliferation through a provoked accumulation of exogenous αKG under hypoxia condition. We speculated that high levels of αKG would result in a boosted PHDs activity with subsequent activation of HIF-1α protein degradation cascade. Although the ketoacid hydrophilic properties constitute a limitation to its membrane permeability, we generated ester analogues of αKG (αKGlogues), in which the metabolite is linked to such hydrophobic carriers via an ester bond allowing to optimise its physicochemical properties and thereby its delivery to the intracellular compartment due to the action of esterases. Consequently, a panel of 7 different αKG-monoesters were synthesised for the purpose of this study, each one bearing a structurally distinct carrier, and their ability to impede HIF-1α stabilisation in low oxygen tension along with cancer cell growth was assessed. Simultaneously, the αKGlogues safety was tested on non-cancer cells counterpart. Further, the respective abundances of TCA cycle intermediates and the molecular consequences likely engendered by such a metabolic state in cancer cells were also investigated. Finally, taking this study a step further in the perspective of proposing an αKG-based adjuvant anti-neoplastic therapy we aimed at translating our main hypothesis in more complex *in vitro* and *in vivo* cancer models that mimic the main features of solid tumors. In this regard, the potency of the most promising analogues and their cytotoxicity was established in 3D-derived tumor spheroids and *in vivo* whole organism namely *Drosophila melanogaster* cancer model.

EXPERIMENTAL PROCEDURES

Chemical synthesis and stability analyses on αKGlogues

Aiming to increase the permeability of exogenous αKG through the plasma membrane and thus achieve cytoplasmic accumulation of the metabolite, αKG was conjugated to chemical carriers of different hydrophobic indexes thereby generating monoester analogues (αKGlogues). The panel of 7 αKGlogues were synthetized as following: the appropriate halo-derivative was added (1.1 eq) to a solution of α-ketoglutaric acid (10 mmol) and dicyclohexylamine (1.2 eq) in dimethyl formamide (50 mL), and the solution was heated at 50°C for 5-16h. The mixture was concentrated under reduced pressure, the residue was resuspended in dichloromethane (100 ml) then washed with 0.5 N aqueous hydrochloric acid (50 mL). The organic layer was dried (sodium sulfate), and the solvent was removed under reduced pressure. The crude products were purified by flash column chromatography (petroleum ether/acetone, in various proportions), or by crystallization from acetone, ethanol, ethyl acetate or petroleum ether. The structures of the final compounds were confirmed by means of ^{1}H-NMR spectra. The ^{1}H-NMR spectra were recorded on a Varian MR 400 MHz (ATB PFG probe) (Data not shown). Following chemical synthesis (Figure 6) and purity assessment using NMR technology, compounds were dissolved in 100% ethanol or in a 1:1 mixture of ethanol:DMSO (αKG-PP) then stored at -20°C. In their organic solvent the panel of αKGlogues displayed overall good stability levels, and only traces of degradation products were detected by thin layer chromatography (TLC) (Figure 7A) and quantitative mass spectrometric analysis revealed the esterified form of the compounds was prevalent to more than 99% (Figure 7B). Likewise, αKGlogues were stable up to 80% in tissue culture media reflecting minor basal hydrolysis and further confirming the compounds stability in aqueous solution (Figure 7C).

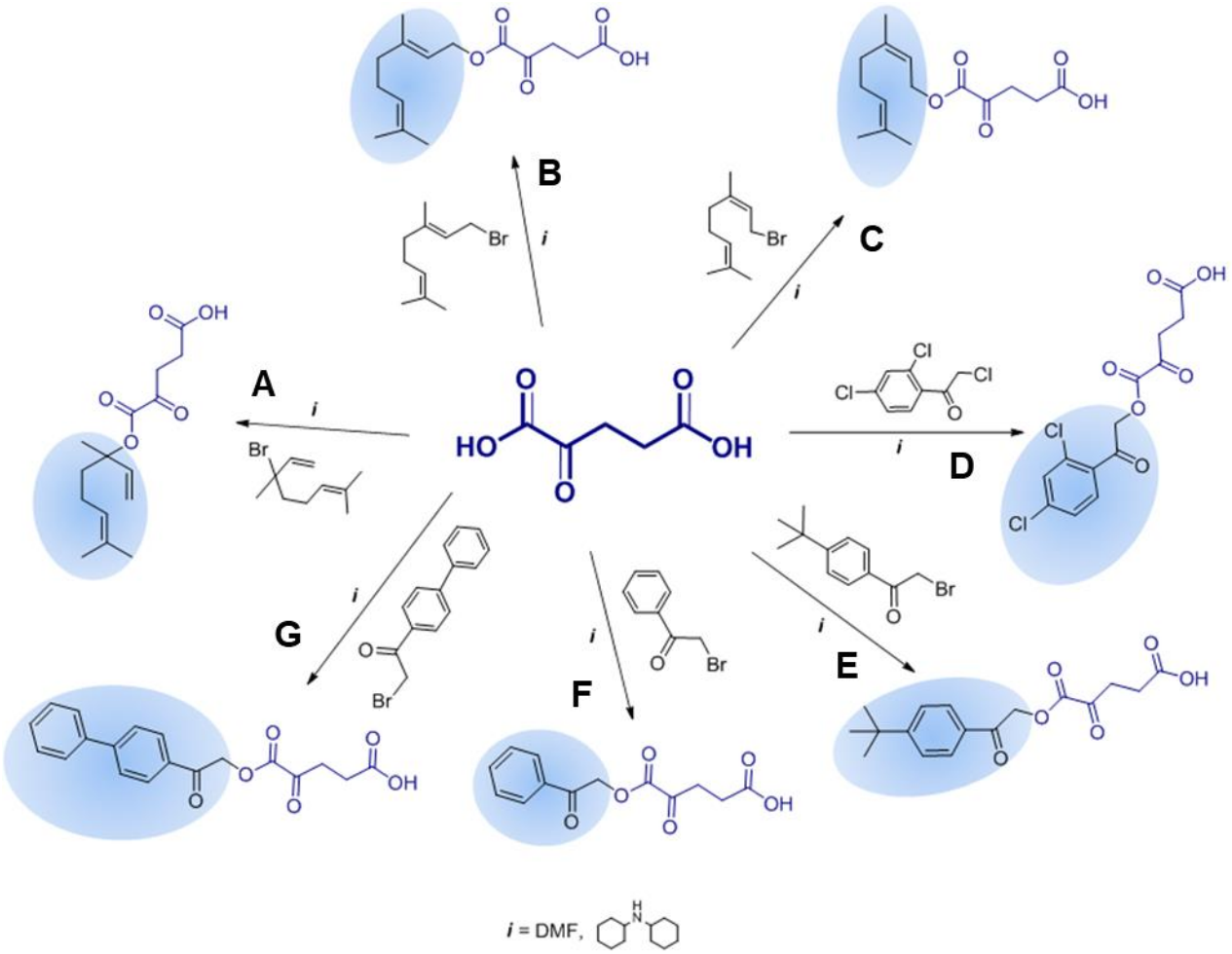

Figure 6: **Schematic representation of αKGlogues chemical synthesis.** Free αKG was coupled to structurally distinct hydrophobic carriers thereby giving rise to monoester analogues of αKG: αKG-L **(A)**, αKG-G **(B)**, αKG-N **(C)**, αKG-Cl **(D)**, αKG-tB **(E)**, αKG-P **(F)** and αKG-PP **(G)** with the aim to enhance the metabolite membrane permeability.

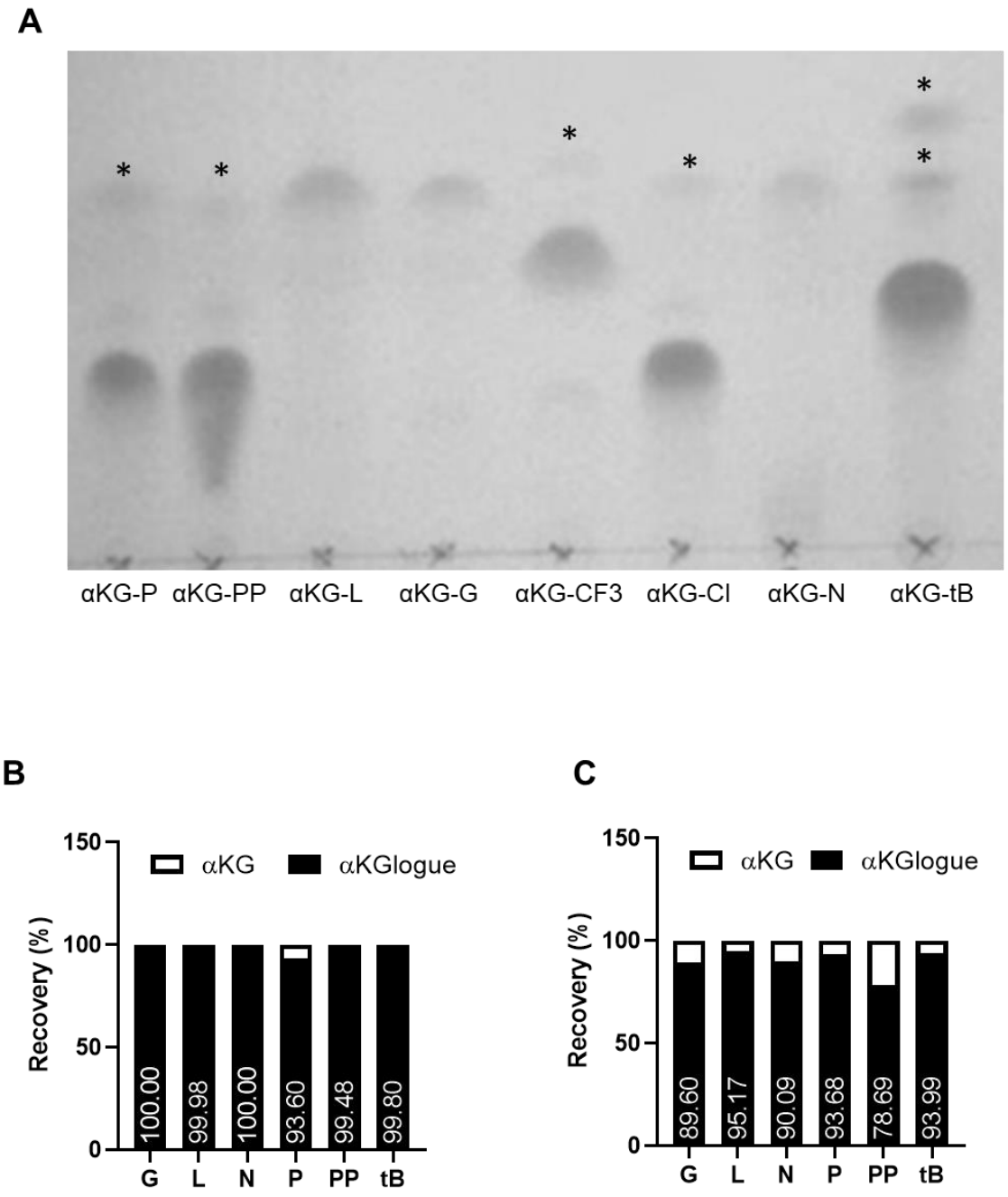

Figure 7: **αKGlogues stability in organic solvent and in aqueous solution. (A)** Thin layer chromatography showing mere traces of degradation of αKGlogues in organic solvent (marked with asterisks*). **(B)** αKGlogues quantitative stability data as assessed by mass spectrometric analysis respectively in organic solvent and in cell growth media unsupplemented with FBS **(C)**.

Cell culture

The cellular models used in this study, namely primary human follicular thyroid cells (N-Thy 3.1) and thyroid papillary carcinoma cells (TPC-1) were cultured in RPMI 1640 (Gibco, #21875091) while normal proximal tubule cells (HK-2) and human kidney carcinoma cells (UOK-257) of an individual with Birt-Hogg-Dubé syndrome (BHD) (Yang et al., 2008) were cultured in Dulbecco's modified Eagle medium (DMEM) high glucose media (Gibco, #21969035). Growth medias were supplemented with 10% heat-inactivated Fetal Bovine serum (FBS) (Gibco, #16000044), 100 units/mL Penicillin/100µg/mL Streptomycin (Gibco, #15140122) and 2mM L-glutamine (Gibco, #25030024). Cells were tested on a regular basis through PCR for mycoplasma detection. Where indicated, cells were exposed to 2mM of commercial αKG-DM (Sigma-Aldrich, #349631). Deferoxamine (DFO) (Novartis, #A020417022) was used at 150µM for 24h as a positive control for PHDs inhibition.

HIF-TM transduction

A non-degradable version of HIF-1α was produced as previously described (Kurelac et al., 2019) by site directed mutagenesis of residues P402A, P564G, and N803A, HIF-targeted sites for hydroxylation by prolyl hydroxylases (PHDs) and Factor inhibiting HIF (FIH1), respectively using Quickchange Site-Directed Mutagenesis kit (Agilent, #200518). Triple-mutant HIF1A (TM-HIF) sequence was priorly transferred onto pMSCV-puro-Retroviral vector (Clontech, #PT3303-5), after which the empty vector and the vector containing HIF-TM were used to transduce TPC-1 and UOK-257 cells by following phxA transduction protocol (Takara, #631317). Cells carrying the vectors were selected with 750 ng/mL puromycin (Sigma-Aldrich, #P8833) and maintained in medium supplemented with 250 ng/mL puromycin. Clonal selection was performed to identify the clones with the highest HIF-TM protein levels in normoxia (21% O_2) and pools of at least 3 clones were made for each cell line.

SDS-PAGE & western-blotting

Where indicated and post-hypoxia exposure in presence of either 200µM unconjugated αKG, αKGlogues or PP carrier, cells were harvested and lysed in RIPA buffer (Tris-HCl 50mM pH 7.4, 1% Triton X-100, 0.1% SDS, 1mM EDTA pH 7, 150mM NaCl) supplemented with a 1X

phosphatases inhibitors (Alfa Aesar, #J63907) and 1X proteases inhibitors (Roche, #4693116001). Proteins were quantified with the Bradford method using BSA as a standard, denatured for 5 minutes at 95°C in Laemmli buffer, then loaded (30-40 µg) onto polyacrylamide gels (SDS-PAGE) and separated in a Mini-PROTEAN® Electrophoresis cell (Bio-Rad). Samples were subsequently transferred in full-wet system (Mini Trans-Blot® Cell, Bio-Rad) onto nitrocellulose membranes (Bio-Rad, #1620115), or Polyvinylidene floride (PVDF) (Bio-Rad, #1620177) for HIF-1α immunoblotting. Following 1h of blocking in 5% non-fat dry milk, 1X TBS (Tris Buffered Saline)-0.05% Tween® 20 (Sigma-Aldrich, #P1379), membranes were incubated overnight at +4°C with primary antibodies: anti-β-Actin (Sigma-Aldrich, #SAB5500001) 1:5000, anti-HIF-1α (GeneTex, #GTX127309) 1:2000; phospho-mTOR (S2448) (Cell Signaling Technology, #5536S) 1:1000; Phospho-Raptor (Ser792) (Cell Signaling Technology, #2083S) 1:1000; Phospho-p70S6K (S371) (Cell Signaling Technology, #9208S) 1:1000; Phospho-4E-BP1 (Thr37/46) (Cell Signaling Technology, 2855T) 1:1000. Anti-GAPDH (Sigma-Aldrich, #G8795) 1:10,000; anti-LC-3 (Sigma-Aldrich, #L7543) 1:1000; Total mTOR (Cell Signaling Technology #2983S) 1:1000; Total Raptor (Cell Signaling Technology, #2280S) 1:1000; Total p70S6K (Cell Signaling Technology, #2708S) 1:1000; were incubated for 2h at room temperature (RT). Horseradish-peroxide-conjugated secondary antibodies (Jackson ImmunoResearch Laboratories, anti-rabbit #111-035-144, anti-mouse #115-035-146) were incubated at RT and proteins developed using Clarity^{TM} Western ECL Substrate (Bio-Rad, #1705061). Images were acquired with Gel Logic 1500 Imaging system (Kodak, Ronchester, NY, USA). Densitometric quantification of the analysed proteins was performed using ImageJ software (NIH Image).

Cell viability

Cells were counted and plated (1 x 10^3 cells/well for cancer cell models and 2 x 10^3 cells/well for non-cancer counterparts) in 96-wells TC-treated plates (Falcon® 96 well, #353072) and left to adhere overnight. Subsequently, fresh media containing treatment (2µM, 20µM and 200µM αKGlogues or corresponding carriers) was added and cells incubated at 37°C in standard conditions (21% O_2 and 5% CO_2). Experiments carried out under low oxygen tension (1% O_2, 5% CO_2) were performed in a hypoxic workstation (Ruskinn INVIVO$_2$ 300). Cell viability was assessed after 0, 24, 48 and 72h of treatment using sulforhodamine B

(SRB) viability assay. Briefly, at the indicated time points, cells were fixed with 50% trichloroactic acid (TCA) (Sigma-Aldrich, #T6399), then colored with SRB (Sigma-Aldrich, #S1402) which reflects intracellular protein content (Vichai and Kirtikara 2006). SRB is an aminoxanthene dye bearing two sulfonic groups which bind to basic amino acids under mild acidic conditions and dissociate in basic conditions. Following a 30-minutes staining step and several washes in 1% acetic acid, SRB was solubilized in 10mM Tris-HCl pH 10.4 and absorbance measured at 560 nm using microplate reader VICTOR3^{TM} (PerkinElmer, Turku, Finland). Cell viability data were expressed as percentage of cell growth with respect to time 0.

Colony forming assay (clonogenic assay)

Cells were seeded at a density of 250cell/well in 6-well plates. 24h post-seeding, treatment (200µM αKGLogues, PP carrier or vehicle) was added and cells incubated at 37°C in low oxygen tension (1% O_2, 5% CO_2, Ruskinn INVIVO$_2$ 300 Hypoxia workstation) for 7 days. Cells were then fixed with 50% TCA and the number of colonies counted. To evaluate protein content, colonies were stained with SRB dye after which absorbance reflecting colony size, was measured as described above.

Cell migration (wound-healing assay)

40-50 x 10^3 cell/well were plated onto Incucyte® ImageLock 96-well plates (Sartorius, #4379) to reach sub-confluency. The subsequent day, a homogenous wound was realized in all wells using Incucyte® WoundMaker (Sortorius), initial media discarded, and cell monolayers washed once with Phosphate Buffer Saline (PBS) after which treatment was added. Cells were then incubated at 37°C with a fresh growth media supplemented with 1% FBS containing either vehicle or treatment (200µM αKG-tB, αKG-PP or PP carrier). Wound confluence was monitored every hour for 24h using the Incucyte® S3 Live cell Analysis System (Sartorius) in O_2 and CO_2 monitored conditions (21% O_2 and 5% CO_2).

LC-MS metabolomics analyses

For the purpose of this experiment, 5 x 10^5 cells were plated in 6-well plates and kept at 37°C in controlled O_2 and CO_2 conditions. 24h later, initial media was replaced, and respective treatments added, namely 200µM αKG-PP alone or in combination with 3-methyl, 2-oxovaleric acid (KMV, 2mM) (Sigma-Aldrich, #K7125), an αKG dehydrogenase complex (αKGDHC) inhibitor that was used as a positive control to induce endogenous accumulation of αKG. Consequently, 1- and 3-hours post-treatment in high oxygen tension (21% O_2), cells were counted and accordingly metabolites extracted with an appropriate volume of ice-cold extraction solution composed of 50% methanol, 30% acetonitrile, 20% ultra-pure H_2O and 5µM d8-Valine as an internal standard. Briefly, following 3 washes in PBS, extraction solution was added (1mL/million cells) and cells incubated on dry ice for 15 minutes. Cells were then scraped, collected in tubes, kept under agitation for 15 minutes at +4°C then incubated at -20°C for 1h. Finally, samples were centrifuged for 10 minutes at 16,000 rpm at +4°C and supernatants collected to be analyzed. Liquid chromatography-mass spectrometry (LC-MS) analyses were performed using an QExactive Orbitrap mass spectrometer (Thermofisher Scientific) as previously described (Sciacovelli et al., 2016). To determine αKG intracellular concentration, standard curves were realized with commercial αKG-DM (Sigma-Aldrich, #349631) and data were normalized to mean cell volume.

Nuclear morphology assessment

30 x 10^3 cells were plated on glass slides (15x15mm) and left overnight, after which initial growth media was replaced with a fresh one containing vehicle, 200µM αKG-PP or PP carrier. 72h post-treatment in high oxygen tension (21% O_2), cells were fixed for 15 minutes in 4% formaldehyde, subsequently washed 3 times in PBS then incubated with DAPI (1µg/mL) for 10 minutes. Following another 3 washes in PBS, slides were mounted using a 50% glycerol solution. Nuclei morphology upon treatment was then analyzed and images captured with an epi-fluorescence microscope (Nikon 90i wide field fluorescence microscope).

Flow cytometric analysis of apoptotic cell death

24h-post seeding, cells were incubated with treatment (vehicle, 200µM αKG-PP or PP carrier) and kept in culture under high oxygen tension (21% O_2, 5% CO_2). 72h after treatment initiation, cells were harvested, counted, washed twice in PBS and centrifuged 5 minutes at 300 *xg*. Cell pellets were then resuspended in provided binding buffer and the prepared cell suspensions co-stained with Annexin V (AV)/Propidium iodide (PI) for 20 minutes following manufacturer's instructions (Annexin V Apoptosis Kit [FITC]) (Novus, #NBP2-29373) after which flowcytometric analysis was performed using an S3 cell sorter (Bio-Rad).

β-galactosidase-associated senescence assay

8 x 10^3 cells were plated onto 24-well plates and treatment (200µM of αKG-PP or PP carrier) added the subsequent day, after which cells were incubated at 37°C in controlled O_2 and CO_2 conditions (21% and 5%, respectively). At experiment endpoint (72h), treatment-containing media was removed, and cells washed once in PBS then fixed for 15 minutes with the provided fixative solution (Senescence Detection Kit, Abnova, #KA0899). After two washes in PBS, cells were stained overnight at 37°C with a staining solution according to manufacturer's instructions for the detection of senescence-associated β-galactosidase activity. Images were captured using a light microscope.

Multicellular cancer-derived spheroids

To generate cancer-derived spheroids, kidney and thyroid cancer cells were seeded in 96-well Ultra Low Attachment plates (Corning, # CLS3474) in a mix of appropriate tissue culture media and 2.5% (v/v) basement membrane extract (Geltrex™) (Thermofisher, #A1413202) to mimic extracellular matrix. Cells were then centrifuged at 130 *xg* for 10 minutes at RT and incubated at 37°C for 72h to allow cell aggregation and formation of homogenously sized single spheroids (Figure 8) after which αKGlogues treatment was initiated. Cytotoxicity induced by αKGlogues and positive control (200nM staurosporine) was evaluated using Promega's CytoTox-Glo™ bioluminescence assay (Promega, #G9291) according to manufacturer's instructions. In addition, 3-(4,5-dimethylthiazol-2-yl)-2,5-diphenyltetrazolium bromide (MTT) assay was used as a complementary method to determine residual live cells in 3D models. Upon treatment with αKG-PP, kidney-derived cancer spheroids were harvested

and stained with MTT dye for 4 hours at 37°C. Exceeding dye was subsequently eliminated and reduced MTT accumulated inside the cells was dissolved in DMSO. Finally, MTT absorbance reflecting metabolically active cells was measured at 560 nm using microplate reader VICTOR3^{TM} (PerkinElmer, Turku, Finland). Spheroids size was determined using ImageJ free software (NIH).

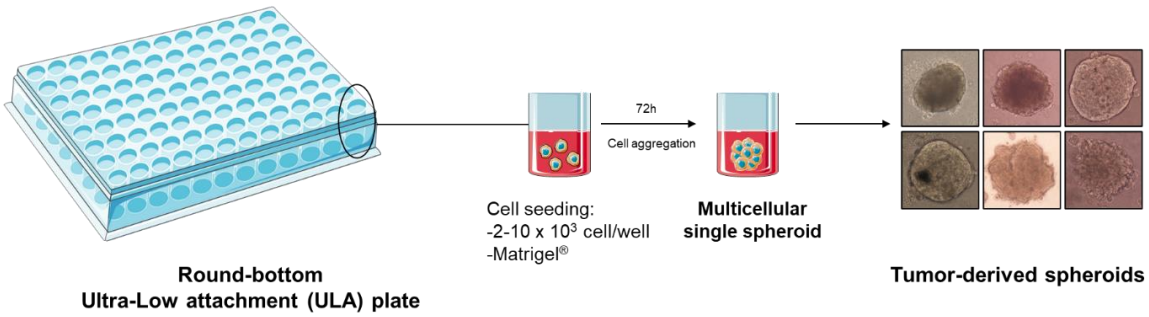

Figure 8: Generation of multicellular single spheroids as *in vitro* 3D cancer models. Cancer cells seeding in a mixture of growth media and basement membrane extract (Matrigel®) allows the formation of homogenously sized single spheroids in 96-well plates in order to test αKGlogues antiproliferative capacity. Servier Medical Art templates (https://smart.servier.com/) were used to generate this figure.

Drosophila imaginal wing discs as tumor model

Drosophila imaginal wing discs are the larval primordium of adult fly wing. They are composed of pseudo-stratified columnar epithelium morphologically and biochemically comparable to mammalian epithelia (Wodarz and Näthke 2007) and represent a good model for proliferation studies. During larval development, the imaginal wing discs are subdivided by the anterior-posterior border (A/P) into a posterior (P) and anterior (A) compartment while the dorsal-ventral border divides the disc into a dorsal and a ventral compartment. The dorsal and ventral compartments are determined by Apterous (Ap) expression in the dorsal compartment of the organs (Butler et al., 2003).

To induce tumor growth in wing discs, UAS-Gal4 genetic system was used (Brand and Perrimon, 1993). The two components of this system are the yeast transcriptional factor Gal4 and its specific Upstream Activating Sequences (UAS). The driver line contains the Gal4 sequence under the control of a specific promoter which permits its expression in specific tissues. The responder line, instead, contains the UAS sequence upstream of a specific

transgene. The two lines are crossed, and transcription is activated in the progeny. In the used model, the contemporary *lethal giant larvae* knockdown (*lgl*^{KD}), an evolutionary preserved polarity gene, and Ras^{V12} mutation under the control of *apterous (ap)* promoter were induced to mimic an oncogenic cooperation mechanism. *lgl*^{KD} and Ras^{V12} expression in the dorsal compartment of the wing discs (in green in Figure 9) allows an unrestrained larval organ overgrowth and a complete altered loss of tissue architecture (Figure 9B) with respect to the wild-type counterpart (Figure 9A). The larval development of ap-*lgl*^{KD}, Ras^{V12} individuals lasts 8-9 days unlike wild-type larvae which take 5 days to complete the larval stages at 25°C. ap-*lgl*^{KD}, Ras^{V12} larvae die at pre-pupa stadium showing wing discs with tumor dorsal compartment filling the entire organs (Figure 9B). To boost the tumor phenotype the experiments was performed at 29°C.

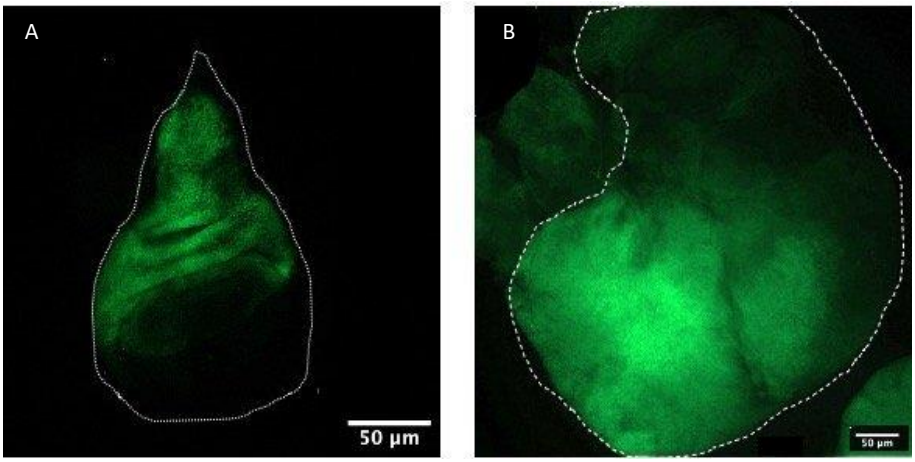

Figure 9: *Drosophila* epithelial tumor model. Wild-type **(A;** ap-GFP) and tumor **(B**; ap-GFP, *lgl*^{KD}, Ras^{V12}) imaginal wing discs. The dorsal compartments are marked in green (GFP^{+}). The wing disc structures are highlighted by a dotted line. Magnification is 400X.

Fly manipulation and volume analysis

6 days after egg laying (AEL), tumor larvae were selected and divided into two groups of 25 individuals each: a control and a treated group which received vehicle and 200µM αKG-PP, respectively. 2 days after the treatment, the wing discs were isolated, photographed, and minor and major axes were measured using ImageJ free software (NIH). For volume calculation the disc shape has been approximated to a spheroid with width=depth.

Statistical analysis

GraphPad Prism 8.0 was used to perform statistical analyses and graphs generation. One-way ANOVA was performed for multiple comparison of HIF-1α/β-Actin densitometric quantification as well as of clonogenic assay data. Two-way ANOVA was performed to analyze cell viability experiments and compounds efficacy. Finally, an unpaired t-test was performed to compare two groups unless stated otherwise. Statistical significance was considered for a *p*-value $p \leq 0.05$.

RESULTS

Selected αKGlogues are able to prevent HIF-1α stabilization in hypoxia

We previously demonstrated that increased levels of intracellular αKG in respiratory complex I defective models are associated with reduced HIF-1α stabilization in hypoxia (Kurelac et al., 2019). Thus, we hypothesize that such condition, termed *pseudonormoxia*, can be obtained through the supplementation of αKG to cells. However, because of its low hydrophobicity, αKG is poorly permeable through the plasma membrane and we pursued the strategy of conjugating the metabolite with hydrophobic substituents to improve its permeability. To investigate the ability of cell permeable αKGlogues to induce a pseudonormoxic state, HIF-1α protein levels in hypoxia (1% O_2) were analysed in thyroid papillary carcinoma (TPC-1) and kidney carcinoma (UOK-257) cells upon incubation with 7 different αKGlogues. Commercial αKG-DM was used as a reference for compound's effectiveness. HIF-1α levels assessed by immunoblotting, revealed that at the dose of 200μM, αKGlogues displayed different effects on HIF-1α protein stabilisation in hypoxia (Figure 10) after 60 and 90 minutes of treatment. In TPC-1 cells, analogues αKG-G, αKG-N, αKG-L, αKG-tB and αKG-Cl significantly reduced HIF-1α destabilisation after 60 and 90 minutes of incubation in hypoxia with respect to the untreated cells (Figure 10A-C). However, among these compounds only αKG-N and αKG-Cl were more effective than commercially available αKG-DM (Figure 10A-C). By contrast, αKG-P and αKG-PP showed a paradoxical effect, by increasing HIF-1α protein levels after 90 minutes of treatment (Figure 10A-C). In UOK-257 cells, αKG-PP stood out as the most potent compound, being able to significantly reduce HIF expression after 60 minutes with respect to control and maintain this effect up to 90 minutes (Figure 10D-F). Interestingly, while the impact of 200μM of αKG-G and αKG-Cl was noted only after 90 minutes of treatment in hypoxia, the effect of αKG-N and αKG-P was transient, since they were effective after 60 minutes in destabilizing HIF-1α, but the levels of the protein increased again after 90 minutes of incubation (Figure 10D-F). However, αKG-PP, αKG-G and αKG-Cl were all more effective than αKG-DM, which in turn seemed to not significantly affect on HIF-1α levels (Figure 10D-F). We tested the effect of such compounds also in non-cancer models derived from the same tissue, namely N-Thy 3.1 for thyroid and HK-2 for kidney. Overall, αKGlogues did not impair HIF stabilisation in the healthy thyroid cells up to 90 min of exposure in hypoxia, with the exception of αKG-L and αKG-Cl which showed a transient slight reduction of HIF-1α abundance at 60 minutes (Figure 11A-C). Similarly, in the healthy kidney counterpart, most compounds had no effect on HIF-1α destabilisation for the duration of treatment, with the only remarkable exception of 60

minutes of exposure to αKG-PP that induced a transient reduction in HIF-1α levels (Figure 11D-F).

Hence, from the first phase of screening, the most potent compounds limiting HIF-1α accumulation in hypoxia were selected for further investigation, namely αKG-N, αKG-L, αKG-Cl and αKG-tB on thyroid cancer cells and αKG-G, αKG-N, αKG-Cl, αKG-P and αKG-PP on the kidney cancer cells.

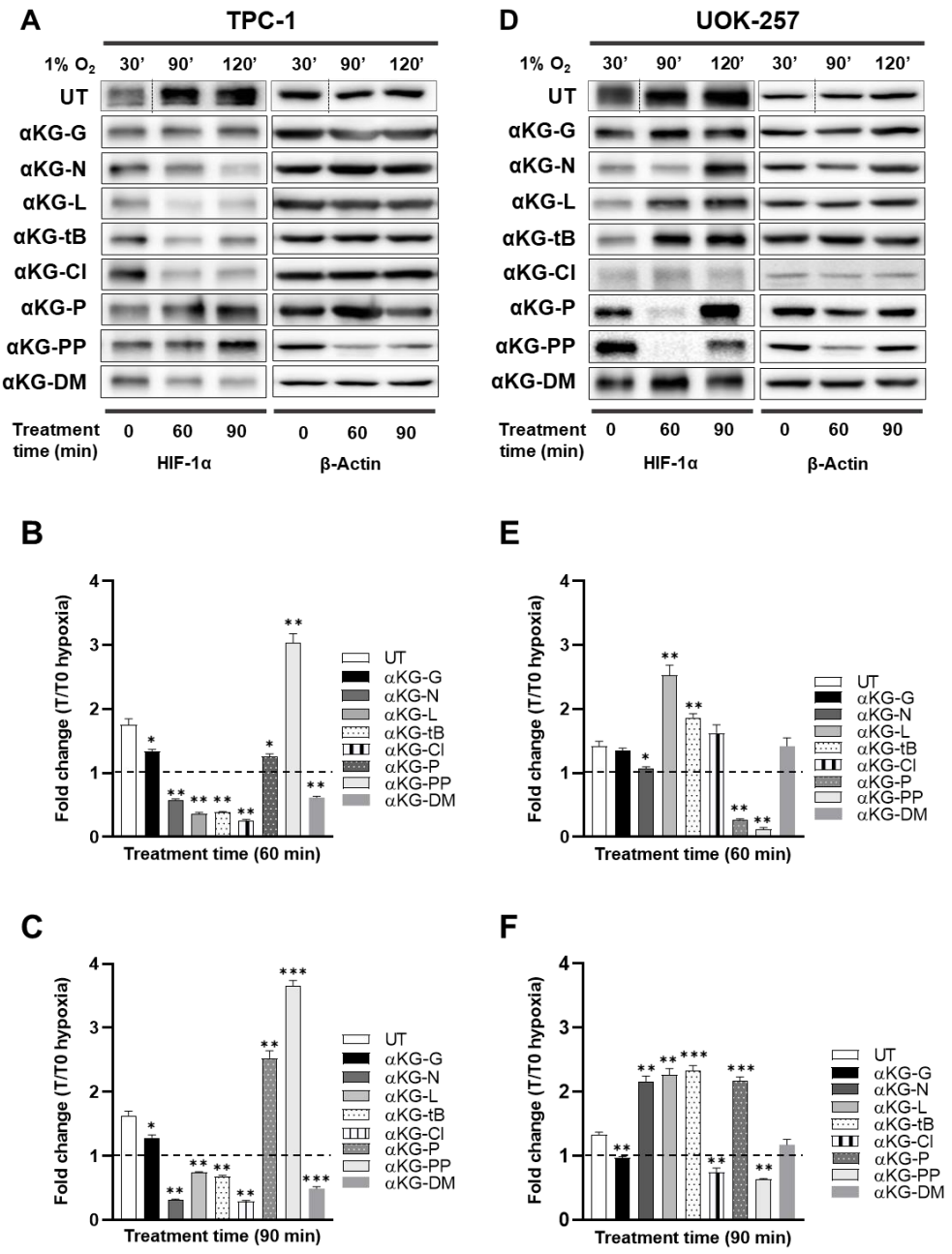

Figure 10: **HIF-1α expression in cancer cell models treated with αKGlogues panel under low oxygen tension reveals promising compounds.** Western blot and related densitometric analysis of HIF-1α levels in TPC-1 **(A-C)** and UOK-257 **(D-F)** cells at 60- and 90-minutes post-treatment with 200µM αKGlogues in hypoxia (1% O_2). β-Actin was used as a loading control. Data (mean ± SD) are expressed as HIF-1α/β-Actin ratio calculated at treatment time (T) and normalised on their respective untreated counterpart at T0 (30 minutes of hypoxia baseline) (n=3). A one-way ANOVA was performed for statical analysis. *$p \leq 0.05$, **$p \leq 0.01$, ***$p \leq 0.001$

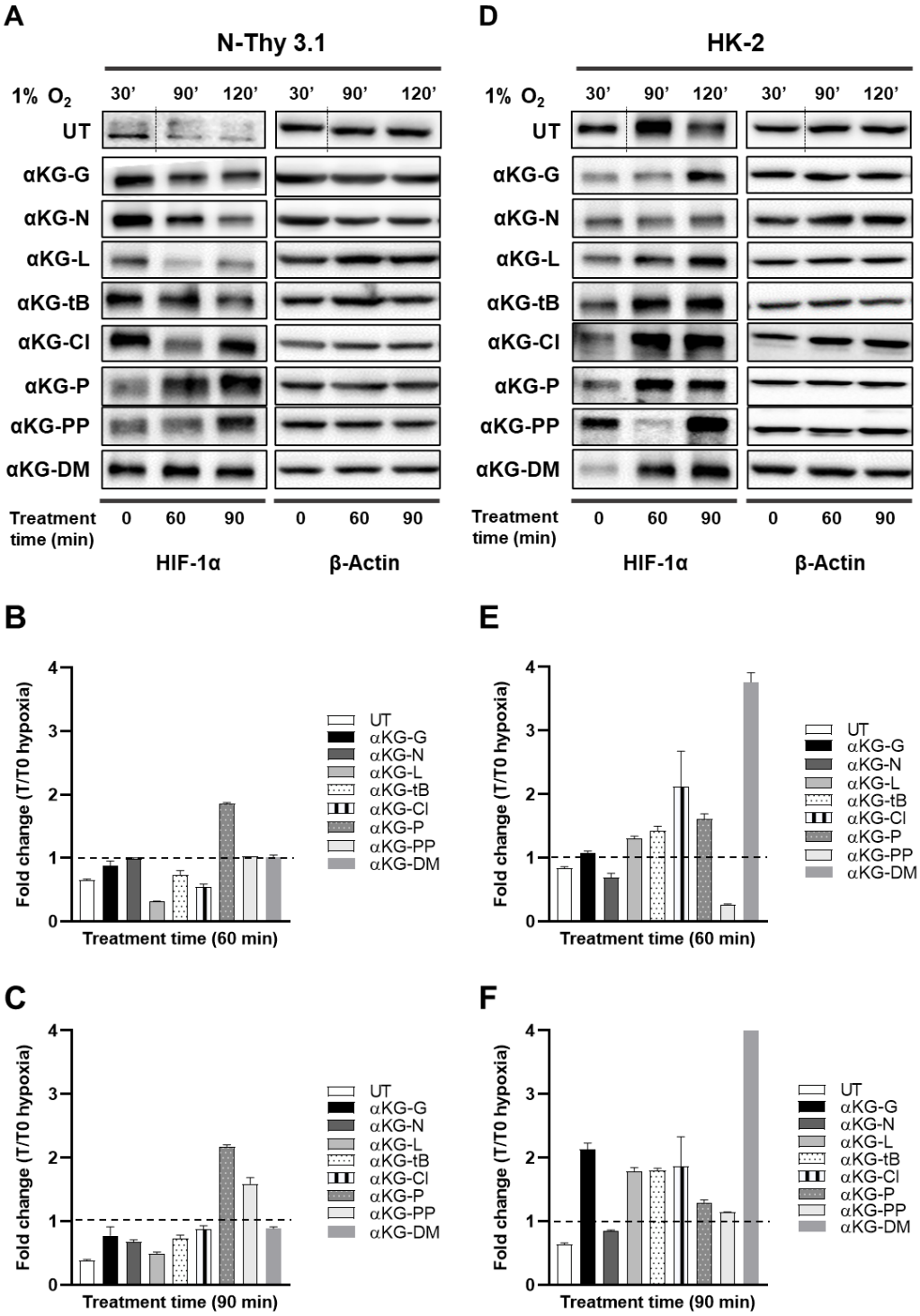

Figure 11: **HIF-1α levels in non-cancer epithelial cells are not influenced by treatment with αKGlogues.** Western blot and related densitometric analysis of HIF-1α levels in N-Thy 3.1 **(A-C)** and HK-2 **(D-F)** cells at 60- and 90-minutes post-treatment with 200μM αKGlogues in hypoxia (1% O_2). β-Actin was used as a loading control. Data (mean ± SD) are expressed as HIF-1 α/β-Actin ratio calculated at treatment time (T) and normalised on their respective untreated counterpart at T0 (30 minutes of hypoxia baseline) (n=2).

αKGlogues specifically alter cancer cells growth and *in vitro* tumorigenic properties

After establishing αKGlogues block HIF-1α stabilisation in hypoxia at a dose of 200μM in our cancer cell models, the most effective compounds selected were then tested for their ability to alter cancer cell growth *in vitro*. Hence, in the presence of increasing concentrations of compounds, the growth of thyroid and renal cancer cells was determined along with their non-cancer counterparts, namely TPC-1/N-Thy 3.1 and UOK-257/HK-2, respectively. Cell viability following treatment was evaluated after 24, 48 and 72h of incubation using the SRB assay both in hypoxia (1% O_2) and normoxia (21% O_2). Despite the significant reduction of HIF-1α levels in hypoxic conditions, αKG-N did not affect the growth of TPC-1 cells after 72h neither in hypoxia nor in normoxia even at the highest dose (200μM) (Figure 12A-B). Likewise, αKG-L was ineffective at lower doses both in hypoxia and normoxia, even if at 200μM the analogue slightly delayed the growth of TPC-1 cells after 3 days in hypoxia (Figure 12C-D). These two compounds resulted ineffective in the non-cancer counterpart N-Thy 3.1 (Figure 13A-D). Conversely, αKG-Cl induced a dose- and time-dependent restriction of TPC-1 cell growth (Figure 12E-F). In particular, 200μM of αKG-Cl was able to completely block the growth of TPC-1 cells already after 24h of treatment both under hypoxic (1% O_2) and normoxic conditions (21% O_2), while at lower doses this compound resulted more effective in hypoxia. Similarly, 20μM αKG-Cl displayed an early severe effect after 24 and 48 hours of incubation of N-Thy 3.1 cells, while high doses of the compound drastically altered their proliferation (Figure 13E-F). Low doses (2 and 20μM) of αKG-tB provoked a mild reduction of TPC-1 cell growth after 72h in low and high oxygen tension, while high doses (200μM) displayed a strong alteration on cells growth already after 24h of treatment independently of oxygen level (Figure 12G-H). Conversely, N-Thy 3.1 cells were not affected by low doses of αKG-tB, and only 200μM of the analogue correlated with a mild growth reduction independently of oxygen conditions as cells maintained their proliferation (Figure 13G-H). To discriminate the effect of the compounds on cancer vs non-cancer cells, compounds efficacy at 72h representing the percentage of dead cells induced by 200μM of treatment was calculated with respect to the untreated control in both cancer and non-cancer cells (Figure 14A-B). This analysis identified αKG-tB as the only compound able to selectively target TPC-1 cells without being deleterious for N-Thy 3.1 cells, as highlighted by a calculated efficacy of 80% in favour of the TPC-1 over N-Thy 3.1 (50%) (Figure 14A-B).

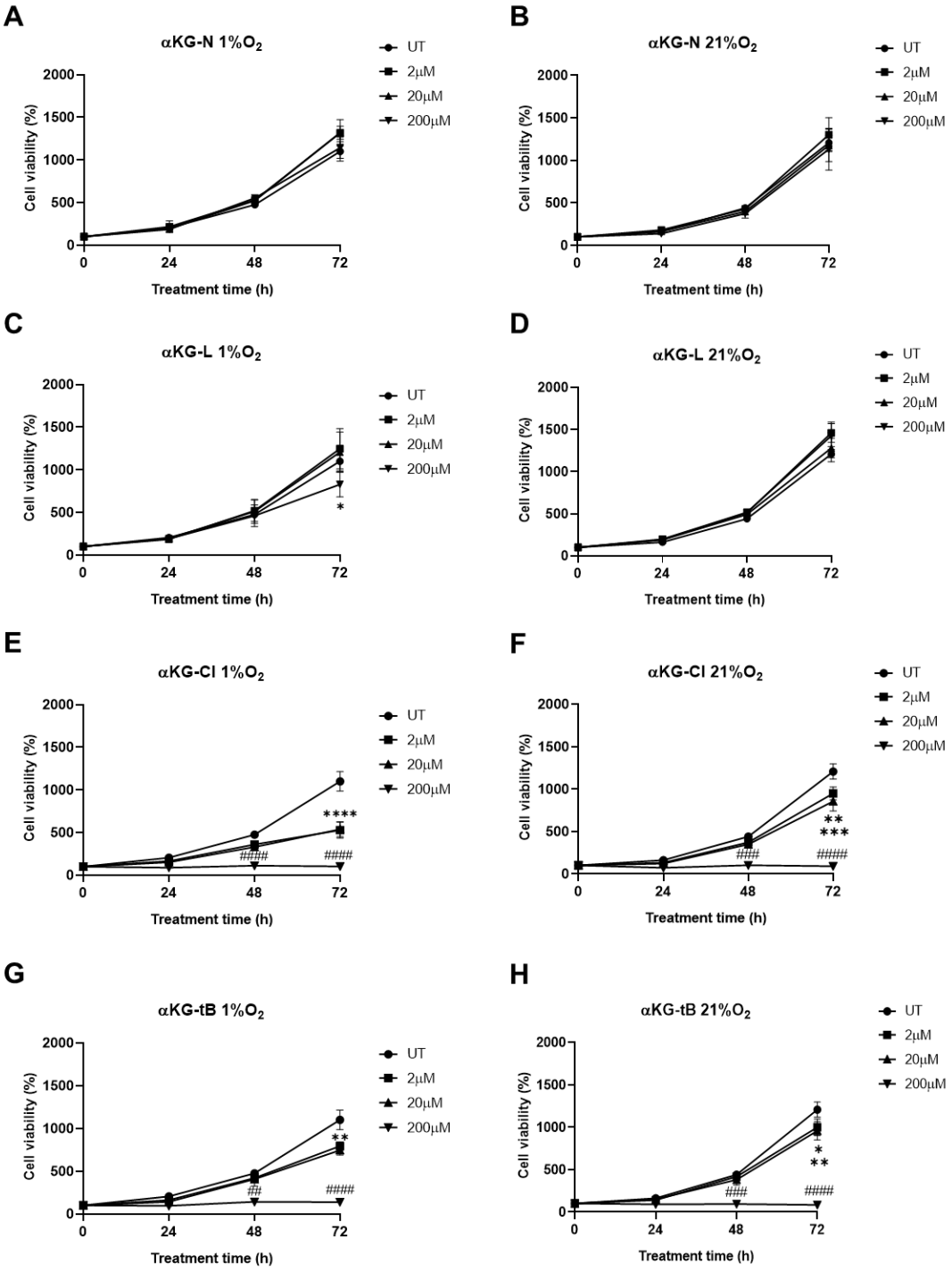

Figure 12: **High doses of αKG-Cl and αKG-tB significantly alter the growth of papillary thyroid carcinoma cells despite of oxygen level.** TPC-1 cell viability was determined by using SRB assay up to 72h of treatment with different doses of αKG-N **(A, B)**, αKG-L **(C, D)**, αKG-Cl **(E, F)**, αKG-tB **(G, H)** respectively in hypoxia (1% O_2) and normoxia (21% O_2). Data (mean ± SE) are expressed as a percentage of cell growth with respect to time 0 considered as 100% (n≥3). *p*-value was calculated with a two-way ANOVA. **p*≤0.05, ***p*≤0.01, ****p*≤0.001, *****p*≤0.0001

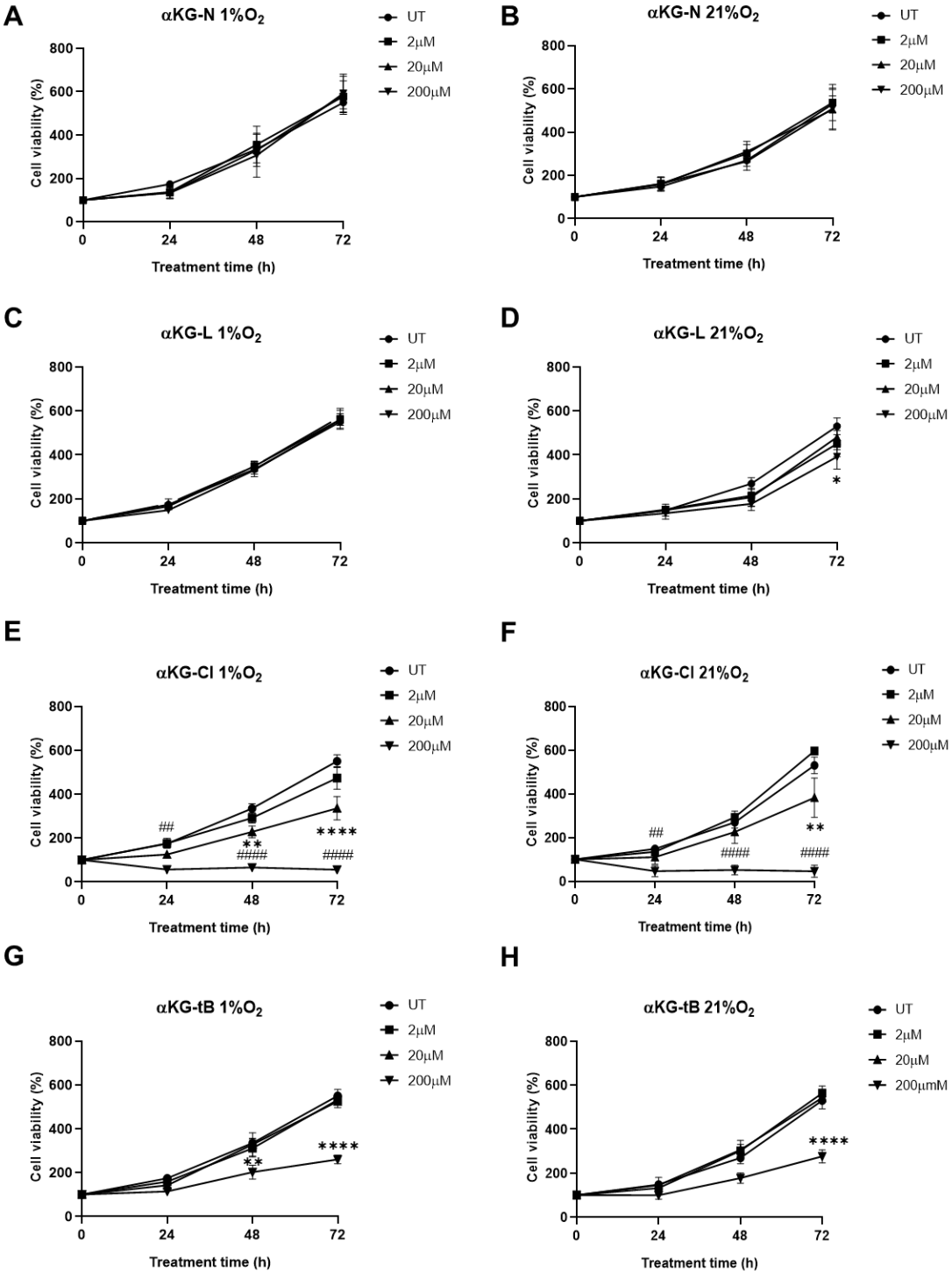

Figure 13: **Proliferation of non-cancer thyroid cells is severely impaired by high doses of αKG-Cl**. N-Thy 3.1 growth rate was determined by using SRB assay up to 72h of treatment with increasing doses of αKG-N **(A, B)**, αKG-L **(C, D)**, αKG-Cl **(E, F)**, αKG-tB **(G, H)** respectively in hypoxia (1% O_2) and normoxia (21% O_2). Data (mean ± SE) are expressed as a percentage of viable cells with respect to time 0 considered as 100% (n≥3). *p*-value was calculated with a two-way ANOVA. *$p \leq 0.05$, **$p \leq 0.01$, ***$p \leq 0.001$, ****$p \leq 0.0001$

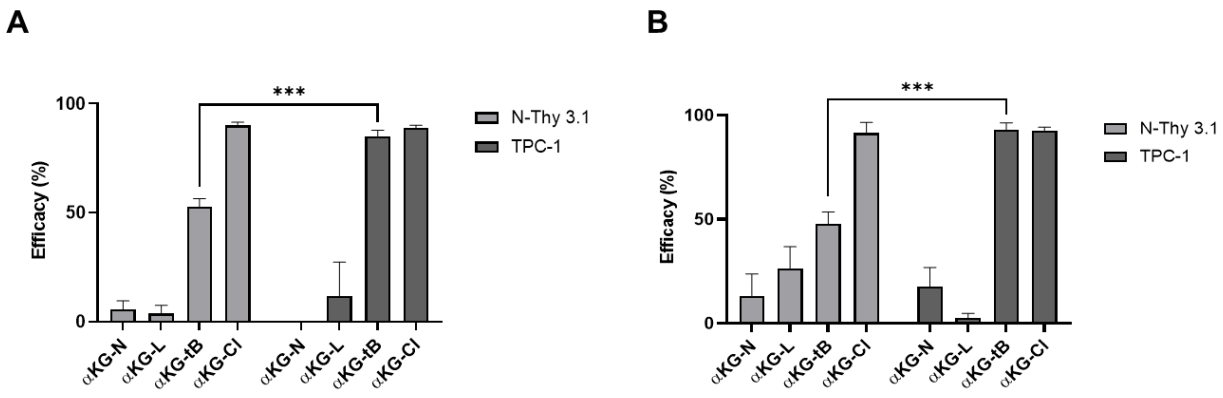

Figure 14: **αKGtB selectively alters the proliferation of papillary thyroid carcinoma cells. (A-B)** Efficacy of selected αKGlogues was determined in thyroid cancer (TPC-1) and non-cancer (N-Thy 3.1) cells under low (1% O_2) **(A)** and high oxygen tension (21% O_2) **(B)**, respectively. Data (mean ± SEM) represent the percentage of dead cells induced by 200µM αKGlogues at 72h calculated with respect to the untreated control for each cell line (n≥3). A two-way ANOVA was used to calculate *p*-value. *$p \leq 0.05$, **$p \leq 0.01$, ***$p \leq 0.001$

With regards to the growth curves of the UOK-257 cells, the kidney carcinoma cells were insensitive to increasing doses of αKG-N, αKG-G and αKG-P up to 200µM either in hypoxia (1% O_2) or normoxia (21% O_2) (Figure 15A-D, G-H) and the three compounds resulted equally non-effective on the proliferation of the epithelial kidney counterparts (Figure 16A-D, G-H). By contrast, αKG-Cl induced a mild yet significant alteration in the growth of UOK-257 cells at low doses (2 and 20µM) 48 and 72h after treatment initiation in hypoxia, while a dose of 200µM caused a severe block in the proliferation of the kidney carcinoma cells during the first 2 days of the treatment in hypoxia to finally induce cell death, an effect that was observed already 24h post-treatment in normoxia (Figure 15E-F). Similarly to αKG-Cl, 2 and 20µM of αKGlogue-PP significantly delayed the proliferation of the UOK-257 cells at day 3 of treatment both in high and low oxygen tension whilst 200µM of compound blocked the growth of the cancer cells and ultimately resulted in a lethal effect at 72h (Figure 15I-J). With regards to the effect of αKG-Cl and αKG-PP on the non-cancer kidney counterpart, HK-2 cells displayed a slightly slowed growth rate after 72h of exposure to low doses of the analogues in hypoxia, and although cells suffered a drop in proliferation with 200µM of αKG-Cl in hypoxic as well as in normoxic conditions (Figure 16E-F), the effect remained relatively harmless as reflected by compound's efficacy (Figure 17A-B). Most importantly, αKG-PP affected the non-cancer renal cells viability to a lesser extent. In fact, it

shows to be more specific on the UOK-257 cells (80%) than on the non-cancer control (50%) in low oxygen levels (Figure 17A-B). Overall, 200µM of αKG-Cl and αKG-PP specifically impaired the growth of the kidney carcinoma cells while displaying safety on the epithelial counterpart (80% vs. 50% of efficacy rate for αKG-Cl and 90% vs. 70% for αKG-PP) (Figure 17A-B).

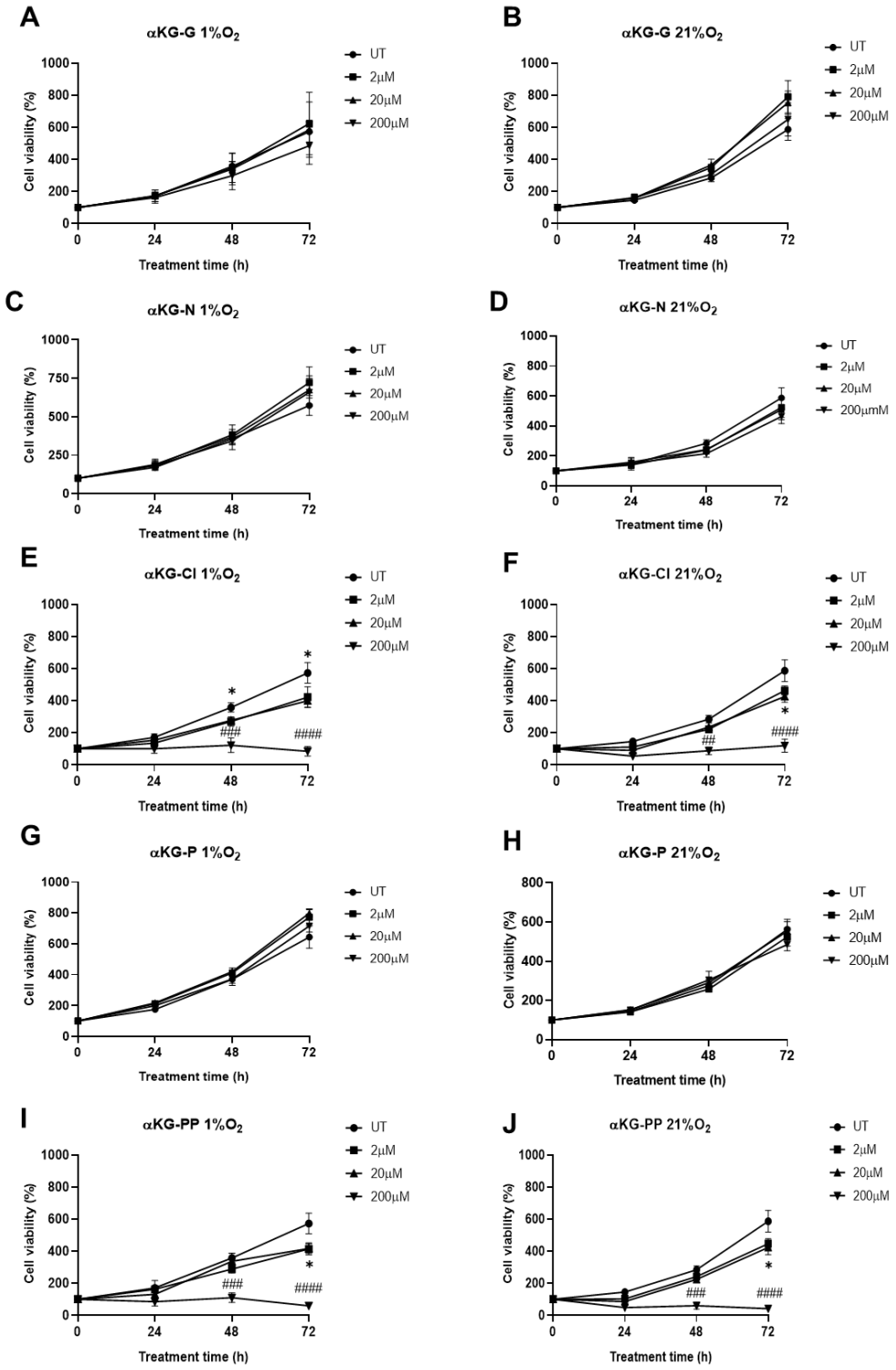

Figure 15: High doses of αKG-Cl and αKG-PP block the growth of kidney carcinoma cells indifferently from oxygen tension. UOK-257 cell viability was determined using SRB assay up to 72h of treatment with growing concentrations of αKGlogues: αKG-G **(A, B)**, αKG-N **(C, D)**, αKG-Cl **(E, F)**, αKG-P **(G, H)** and αKG-PP **(I, J)** respectively in hypoxia (1% O_2) and normoxia (21% O_2). Data (mean ± SE) are expressed as a percentage of viable cells with respect to time 0 considered as 100% (n≥3). *p*-value was calculated using a two-way ANOVA. *$p \leq 0.05$, **$p \leq 0.01$, ***$p \leq 0.001$, ****$p \leq 0.0001$

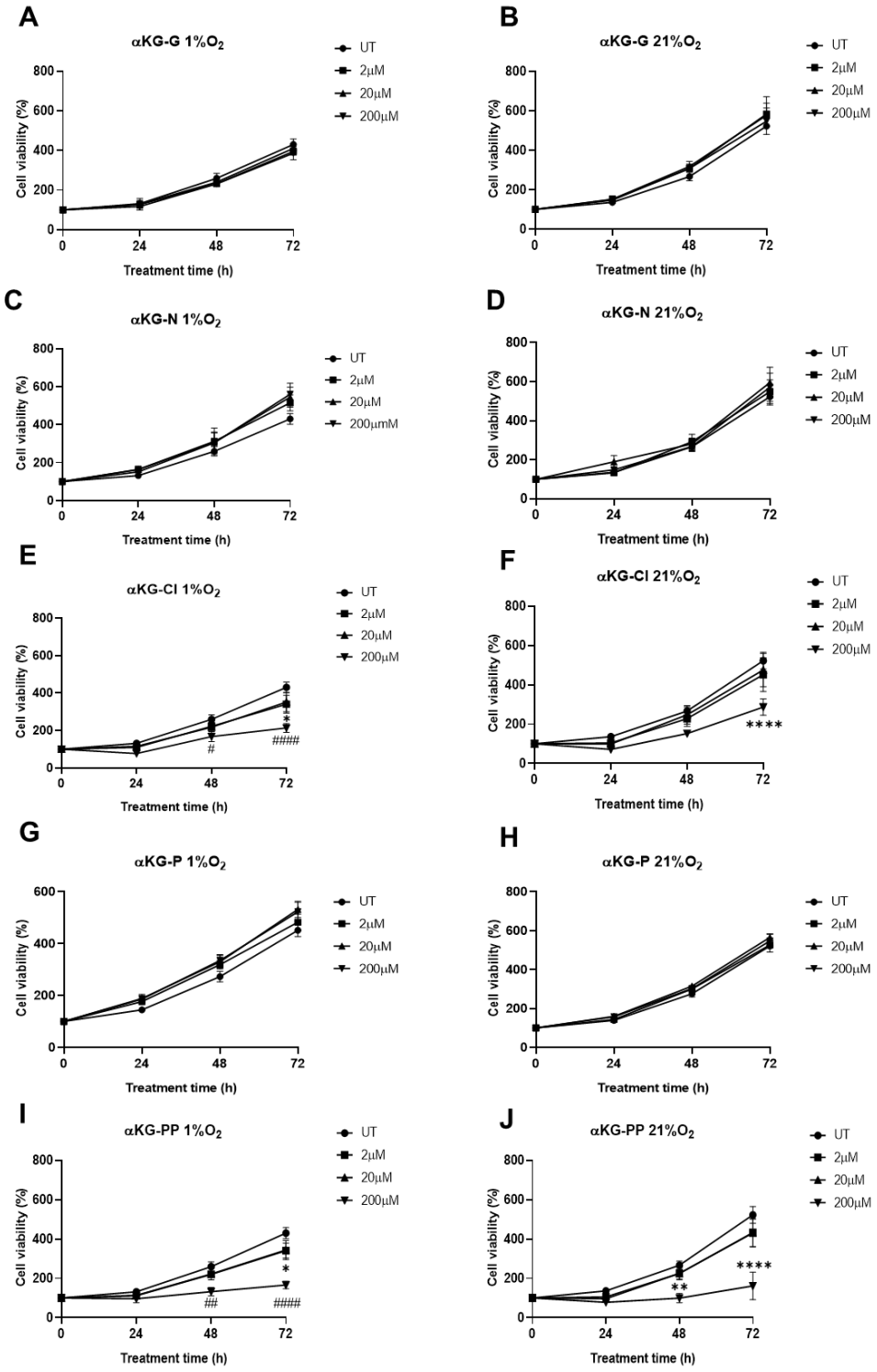

Figure 16: **High doses of αKG-Cl and αKG-PP mildly delay the growth of epithelial kidney cells.** HK-2 growth rate was determined using SRB assay up to 72h of treatment with increasing doses of αKGlogues: αKG-G **(A, B)**, αKG-N **(C, D)**, αKG-Cl **(E, F)**, αKG-P **(G, H)** and αKG-PP **(I, J)** respectively in hypoxia (1% O_2) and normoxia (21% O_2). Data (mean ± SE) are expressed as a percentage of viable cells with respect to time 0 considered as 100% (n≥3). *p*-value was calculated with a two-way ANOVA. *$p \leq 0.05$, **$p \leq 0.01$, ***$p \leq 0.001$, ****$p \leq 0.0001$

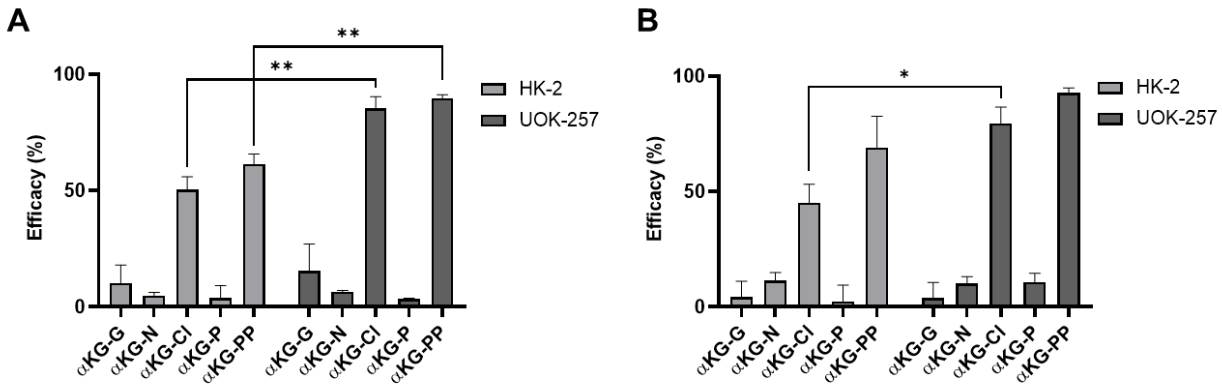

Figure 17: **αKG-Cl and αKG-PP selectively impair the proliferation of kidney carcinoma cells in hypoxia. (A-B)** Efficacy of selected αKGlogues was determined in kidney cancer (UOK-257) and non-cancer (HK-2) cells under low (1% O_2) **(A)** and high oxygen tension (21% O_2) **(B)**, respectively. Data (mean ± SEM) represent the percentage of dead cells induced by 200μM αKGlogues at 72h calculated with respect to the untreated control (n≥3). A two-way ANOVA was used to calculate *p*-value. *$p \leq 0.05$, **$p \leq 0.01$, ***$p \leq 0.001$

To correlate the effect of αKGlogues on cell viability with HIF-1α stabilization, we evaluated the levels of HIF-1α in hypoxia upon treatment with the most effective compounds for long incubation times (6h and 12h). αKG-Cl and αKG-tB were chosen for TPC-1 cells, while αKG-Cl and αKG-PP were selected for UOK-257 cells. In TPC-1 cells, HIF-1α expression was mildly reduced in presence of αKG-Cl at 6h but recovered after 12 hours (Figure 18A, 18C), while αKG-tB sustained HIF-1α degradation up to 12h as the protein levels were two-fold lower with respect to untreated cells (Figure 18B-C). Similarly, in UOK-257 cells αKG-Cl significantly reduced the protein abundance after 12h of treatment while αKG-PP was as potent at 6 and 12h of exposure reducing HIF-1α levels to their half with respect to the untreated (Figure 18E-F). Interestingly, at these time points unconjugated αKG was unable to affect the hypoxic HIF-1α protein stabilisation in both TPC-1 and UOK-257 cells, confirming its low cell permeability (Figure 18B-C, 18E-F).

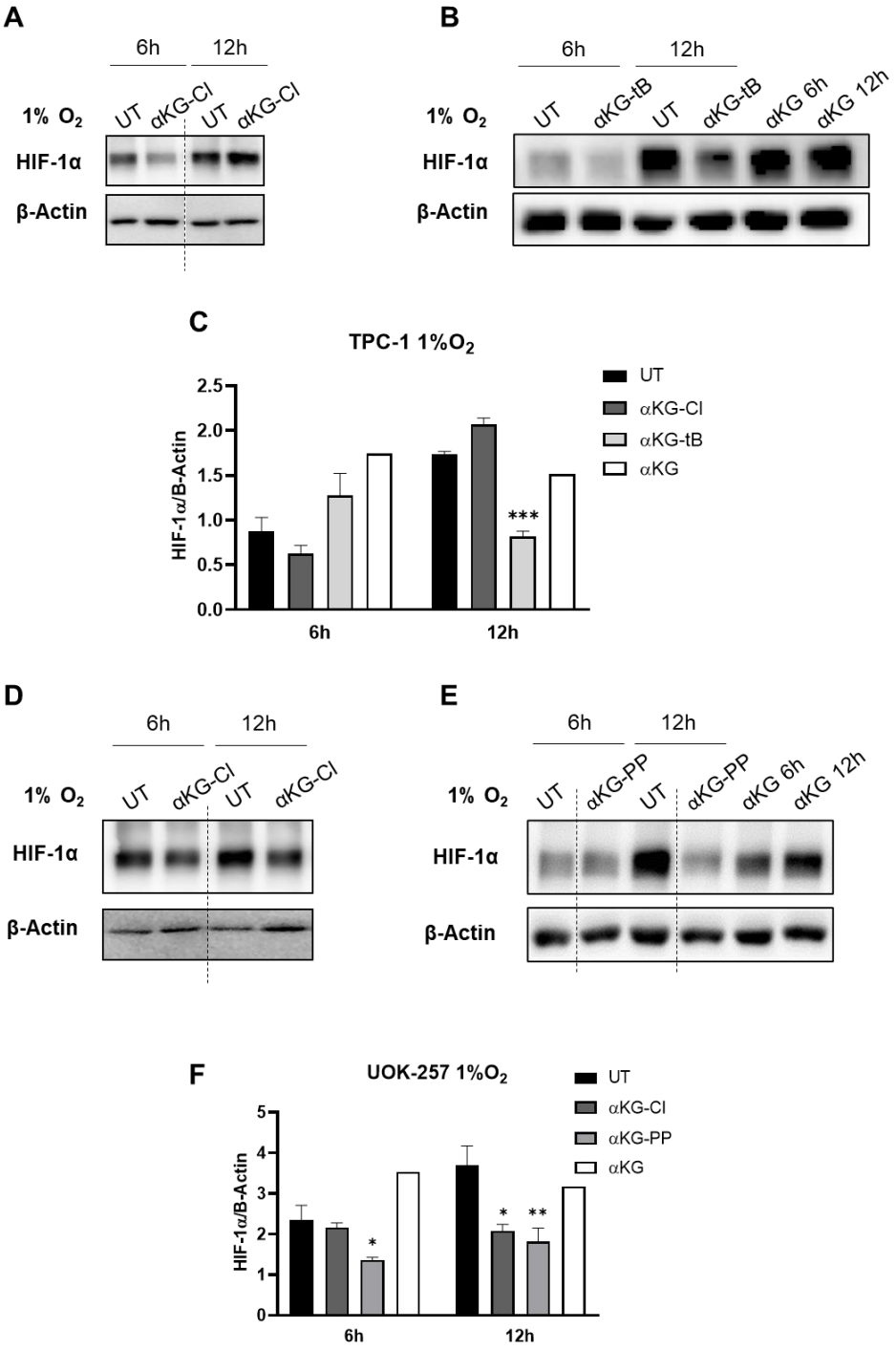

Figure 18: **Selected αKGlogues sustain HIF-1α destabilization in low oxygen tension.** Western blot analysis of HIF-1α expression in TPC-1 cells exposed to 200μM αKG-Cl **(A)**, αKG-tB and unesterified αKG **(B)**. Western blot analysis of HIF-1α expression in UOK-257 cells treated with 200μM αKG-Cl **(D)**, αKG-PP or unconjugated αKG **(E)** for 6 and 12 hours. Densitometric quantification of HIF-1α protein levels both in TPC-1 **(C)** and UOK-257 **(F)** cells was performed using ImageJ software and normalised to loading control β-actin. Results (mean ± SEM) are representative of at least 2 experiments. A two-way ANOVA was performed for statical analysis. *$p \leq 0.05$, **$p \leq 0.01$, ***$p \leq 0.001$

To test the ability of our selected hits to alter malignant cells tumorigenic properties *in vitro,* TPC-1 and UOK-257 cells were incubated in low oxygen conditions (1% O_2) with 200µM of selected αKGlogues. To this aim, we performed a colony formation assay in hypoxia to assess clonogenic properties and a wound-healing assay to determine cell migration upon treatment with selected compounds. In colony formation assay, cells were incubated for 7 days with αKGlogues and colonies were stained with SRB in order to determine the colony number and the quantification of protein content as an indicator of colony size. In these experiments, αKG-Cl was not investigated since we identify an intrinsic detrimental effect on the healthy thyroid cells even at low doses, thereby only leaving αKG-tB and αKG-PP as the most promising compounds on the TPC-1 and UOK-257, respectively. In line with the viability data, 200µM αKG-tB drastically reduced the number and the size of colonies of TPC-1 cells (Figure 19A). The same parameters were severely affected by the treatment of UOK-257 cells with 200µM αKG-PP (Figure 19B). These results suggest that the analogues able to induce HIF-1α degradation in hypoxia up to 12h and to block cell growth are also able to impinge the clonogenic ability of cancer cells. Then, we analysed cancer cell mobility in a wound-healing assay. Cells were seeded in order to reach confluence after 24h, when wound was produced followed by incubation with 200µM of selected compounds. The analysis of wound confluence after 24h from the wounding event revealed that TPC-1 cells treated with 200µM αKG-tB showed a wound confluence of about 40% while untreated cells were almost able to close the wound with a confluence of 70% (Figure 19C). Similarly, after 24h the wound surface in untreated UOK-257 was at 45% confluence, while UOK-257 treated with 200µM αKG-PP showed a wound with a confluence of 15% (Figure 19D) highlighting the effectiveness of the two αKGlogues in limiting cancer cells migration ability *in vitro*.

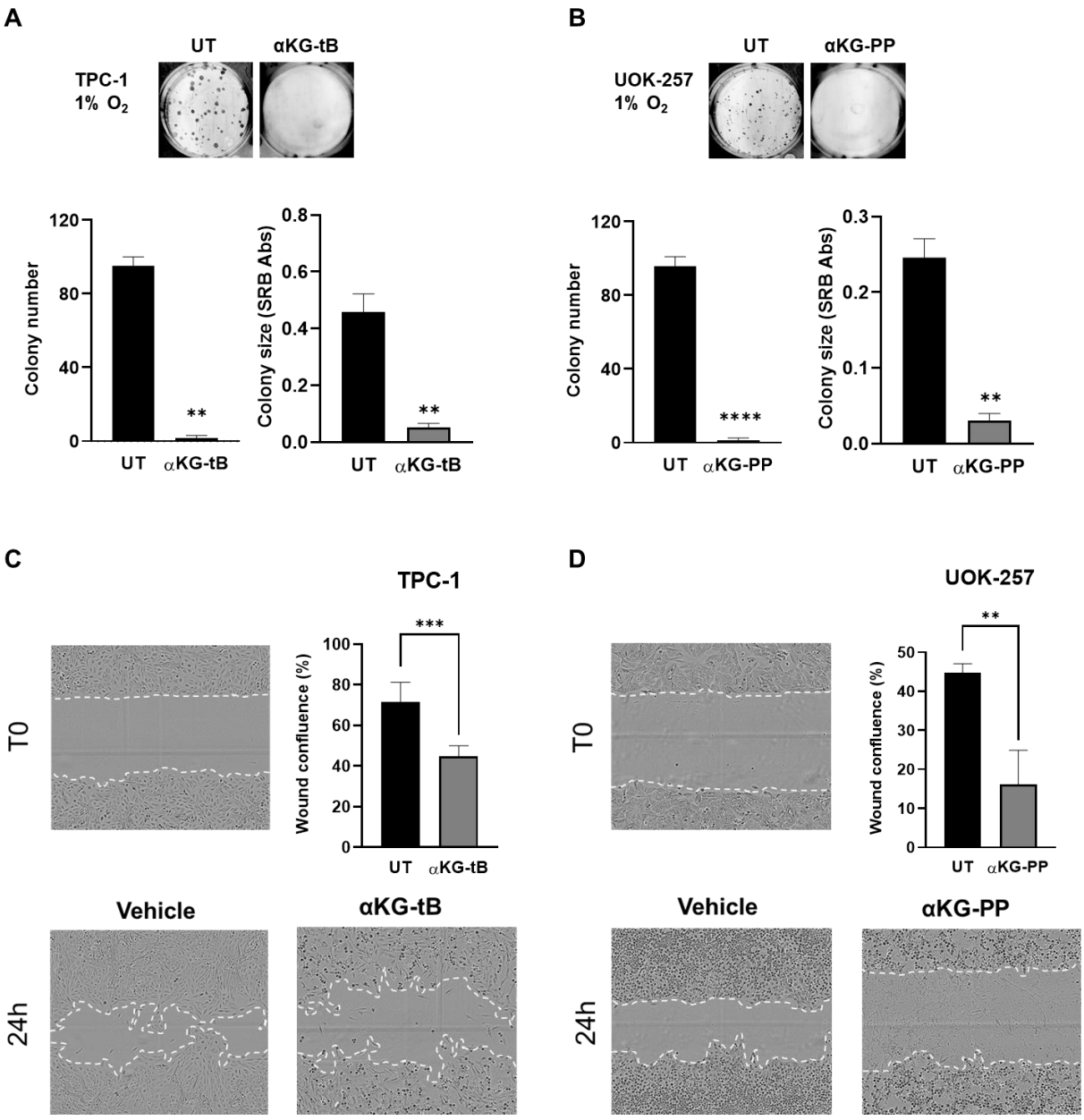

Figure 19: **αKGlogues severely hamper tumorigenic properties of thyroid and kidney cancer cells *in vitro*. (A, B)** Clonogenic assay was performed on untreated (UT) and treated TPC-1 and UOK-257 cells after incubation with 200µM αKG-tB or αKG-PP respectively, for 7 days in low oxygen conditions (1% O_2). Colony number was counted, and colony size determined by SRB dye absorbance measured at 560 nm. An unpaired t-test was performed for statistical analysis of data (mean ± SEM) (n=3) *$p \leq 0.05$, **$p \leq 0.01$, ***$p \leq 0.001$, ****$p \leq 0.0001$. **(C, D)** Cell migration was evaluated through a wound-healing assay in presence of the most promising analogues: αKG-tB in TPC1 and αKG-PP in UOK-257 under high oxygen tension (21% O_2). Wound making was realised on cell monolayers at time 0 (T0) and wound closure monitored for 24h using Incucyte® S3 Live cell Analysis System. Wound confluence in TPC-1 **(C)** and UOK-257 **(D)** monolayers was calculated at experiment endpoint using Incucyte® S3 Live cell Analysis System Software. An unpaired t-test was used for statistical analysis of data (mean ± SEM) (n=3) *$p \leq 0.05$, **$p \leq 0.01$, ***$p \leq 0.001$

Long-term effect on cancer cell viability is partially related to HIF pathway alteration

Selected αKGlogues, namely αKG-PP and αKG-tB, induced HIF-1α degradation in hypoxia, which correlated with impaired cell proliferation and repressed tumorigenic properties. In order to investigate whether such alterations are caused by the shut-off of HIF-1α signalling the two cell models were transduced to stably express a triple-mutant non-degradable version of HIF-1α (HIF-TM). After showing the cells successfully stabilise HIF-1α in high oxygen levels (Figure 20A, 20E), their proliferation rate was subsequently determined in presence of the selected compounds and the respective hydrophobic carriers (Figure 20B-C, 20F-G). Surprisingly, TPC-1 cells expressing HIF-TM were as sensitive to αKG-tB as to tB hydrophobic carrier (Figure 20B-D). Indeed, 200µM of both treatments blocked the growth of the transduced cell line, leaving only 10% viable cells after 72h and thus suggesting a non-specific effect of the carrier. Moreover, parental TPC-1 cells displayed a similar growth alteration in response to treatment with 200µM αKG-tB or the corresponding hydrophobic carrier (Figure 20B-D). These data suggest that the anti-proliferative effect observed with αKG-tB is independent of HIF-1α destabilisation and solely due to the activity of the carrier, and thus not related to increased intracellular levels of αKG. By contrast, in the parental UOK-257 the residual viability in response to treatment with 200µM αKG-PP was of 10% viable cells, while the counterpart expressing HIF-TM is less affected by the compound with a 60% residual viable cells after 72h (Figure 20F, 20H). Interestingly, PP carrier alone similarly reduced to 60% the viability in both parental and HIF-TM expressing cells, thereby suggesting this molecule alters kidney cancer cell proliferation independently of HIF-1α status by 40% (Figure 20F-H). Hence, PP carrier appears to contribute in part to the reduced cell proliferation and displays an additive effect to that of αKG. In light of these results, αKG-tB was therefore excluded from the study thus leaving only αKG-PP as a selected hit.

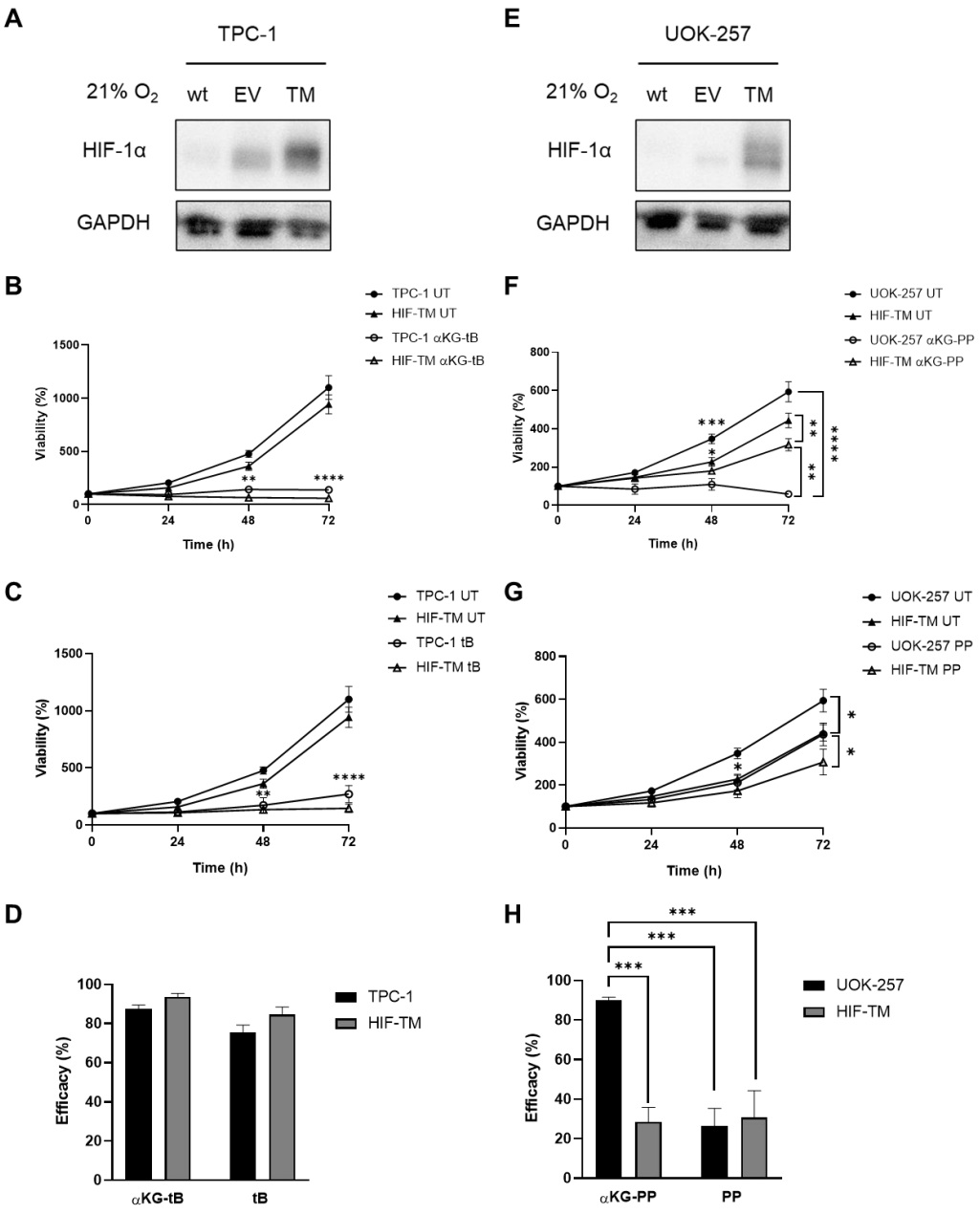

Figure 20: **Hydrophobic carriers contribute to the alteration of cancer cell growth independently of HIF-a signalling.** Growth curves of TPC-1 **(A)** and UOK-257 **(E)** cells transduced with non-degradable HIF-1α (HIF-TM) in presence of 200μM αKG-tB and tB carrier **(B, C)** or αKG-PP and PP carrier **(F-G)** in normoxia (21% O_2). Curves are plotted along with the corresponding parental cell lines expressing wild-type HIF-1α exposed to the same treatments in hypoxia (1% O_2). A two-way ANOVA was used for statistical analysis of data (mean ± SEM) (n≥3) *p≤0.05, **p≤0.01, ***p≤0.001****p≤0.0001. Efficacy of treatment with 200μM αKG-tB and αKG-PP along with their respective carriers on TPC-1 **(D)** and UOK-257 **(H)** cell lines. Data (mean ± SEM) represent the percentage of dead cells induced by treatment at 72h calculated with respect to the untreated control in transduced and parental cell lines (n≥3). A two-way ANOVA was used for statistical analysis *p≤0.05, **p≤0.01, ***p≤0.001****p≤0.0001

The evaluation of colony formation and cell migration of UOK-257 cells treated with 200µM PP carrier confirmed its synergistic anti-proliferative activity. Indeed, UOK-257 cells treated with 200µM PP carrier showed an impairment in their clonogenic properties, which is however significantly lower compared with αKG-PP treatment (Figure 21A). Similarly, cell migration was impaired in cells treated with 200µM PP carrier, but not as much as those incubated with αKG-PP (wound confluence 30% and 15%, respectively) (Figure 21B), thereby suggesting an additive effect in this property as well. Lastly, the PP carrier alone resulted mostly well tolerated by epithelial non-cancer cells HK-2 and N-Thy 3.1 cells which were respectively viable to 70% and 50% after 72h of treatment with 200µM of carrier (Figure 21C-D).

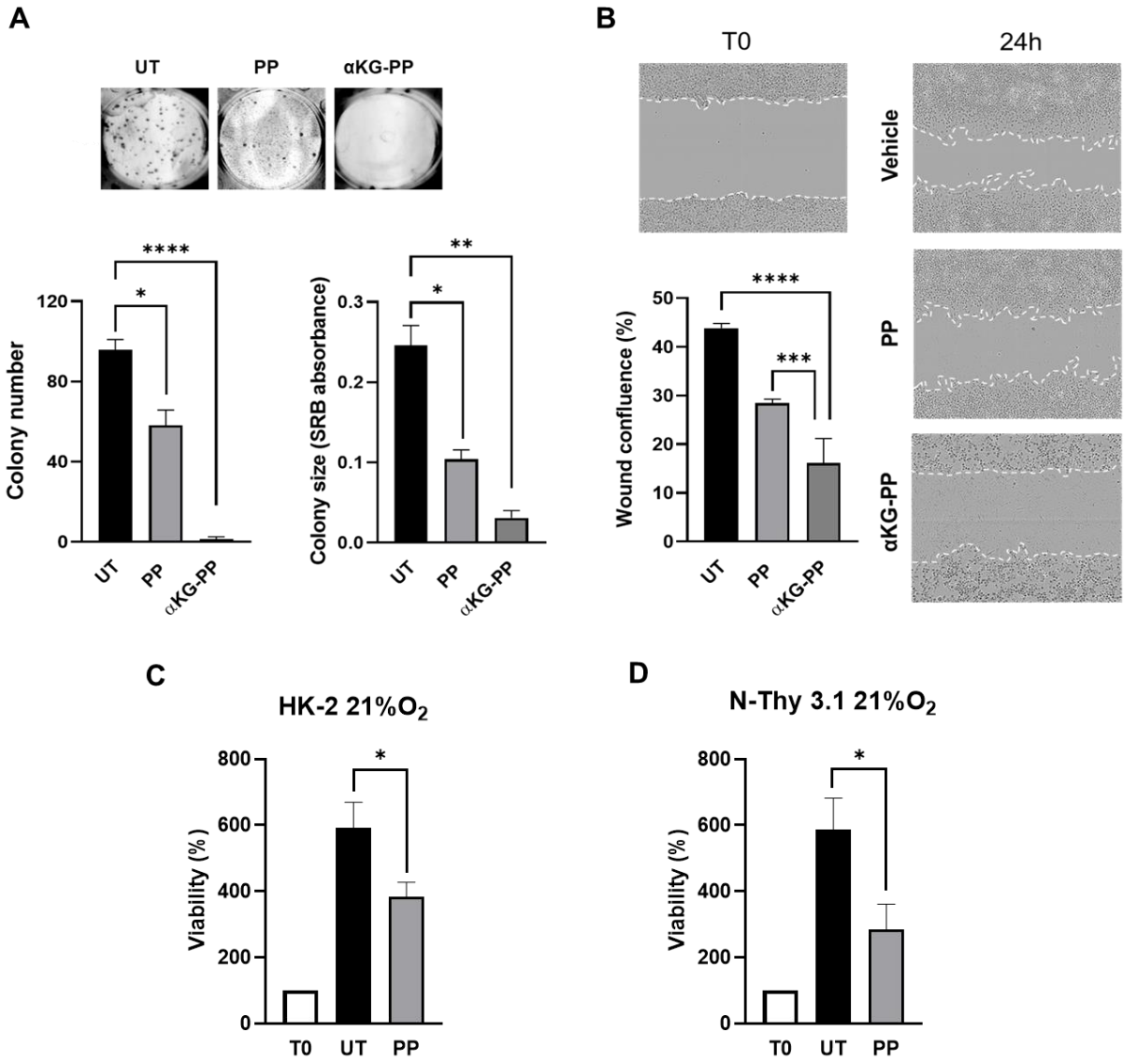

Figure 21: **PP carrier *per se* displays a synergistic effect on kidney carcinoma cell migration properties. (A)** Clonogenic abilities were determined in presence of 200µM αKG-PP or PP carrier for 7 days in low oxygen conditions (1% O_2). Colony number was counted, and colony size determined by SRB dye absorbance measured at 560 nm. A one-way ANOVA was performed for statistical analysis of data (mean ± SEM) (n=3) *$p \leq 0.05$, **$p \leq 0.01$, ***$p \leq 0.001$, ****$p \leq 0.0001$. **(B)** Cell migration in UOK-257 cells was evaluated through a wound-healing assay in presence of 200µM αKG-PP or PP carrier under high oxygen tension (21% O_2). Wound making was realised on cell monolayers at time 0 (T0) and wound closure monitored for 24h using Incucyte® S3 Live cell Analysis System. Wound confluence in UOK-257 monolayers **(B)** was calculated at experiment endpoint using Incucyte® S3 Live cell Analysis System Software. A one-way ANOVA was used for statistical analysis of data (mean ± SEM) (n=3) *$p \leq 0.05$, **$p \leq 0.01$, ***$p \leq 0.001$. **(C-D)** Cell viability of normal epithelial cells HK-2 **(C)** and N-Thy 3.1 **(D)** in high oxygen tension (21% O_2) was determined after 72h of treatment in presence of 200µM PP carrier using SRB assay. An unpaired t-test was used for statistical analysis of data (mean ± SEM) (n=3). *$p \leq 0.05$

αKGlogue PP provokes αKG intracellular accumulation and imbalanced αKG/SA ratio

We previously described that CI-deficient cells are unable to stabilise HIF-1α even in low oxygen tension as a result of PHDs chronic activation. At the metabolic level, these cells displayed increased αKG levels and reduced succinate reflecting a disrupted TCA cycle. To demonstrate that the selected αKG-PP permeates the cell membrane and causes increased αKG intracellular levels, LC-MS-based metabolomics analysis was carried out on UOK-257 cells after exposure to the compound for 1h and 3h. In these experiments, we used 2mM 3-methyl, 2-oxovaleric acid (KMV) to inhibit the αKG dehydrogenase complex (αKGDHC) and push the accumulation of endogenous as well as exogenous αKG, and we considered it as a positive control. UOK-257 cells incubated with 200μM αKG-PP for 1h or 3h showed a time-dependent increased levels of αKG (Figure 22A), reduced succinate levels (Figure 22B) correlating with an elevated αKG/succinate ratio (Figure 22C), while not altering 2-hydroxyglutarate (2-HG) levels (Figure 22D). In such context, the latter result indicates that, once uptaken, αKG is quickly metabolised by αKGDHC. Indeed, 2-HG levels rapidly increase when cells are treated with the combination of 200μM αK-PP and 2mM KMV (Figure 22D). Interestingly, the observed peak in αKG levels after 3 hours of treatment corresponds to reduced HIF-1α abundance that is maintained even after 6 hours, while PP carrier has no effect at the same time points, thereby confirming that αKG-PP, and not the hydrophobic carrier, interferes with HIF-1α stabilisation likely by activating prolyl hydroxylases (Figure 22E-F). Metabolomic analysis revealed that after 1 hour of incubation with αKG-PP only a slight decrease of glutamate was detected, while 3 hours post-treatment a consistent alteration of the TCA cycle was observed. Indeed, aconitate and glutamate levels were significantly reduced (Figure 23A, 23E), while fumarate and malate levels were increased (Figure 23C-D). Citrate and aspartate levels remained unchanged (Figure 23B, 23F). Interestingly, inhibition of αKGDHC by KMV pushes the TCA cycle to its extreme, inducing after just 1 hour a profound depletion of citrate, aconitate, glutamate and aspartate, while causing a striking accumulation of fumarate and malate (Figure 23A-F).

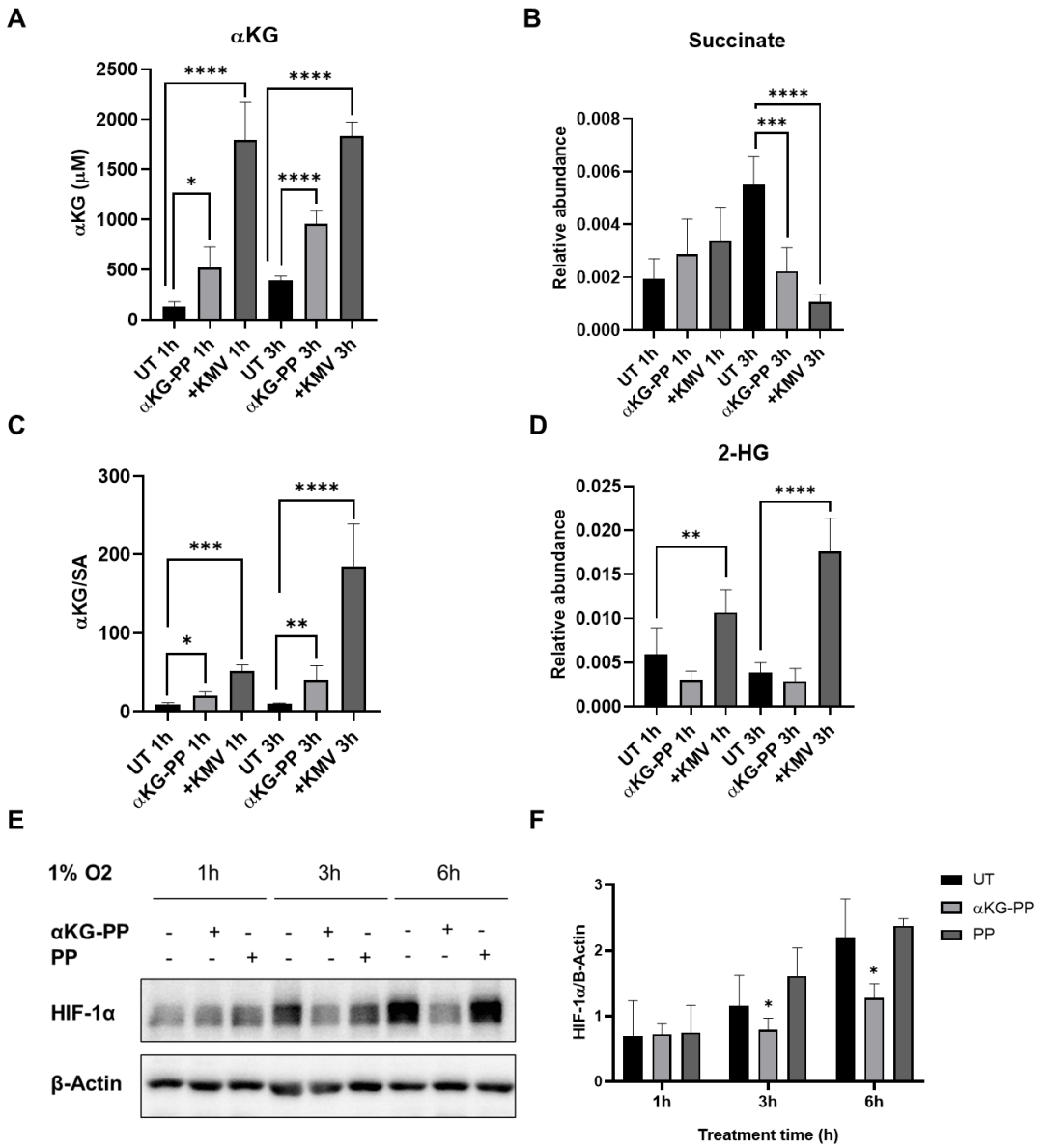

Figure 22: **αKG-PP treatment triggered an increase of intracellular αKG correlated with HIF-1α destabilisation in kidney carcinoma cells. (A)** Intracellular αKG levels after 1 and 3 hours of exposure to 200µM αKG-PP were quantified using LC-MS approach under normoxia (21% O_2). To determine αKG intracellular levels, a calibration curve of the ketoacid was prepared and raw data normalised to mean cell volume. 3-methyl, 2-oxovaleric acid (KMV; 2mM) was used as a positive control for human αKGDH inhibition. **(B)** Succinate (SA) and 2-hydroxyglutarate (2-HG) **(D)** relative abundance values correspond to metabolites ion intensity normalised to internal standard Valine-d8. **(C)** αKG/SA ratio was calculated by the proportion of relative abundances of each metabolite. Metabolomics data (mean ± SD) are representative of 6 technical replicates. A one-way ANOVA was performed for statistical analysis *$p \leq 0.05$, **$p \leq 0.01$, ***$p \leq 0.001$, ****$p \leq 0.0001$. **(E)** Western blot analysis of HIF-1α levels in UOK-257 cells untreated and treated with 200µM αKG-PP or PP carrier under hypoxia (1% O_2) for 1, 3 and 6 hours and respective densitometric quantification of protein levels reported to loading control β-actin **(F)**. Data analysis (mean ± SEM) (n=3) was carried out using a one-way ANOVA (mean ± SEM). *$p \leq 0.05$

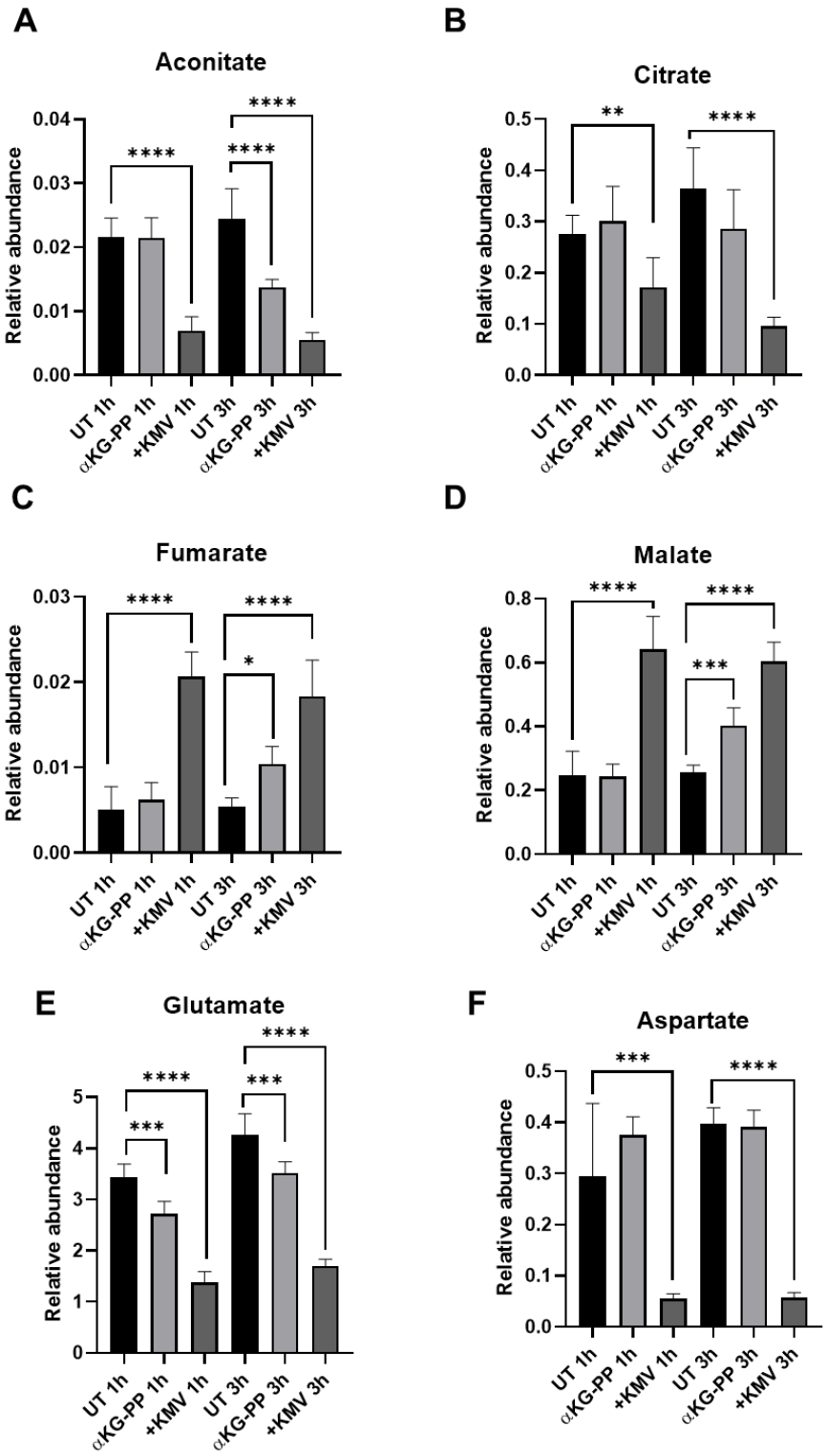

Figure 23: αKG-PP causes TCA cycle rewiring in kidney carcinoma cells. Relative abundance of aconitate **(A)**, citrate **(B)**, fumarate **(C)**, malate **(D)**, glutamate **(E)** and aspartate **(F)** were obtained after 3 hours of treatment under normoxia (21% O_2). Values correspond to metabolites ion intensity normalised to internal standard Valine-d8. Data (mean ± SD), are representative of 6 technical replicates. A one-way ANOVA was performed for statistical analysis *$p \leq 0.05$, **$p \leq 0.01$, ***$p \leq 0.001$, ****$p \leq 0.0001$.

The molecular mechanisms underlying αKG-PP effect imply the block of mTORC1 pathway

As reported in previous sections, αKG-PP and its corresponding carrier are capable of impairing cancer cell growth at high doses (200µM), and αKG-PP was much more potent in doing so. In this regard, and with the aim to investigate the modalities underlying the effect of αKG-PP on UOK-257 cell viability, we started by exploring apoptosis induction resulting from αKG-based treatment as previously reported in literature (Tennant and Gottlieb 2010). In this regard, DAPI-stained nuclear structures of untreated UOK-257 cells or treated with either αKG-PP or PP carrier did not show any sensitive alterations or apoptotic features up to 72h of treatment in normoxia (21% O_2) (Figure 24A) nor in hypoxia (1% O_2) (data not shown) thereby eliminating a hypothetical apoptotic cell death that would be due to αKG-PP or corresponding carrier. Furthermore, a flow cytometry analysis was performed on UOK-257 cells 72h post-treatment with 200µM of αKG-PP or PP carrier in normoxia (21% O_2), using Annexin V (AV) as a marker for apoptotic cell death along with propidium iodide (PI). Both experiment and analysis were carried out in high oxygen tension since flow cytometer does not allow a controlled oxygen supply in order to maintain cells under low oxygen conditions. At the experiment endpoint, results revealed a shift in cell populations. While the untreated condition counted around 89% of live cells, this percentage was of 86.3% in cells treated with PP carrier and to 82.9% in αKG-PP-treated cells (Figure 24B). In this latest condition, the proportion of dead cells was twice as much as in the untreated control (5.73%) with 12.5% dead cells, while 200µM PP provoked 8.70% cell death (Figure 24B). These data thus support cell viability experiments previously described, showing that αKG-PP induces cell death on the one hand and confirming the contribution of PP carrier. However, it is worth to note that the proportion of dead cells induced by the analogue in this last case was less marked than in SRB viability assay. Moreover, the induction of senescence in these cells was also investigated. In this frame, treated and untreated kidney carcinoma cells stained negative to senescence-specific β-galactosidase assay (Figure 24C, *upper panel*) 72h after treatment with either 200µM of αKG-PP or PP carrier in normoxia, thus ruling out this pathway as a possible mechanistic consequence of αKG accumulation. Similarly, no differences in LC-3 protein levels or processing were observed up to 6h of treatment with αKG-PP or PP carrier in hypoxia (Figure 24C, *lower panel*) excluding the induction of autophagy as a consequence of αKG accumulation at least not as an early event during treatment.

Being a precursor of glutamine, αKG is tightly involved in amino acids metabolism. On the other hand, mammalian Target of Rapamycin Complex 1 (mTORC1), constitutes the master regulator of protein synthesis in response to nutrients availability and proliferation needs of rapidly growing cancer cells (Saxton and Sabatini 2017). Interestingly, analysing proteins of this pathway through western blot in a context of αKG accumulation surprisingly revealed treatment with αKG-PP and not PP carrier correlated with an inhibition of mTORC1 pathway after 1, 3 and 6 hours in hypoxia. Indeed, Raptor, one of mTORC1 associated regulatory proteins necessary for the complex binding to its targets, was phosphorylated at Serine 792 only in samples treated with αKG-PP (Figure 24D), highlighting the protein inactivation and thus the shut-off of mTORC1 signalling. Next to that, no notable differences in total or phosphorylated mTOR levels were observed (Figure 24D). Such results thus suggest increased intracellular αKG levels in UOK-257 cells correlate with a rapid inhibition of mTORC1 signalling. Furthermore, the phosphorylated forms of p70S6K and 4E-BP1, two downstream substrates of mTORC1 involved in the initiation of cap-dependent translation and protein synthesis, were notably reduced in UOK-257 cells exposed to αKG-PP for 48h with respect to the untreated (Figure 24E), indicating αKGlogue PP represses mTORC1 signalling and protein synthesis at 48h in low oxygen tension while no such effect was notable at earlier times, namely 16 and 24h of treatment. Surprisingly, PP carrier also appeared to downmodulate mTORC1 pathway in UOK-257 cells after 48h, although less marked than the analogue itself, suggesting once more an additive effect of the carrier in this context (Figure 24E). Notably, total and phosphorylated mTOR levels remained unchanged between 16h to 48h of treatment (Figure 24E).

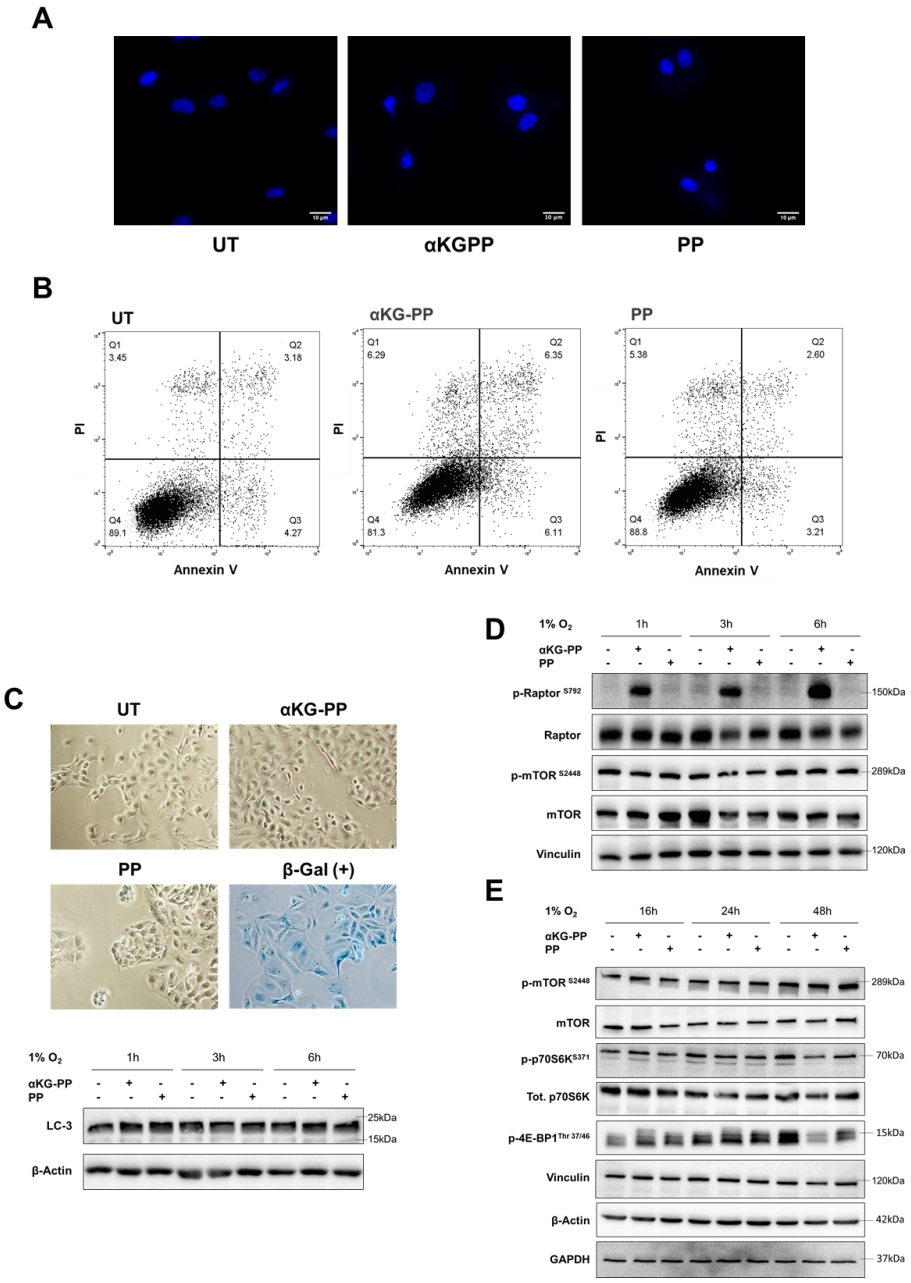

Figure 24: Molecular mechanisms underlying αKG-PP effect in UOK-257 cells imply the block of protein synthesis via mTORC1 signalling. (A) Nuclei morphology was visualized by DAPI staining upon exposure to 200µM αKG-PP and PP carrier for 72h under normoxia (21% O_2). **(B)** Apoptotic death was evaluated using PI and AV as markers in flow cytometry after 72h of αKG-PP and PP treatment under normoxia (21% O_2). **(C)**, Senescence-specific β-galactosidase staining of UOK-257 cells untreated or treated with 200µM αKG-PP and PP for 72h under normoxia (21% O_2) (*upper panel)*. Western blot analysis of autophagy marker LC-3 up to 6h of treatment with αKG-PP and PP under hypoxia (1% O_2) (*lower panel*). **(D, E)** Western blot analysis of mTOR pathway at different times of treatment with αKG-PP and PP under hypoxia (1% O_2).

αKG-PP displays anti-proliferative properties in cancer-derived spheroids and *in vivo*

At this stage, we aimed at translating the use of αKG-PP in more complex models such as 3D cultures and animal models. Hence, multicellular spheroids derived from TPC-1 and UOK-257 cells were generated in ULA plates. The obtained 3D models of approximately 200µm diameter were described to recapitulate several properties (oxygen and nutrients gradient, heterogenous cell population) of solid tumors *in vivo.* Spheroids were consequently treated with 200µM αKG-PP, while 200nM staurosporine (STS) was used as a positive control. In this regard, results revealed that the two tested models treated with αKG-PP showed no difference in the proportion of dead cells compared to the untreated control (Figure 25A-B) after 3 days of treatment, while 200nM STS induced a significant cell death. It is possible that at this dose, a treatment duration of 3 days is too short to see any effect on the growth of complex structures such as spheroids. Consequently, treatment was extended to longer periods, as most reports in literature often refer to 7 days as a mean duration. A subsequent experiment in which UOK-257-derived spheroids were maintained in presence of αKG-PP for 7 days confirmed the absence of significant differences in spheroids size 3 days post-treatment (Figure 25C), whereas at day 7 the 3D cancer model exposed to αKG-PP and PP carrier looked significantly smaller in size compared to the untreated control (Figure 25C). These data are comforted by an MTT viability assay that showed the proportion of metabolically active cells was significantly lower in spheroids exposed to 200µM αKG-PP compared to untreated control. Moreover, the percentage of viable cells in presence of αKG-PP was 50% less than in spheroids exposed to PP carrier after 7 days of treatment (Figure 25C). Hence, these preliminary data strongly corroborate an anti-proliferative effect of αKG-PP in the 3D kidney cancer model as well as a synergistic action of the PP carrier in this model.

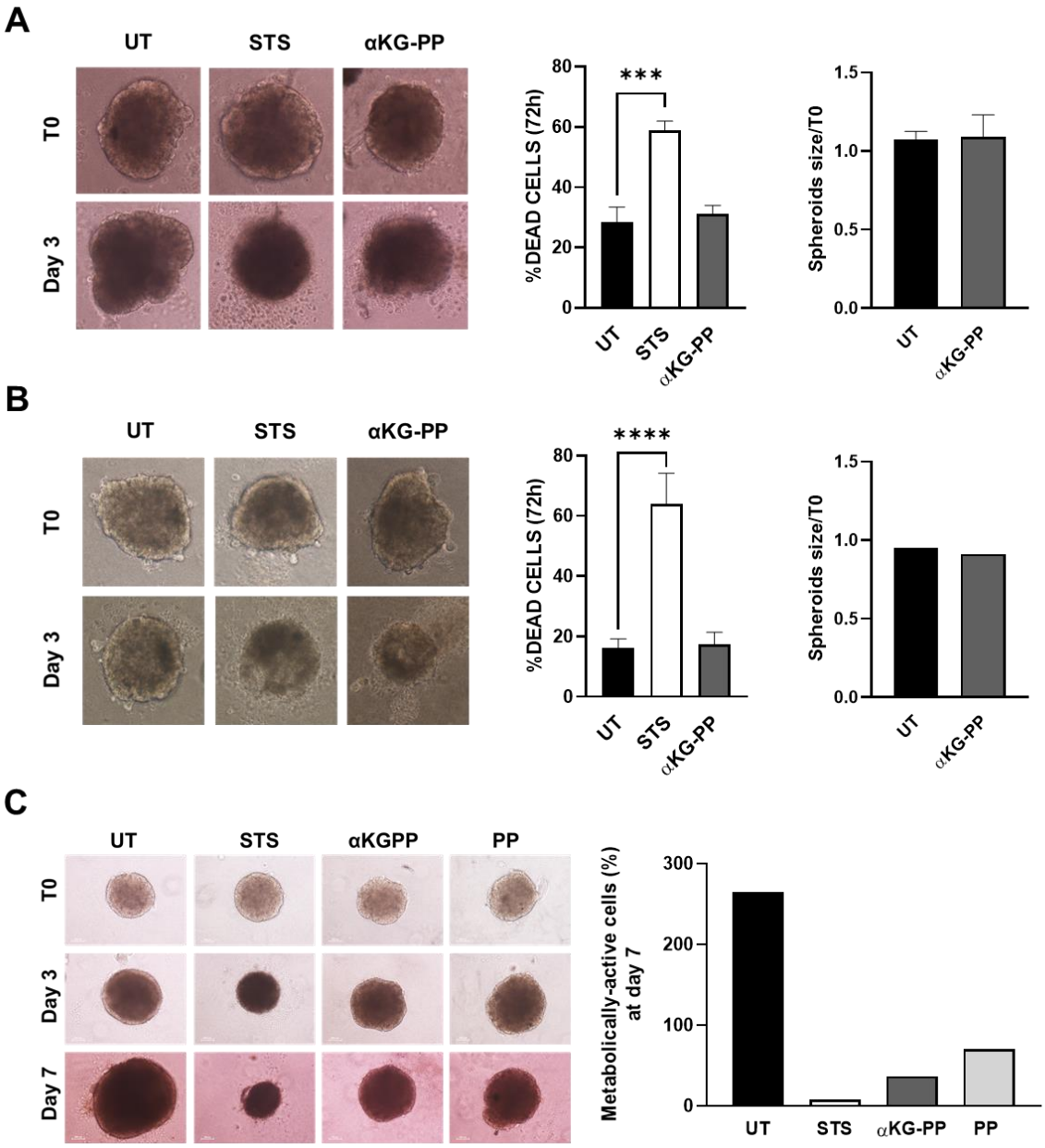

Figure 25: **αKG-PP alters 3D spheroids size and viability.** Size and cytotoxicity assessment in UOK-257 **(A)** and TPC-1-derived spheroids **(B)** after 3 days of treatment with 200µM αKG-PP. 200nM staurosporine (STS) was used as a positive control. Quantitative analysis of dead cells was determined using Promega's CytoTox-Glo™ bioluminescence assay. A one-way ANOVA was used for statistical analysis of data (mean ± SEM, n≥4) **p*≤0.05, ***p*≤0.01, ****p*≤0.001. Spheroids size (mean ± SD) was measured using ImageJ free software (NIH) and normalised to their size at Time 0. **(C)** Growth of UOK-257-derived spheroids up to 7 days of treatment (n=1) with 200µM αKG-PP and PP carrier. Percentage of viable cells at day 7 in UOK-257-derived spheroids was determined using MTT assay. Data were normalised to viable cells at time 0 considered as 100% (n=1).

Drosophila melanogaster is considered a handful *in vivo* model to study the complex features of cancer thanks to signaling pathways and regulatory system preservation from human to flies (Mirzoyan et al., 2019). The use of specific and advanced genetic tools and its short life cycle (10 days at 25°C) make flies easy to manipulate. *Drosophila* is also an excellent model for drug screening studies because, in addition to closely reproducing the typical human cancer traits, it allows the analysis of a large number of individuals. To investigate the consequence of αKG-PP treatment *in vivo*, tumor growth in the dorsal compartment of imaginal wing discs was induced. 6 days after egg laying (AEL) tumor individuals were selected and exposed to 200µM αKG-PP for 2 days. Wing disc isolation revealed a 34% decrease in tumor size of treated individuals with respect to the untreated counterpart as highlighted by volume analysis (Figure 26). These preliminary data thus confirm αKG-PP potency to slowdown tumor growth *in vivo*. However, whether the analogue-mediated effect in *Drosophila* wing discs is due to increased cell death or to reduced proliferation remains to be determined.

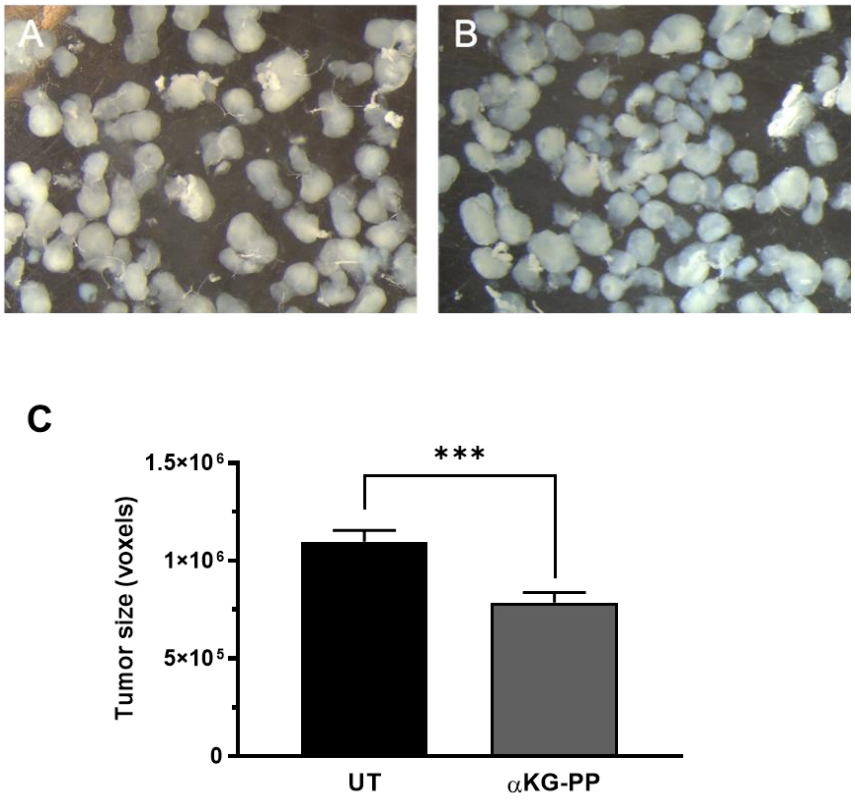

Figure 26: αKG-PP displays antiproliferative properties *in vivo*. Tumors isolated from ap-*lgl*^{KD}, *Ras*^{V12} untreated samples **(A)** or treated with 200µM αKG-PP **(B)** for 2 days. **(C)** Volume analysis of ap-*lgl*^{KD}, *Ras*^{V12} tumor samples untreated (n=46) and treated with αKG-PP analogue (n=48). An unpaired t-test was used for statistical analysis ***p≤0.001

DISCUSSION

Targeting hypoxic adaptation in cancer has long constituted an attractive approach to tackle tumor progression. Although focused approaches as represented by HIF inhibitors seem to constitute an interesting alternative, their use as single therapies in cancer patients is seriously limited by the high resistance rates and relapse. For this reason, now more than ever, the perspective of combining classical chemotherapy/radiotherapy to emerging complementary approaches among which targeting metabolism and hypoxia adaptation appears to be more convenient to enhance the chances of treatment success and are consequently being investigated in clinical trials.

Here, we propose an adjuvant and safe metabolic-based therapeutic approach taking into account that TCA metabolites may also act as tumor growth modulators. In this framework, we have previously demonstrated that a severe mitochondrial CI impairment triggers an increase of both NADH/NAD^+ and αKG/SA ratio, causing chronic HIF-1α degradation (*pseudonormoxia*) and in turn, tumor growth arrest (Porcelli et al., 2010) (Gasparre et al., 2011) (Calabrese et al., 2013) (Iommarini et al., 2014) (Kurelac et al., 2019). To recapitulate this low-proliferative phenotype we exploited the use of cell-permeable αKGlogues to provoke the increase of the physiological substrate of PHDs feeding their activity. Indeed, it is well known that the slightest fluctuations in αKG levels feeds the PHDs reaction (K_m around 50μM). Hence, we generated a panel of 7 novel αKGlogues that maintain their structural integrity both in organic solvents and in aqueous solution. We screened the analogues, to assess their ability to stimulate HIF-1α degradation under hypoxic conditions and to consequently impair cancer cells proliferation without exerting broad cytotoxicity on non-cancer controls. Consequently, only the most selective compounds displaying the least toxic side-effects on the non-cancer cells were considered for further investigations.

Surprisingly, testing the 7 analogues on thyroids carcinoma (TPC-1) and kidney carcinoma (UOK-257) cell lines revealed different sensitivities in terms of HIF-1α degradation. We observed that while TPC-1 cells responded more to 200μM of αKG-tB, αKG-N, αKG-Cl, αKG-L and αKG-G, UOK-257 cells were more sensitive to αKG-PP, αKG-Cl, αKG-P, αKG-N and αKG-G, to a lesser extent. Such a disparity between the two cancer cell models may be attributed to each cell respective membrane composition, which make them more permeable to some analogues harbouring specific hydrophobic groups and less to others. In this regard, the commercial αKG-DM is unable to influence HIF-1α expression levels which remained as high as the untreated control in UOK-257 cells whereas the same dose of compound significantly reduced HIF-1α abundance 60 and 90 minutes after exposure in TPC-1 cells.

Such results thus suggest UOK-257 cells membrane permeability is more selective compared to TPC-1. Moreover, the rate of delivery and use of the compounds which likely varies from one cell to another based on their metabolic profile could strongly influence the analogues intracellular kinetics. This can account for the transient effect observed with αKG-N and αKG-P in UOK-257 cells suggesting these compounds have a short half-life and possibly they are quickly metabolized following cell uptake. Indeed, in a study carried out by Tennant and collaborators, the authors reported a peak in αKG intracellular levels as early as 45 minutes following αKG-analogues administration, after which the metabolite's concentration rapidly decreased to reach the baseline at 120 minutes. Interestingly, structure optimisation of monoester TαKG to produce diester ETαKG was able to prolong αKG accumulation inside the cells up to 4h thereby directly linking the analogues structure with their ability to maintain steady delivery of αKG to the cell (Tennant et al., 2009). It is worth to add that in our tested cancer cell models, un-conjugated αKG was unable to affect HIF-1α protein levels under hypoxic conditions further confirming similar observations by Gottlieb and his group (MacKenzie et al., 2007; Tennant et al., 2009) who showed free αKG inability to cross the plasma membrane as reflected by unchanged metabolite's intracellular levels.

In light of the screening results, we were able to select 4 analogues on the thyroid carcinoma cell line namely, αKG-N, αKG-L, αKG-tB and αKG-Cl, and 5 for the kidney carcinoma cells (αKG-G, αKG-N, αKG-Cl, αKG-P and αKGPP), based on their respective abilities to induce HIF-1α degradation under hypoxic conditions. Next, we investigated the effect of the selected compounds on cancer cells proliferation in a context of HIF-1α destabilisation. In this regard, 200µM αKG-G, αKG-N and αKG-L showed little or no effect on the proliferation of thyroid carcinoma cells (TPC-1) nor on the non-cancer thyroid epithelial cells (N-Thy 3.1) up to 72h under hypoxic condition. Similarly, we noted that αKG-G and αKG-N or αKG-P were unable to affect the growth of the kidney cell models up to 200µM independently from oxygen conditions. These analogues showed a transient effect on HIF-1α protein expression which was recovered after 90 minutes of treatment, potentially hinting that the compounds display an early biological effect on HIF-1α protein levels which is overcome due to the fast use of the metabolite. Interestingly, in the literature αKG analogues were reportedly used at concentration ranging from 2mM to 5mM, albeit at least 10 times more than in the present study. In light of PHDs affinity for their substrate (K_m around 50µM), this might account for the low potency of doses as small as 2µM and 20µM which maybe too weak to influence the

hydroxylases activity, further highlighting the necessity to use doses at least equal or superior to αKG physiological levels in order to observe a biological effect.

In addition, we show that αKG-Cl displayed a dose-dependent effect on the proliferation of both TPC-1 and UOK-257 cells with doses as low as 2µM ultimately resulting in a blocked proliferation at 200µM independently of oxygen tension, suggesting the analogue's effect on cell growth is likely independent from HIF-1α status. Such an observation could be due to an off-target effect or attributed to the activity of the hydrophobic carrier *per se*. Overall, despite being well tolerated by the epithelial kidney cells, this analogue severely hampered the growth of the non-cancer thyroid cells at 200µM and was therefore discarded from the study. These results highlight the sensitivity to different treatments is strongly related to the cells tissue of origin, a parameter often recognised to further complicate the development of anti-cancer therapies.

Although it is well known that coupling αKG to hydrophobic groups enhances its membrane permeability, however, the possibility that these carriers alone, may display a biological activity cannot be excluded. In this regard, we show that αKG-tB selectively hampered the growth thyroid carcinoma cells and *in vitro* tumorigeneic properties at 200µM without inducing marked toxicity on the non-cancer N-Thy 3.1 cells up to 72h of treatment. However, despite its high potency in recreating a *pseudonormoxic* state up to 12h of exposure (Figure 18A-C) we were able to demonstrate that the anti-proliferative effect of αKG-tB on the thyroid cancer cells was independent from HIF-1α destabilisation and is, instead solely due a non-specific activity of the hydrophobic carrier tB, thereby leading to its exclusion. Hence, at the term of the screening phase and based on each analogue's effectiveness and safety properties which constituted our main criteria in this study, αKG-PP was selected as the most promising hit and all the other analogues were discarded.

Indeed, the potential of αKG-PP lied in its ability to impair the growth of the kidney carcinoma cells at 200µM ultimately leading to cell death with good safety levels on the kidney epithelial counterparts under hypoxic conditions, overall correlating with a sustained HIF-1α destabilisation at long term and the repression of cancer cells *in vitro* clonogenic and migration abilities. Further, taking advantage of HIF-TM overexpressing cells, we were able to establish a direct link between αKG-PP treatment, HIF-1α expression and altered cancer cells growth. We demonstrated that the growth alteration provoked by αKG-PP in UOK-257 cells is in part dependent on blocked HIF signalling, the other part being due to a synergistic

activity of the PP carrier independently from HIF-1α status. To our knowledge, this is the first time the single activity of the carriers is reported unveiling an additive effect on cancer cells growth and tumorigenic properties. We provide evidence that exposure to αKG-PP and not PP carrier specifically blocked HIF-1α stabilisation in UOK-257 cells. At the intracellular level, this correlated with a peak in αKG concentration 1 and 3h post-treatment culminating in increased αKG/SA ratio. Consistently with former studies, these data give further insight at two levels: first by confirming the ability of our synthetised analogue to permeate through the plasma membrane and cause the accumulation of the ketoacid inside the cells (Mackenzie et al., 2007; Tennant et al., 2009). On the other hand, and as previously emphasized, a high αKG/SA is one of the main features of CI-deficient cells thus confirming our initial hypothesis that αKG supplementation is able to recapitulate some features of CI-deficient cells, namely a high αKG /SA ratio together with chronic HIF-1α destabilisation.

Besides αKG accumulation, metabolomics data revealed oncometabolite 2-HG levels remained stable 3h post-treatment indicating that the exogenous αKG is quickly metabolised. On the other hand, the low levels of SA coupled to an increased malate/aspartate ratio, a direct indicator of NADH accumulation, hint to the reduction in the oxidative flux of the TCA cycle usually endorsed by αKGDHC. Indeed, the activity of the enzymatic complex is known to be negatively regulated by increased $NADH/NAD^+$, especially in a context of severe mitochondrial defects (Calabrese et al., 2013) (Vatrinet et al., 2017). However, further analysis is likely warranted to clearly sustain these observations. At the metabolic level, other works reported ester analogues of the ketocid to reverse the glycolytic profile characterising hypoxic cancer cells, by reducing their glucose consumption and lactate production *in vitro* and *in vivo* to finally converge in PHD3-mediated apoptotic cell death (Tennant et al., 2009) (Tennant and Goettlieb 2010). Independently of HIF-1α and far from its effect in a hypoxic context, αKG-DM, a commercial ester analogue, was recently reported to induce synthetic lethality in a panel of cancer cells when combined to a well-known OXPHOS inhibitor, namely BAY87-2243. In addition to blocking oxidative phosphorylation, the drug combination displayed a synergistic effect to suppress glycolysis through a mechanism involving MDM2 transcriptional response culminating in a bioenergetic crisis and triggering cell death in a panel of cancer cell models (Sica et al., 2019). More recently, a strong line of evidence highlights the anti-tumorigenic activity of the ketoacid mediated through the stimulation of other dioxygenases of the αKGDDs family, namely DNA and histone demethylases TETs and KDMs ultimately reversing pro-tumorigenic epigenetic signals. In

this regard, αKG-DM was described to recapitulate p53 transcriptional response and favour cell differentiation via the reactivation of TETs enzymes in a model of pancreatic ductal adenocarcinoma (Morris et al., 2019).

In our hands, although UOK-257 exposure to αKG-PP or PP carrier induced a cytotoxic cell death, cells showed no morphological features of apoptosis, thus indicating the analogue and carrier anti-proliferative activity is mediated through a different mechanism. Similarly, αKG-PP did not trigger senescence nor autophagy in the kidney carcinoma cells. Instead, the supplementation of the ketoacid seemed to mediate a rapid repression of mTORC1 signalling. These data suggest that in addition to inducing a state of *pseudonormoxia*, the intracellular accumulation of αKG secondary to treatment also correlated with the inhibition of mTOR signalling, potentially accounting for the growth arrest observed in these cells. Interestingly, mTOR signalling cascade is well known to act upstream of HIF-1α thereby promoting *HIF1A* mRNA transcription and translation (Iommarini et al., 2017). Hence, by downmodulating mTORC1 pathway, it is possible that exogenous αKG indirectly potentiates its repressive activity on HIF-1α expression. In addition, preliminary data at longer terms revealed that αKG-PP-mediated mTORC1 repression is maintained over time and in such a context, PP carrier *per se* also appeared to contribute to the downregulation of the mitogenic pathway further confirming its synergistic activity on cell growth as previously related. Analogous effects were described during the response to pro-apoptotic and cytotoxic compounds like staurosporine, which reportedly inhibited mTOR-dependent protein synthesis by directly acting on its downstream targets (Tee and Proud 2001). Similarly to staurosporine, treatment with αKG was shown to impair the proliferation of colon adenocarcinomas cell lines by inducing cell cycle arrest in normoxia (Rzeski et al., 2012). It is therefore possible that αKG-PP and PP carrier block cell cycle progression by inactivating mTOR downstream targets and shutting down protein synthesis to finally trigger cell death. In this regard, αKG accumulation may induce an immediate cell death following the double repression of HIF-1α and mTOR signalling while the PP carrier may provide a late additive effect thereby sustaining cell death. Nevertheless, further investigations are ongoing to confirm the previous observations and clearly determine the mechanisms underlying αKG-PP and PP carrier anti-proliferative activity in other cancer cell models.

To conclude, the pleiotropic implication of the metabolite highlights its multiple targets and thus considerably widens the scope of its therapeutic applications. This study sustains previous reports in shedding light on the great potential αKG holds to modulate cancer

progression. At the present time, no clinical studies have included αKG as a therapeutic agent in the context of cancer and studies have been restricted to murine models so far. On the other hand, thanks to the preservation of signaling pathways from human to flies and their facility of use, *Drosophila* constitutes an excellent model for drug screening studies. In this regard, our preliminary data confirmed the anti-proliferative activity of αKG-PP *in vivo* on a *Drosophila* cancer model thereby strengthening the anti-tumorigenic potential of αKG analogues and paving the way to further studies. The encouraging results presented herein along with those increasingly reported in literature support the hypothetic anti-cancer activity of the ketoacid and open the possibility to the application of an αKG-based therapy in combination with conventional or novel chemotherapeutic drugs in the frame of a synthetic lethality approach, however, before considering the translation in cancer patients in the clinic the candidate analogues would priorly need to be validated through pre-clinical studies.

REFERENCES

Abla H, Sollazzo M, Gasparre G, Iommarini L, Porcelli AM. The multifaceted contribution of α-ketoglutarate to tumor progression: An opportunity to exploit? Semin Cell Dev Biol. 2020 Feb;98:26-33. doi: 10.1016/j.semcdb.2019.05.031.

Aik W, McDonough MA, Thalhammer A, Chowdhury R, Schofield CJ. Role of the jelly-roll fold in substrate binding by 2-oxoglutarate oxygenases. Curr Opin Struct Biol. 2012 Dec;22(6):691-700. doi: 10.1016/j.sbi.2012.10.001.

Akatsuka A, Kojima N, Okamura M, Dan S, Yamori T. A novel thiophene-3-carboxamide analog of annonaceous acetogenin exhibits antitumor activity via inhibition of mitochondrial complex I. Pharmacol Res Perspect. 2016 Jul 12;4(4):e00246. doi: 10.1002/prp2.246.

Andrzejewski S, Gravel SP, Pollak M, St-Pierre J. Metformin directly acts on mitochondria to alter cellular bioenergetics. Cancer Metab. 2014 Aug 28;2:12. doi: 10.1186/2049-3002-2-12.

Appelhoff RJ, Tian YM, Raval RR, Turley H, Harris AL, Pugh CW, Ratcliffe PJ, Gleadle JM. Differential function of the prolyl hydroxylases PHD1, PHD2, and PHD3 in the regulation of hypoxia-inducible factor. J Biol Chem. 2004 Sep 10;279(37):38458-65. doi: 10.1074/jbc.M406026200.

Atlante S, Visintin A, Marini E, Savoia M, Dianzani C, Giorgis M, Sürün D, Maione F, Schnütgen F, Farsetti A, Zeiher AM, Bertinaria M, Giraudo E, Spallotta F, Cencioni C, Gaetano C. α-ketoglutarate dehydrogenase inhibition counteracts breast cancer-associated lung metastasis. Cell Death Dis. 2018 Jul 9;9(7):756. doi: 10.1038/s41419-018-0802-8.

Bastian A, Matsuzaki S, Humphries KM, Pharaoh GA, Doshi A, Zaware N, Gangjee A, Ihnat MA. AG311, a small molecule inhibitor of complex I and hypoxia-induced HIF-1α stabilization. Cancer Lett. 2017 Mar 1;388:149-157. doi: 10.1016/j.canlet.2016.11.040.

Battelli C, Cho DC. mTOR inhibitors in renal cell carcinoma. Therapy. 2011 Jul;8(4):359-367. doi: 10.2217/thy.11.32.

Bayliak MM, Shmihel HV, Lylyk MP, Vytvytska OM, Storey JM, Storey KB, Lushchak VI. Alpha-ketoglutarate attenuates toxic effects of sodium nitroprusside and hydrogen peroxide in Drosophila melanogaster. Environ Toxicol Pharmacol. 2015 Sep;40(2):650-9. doi: 10.1016/j.etap.2015.08.016.

Baysal BE. A recurrent stop-codon mutation in succinate dehydrogenase subunit B gene in normal peripheral blood and childhood T-cell acute leukemia. PLoS One. 2007 May 9;2(5):e436. doi: 10.1371/journal.pone.0000436

Berra E, Benizri E, Ginouvès A, Volmat V, Roux D, Pouysségur J. HIF prolyl-hydroxylase 2 is the key oxygen sensor setting low steady-state levels of HIF-1alpha in normoxia. EMBO J. 2003 Aug 15;22(16):4082-90. doi: 10.1093/emboj/cdg392.

Bertout JA, Patel SA, Simon MC. The impact of O2 availability on human cancer. Nat Rev Cancer. 2008 Dec;8(12):967-75. doi: 10.1038/nrc2540.

Birsoy K, Possemato R, Lorbeer FK, Bayraktar EC, Thiru P, Yucel B, Wang T, Chen WW, Clish CB, Sabatini DM. Metabolic determinants of cancer cell sensitivity to glucose limitation and biguanides. Nature. 2014 Apr 3;508(7494):108-12. doi: 10.1038/nature13110.

Brand AH, Perrimon N. Targeted gene expression as a means of altering cell fates and generating dominant phenotypes. Development. 1993 Jun;118(2):401-15.

Bridges HR, Jones AJ, Pollak MN, Hirst J. Effects of metformin and other biguanides on oxidative phosphorylation in mitochondria. Biochem J. 2014 Sep 15;462(3):475-87. doi: 10.1042/BJ20140620.

Brière JJ, Favier J, Bénit P, El Ghouzzi V, Lorenzato A, Rabier D, Di Renzo MF, Gimenez-Roqueplo AP, Rustin P. Mitochondrial succinate is instrumental for HIF1alpha nuclear translocation in SDHA-mutant fibroblasts under normoxic conditions. Hum Mol Genet. 2005 Nov 1;14(21):3263-9. doi: 10.1093/hmg/ddi359..

Brunmair B, Lest A, Staniek K, Gras F, Scharf N, Roden M, Nohl H, Waldhäusl W, Fürnsinn C. Fenofibrate impairs rat mitochondrial function by inhibition of respiratory complex I. J Pharmacol Exp Ther. 2004 Oct;311(1):109-14. doi: 10.1124/jpet.104.068312.

Butler MJ, Jacobsen TL, Cain DM, Jarman MG, Hubank M, Whittle JR, Phillips R, Simcox A. Discovery of genes with highly restricted expression patterns in the Drosophila wing disc using DNA oligonucleotide microarrays. Development. 2003 Feb;130(4):659-70. doi: 10.1242/dev.00293.

Calabrese C, Iommarini L, Kurelac I, Calvaruso MA, Capristo M, Lollini PL, Nanni P, Bergamini C, Nicoletti G, Giovanni CD, Ghelli A, Giorgio V, Caratozzolo MF, Marzano F, Manzari C, Betts CM, Carelli V, Ceccarelli C, Attimonelli M, Romeo G, Fato R, Rugolo M, Tullo A, Gasparre G, Porcelli AM. Respiratory complex I is essential to induce a Warburg profile in mitochondria-defective tumor cells. Cancer Metab. 2013 Mar 18;1(1):11. doi: 10.1186/2049-3002-1-11.

Carey BW, Finley LW, Cross JR, Allis CD, Thompson CB. Intracellular α-ketoglutarate maintains the pluripotency of embryonic stem cells. Nature. 2015 Feb 19;518(7539):413-6. doi: 10.1038/nature13981.

Castro-Vega LJ, Buffet A, De Cubas AA, Cascón A, Menara M, Khalifa E, Amar L, Azriel S, Bourdeau I, Chabre O, Currás-Freixes M, Franco-Vidal V, Guillaud-Bataille M, Simian C, Morin A, Letón R, Gómez-Graña A, Pollard PJ, Rustin P, Robledo M, Favier J, Gimenez-Roqueplo AP. Germline mutations in FH confer predisposition to malignant pheochromocytomas and paragangliomas. Hum Mol Genet. 2014 May 1;23(9):2440-6. doi: 10.1093/hmg/ddt639.

Castro-Vega LJ, Buffet A, De Cubas AA, Cascón A, Menara M, Khalifa E, Amar L, Azriel S, Bourdeau I, Chabre O, Currás-Freixes M, Franco-Vidal V, Guillaud-Bataille M, Simian C, Morin A, Letón R, Gómez-Graña A, Pollard PJ, Rustin P, Robledo M, Favier J, Gimenez-Roqueplo AP. Germline mutations in FH confer predisposition to malignant pheochromocytomas and paragangliomas. Hum Mol Genet. 2014 May 1;23(9):2440-6. doi: 10.1093/hmg/ddt639.

Chen W, Hill H, Christie A, Kim MS, Holloman E, Pavia-Jimenez A, Homayoun F, Ma Y, Patel N, Yell P, Hao G, Yousuf Q, Joyce A, Pedrosa I, Geiger H, Zhang H, Chang J, Gardner KH, Bruick RK, Reeves C, Hwang TH, Courtney K, Frenkel E, Sun X, Zojwalla N, Wong T, Rizzi JP, Wallace EM, Josey JA, Xie Y, Xie XJ, Kapur P, McKay RM, Brugarolas J. Targeting renal cell carcinoma with a HIF-2 antagonist. Nature. 2016 Nov 3;539(7627):112-117. doi: 10.1038/nature19796.

Chin RM, Fu X, Pai MY, Vergnes L, Hwang H, Deng G, Diep S, Lomenick B, Meli VS, Monsalve GC, Hu E, Whelan SA, Wang JX, Jung G, Solis GM, Fazlollahi F, Kaweeteerawat C, Quach A, Nili M, Krall AS, Godwin HA, Chang HR, Faull KF, Guo F, Jiang M, Trauger SA, Saghatelian A, Braas D, Christofk HR, Clarke CF, Teitell MA, Petrascheck M, Reue K,

Jung ME, Frand AR, Huang J. The metabolite α-ketoglutarate extends lifespan by inhibiting ATP synthase and TOR. Nature. 2014 Jun 19;510(7505):397-401. doi: 10.1038/nature13264.

Chowdhury R, Yeoh KK, Tian YM, Hillringhaus L, Bagg EA, Rose NR, Leung IK, Li XS, Woon EC, Yang M, McDonough MA, King ON, Clifton IJ, Klose RJ, Claridge TD, Ratcliffe PJ, Schofield CJ, Kawamura A. The oncometabolite 2-hydroxyglutarate inhibits histone lysine demethylases. EMBO Rep. 2011 May;12(5):463-9. doi: 10.1038/embor.2011.43.

Colvin H, Nishida N, Konno M, Haraguchi N, Takahashi H, Nishimura J, Hata T, Kawamoto K, Asai A, Tsunekuni K, Koseki J, Mizushima T, Satoh T, Doki Y, Mori M, Ishii H. Oncometabolite D-2-Hydroxyglurate Directly Induces Epithelial-Mesenchymal Transition and is Associated with Distant Metastasis in Colorectal Cancer. Sci Rep. 2016 Nov 8;6:36289. doi: 10.1038/srep36289.

Cooper AJ, Shurubor YI, Dorai T, Pinto JT, Isakova EP, Deryabina YI, Denton TT, Krasnikov BF. ω-Amidase: an underappreciated, but important enzyme in L-glutamine and L-asparagine metabolism; relevance to sulfur and nitrogen metabolism, tumor biology and hyperammonemic diseases. Amino Acids. 2016 Jan;48(1):1-20. doi: 10.1007/s00726-015-2061-7. Epub 2015 Aug 11. Erratum in: Amino Acids. 2015 Dec;47(12):2671-2.

Cummins EP, Berra E, Comerford KM, Ginouves A, Fitzgerald KT, Seeballuck F, Godson C, Nielsen JE, Moynagh P, Pouyssegur J, Taylor CT. Prolyl hydroxylase-1 negatively regulates IkappaB kinase-beta, giving insight into hypoxia-induced NFkappaB activity. Proc Natl Acad Sci U S A. 2006 Nov 28;103(48):18154-9. doi: 10.1073/pnas.0602235103.

Dang L, White DW, Gross S, Bennett BD, Bittinger MA, Driggers EM, Fantin VR, Jang HG, Jin S, Keenan MC, Marks KM, Prins RM, Ward PS, Yen KE, Liau LM, Rabinowitz JD, Cantley LC, Thompson CB, Vander Heiden MG, Su SM. Cancer-associated IDH1 mutations produce 2-hydroxyglutarate. Nature. 2009 Dec 10;462(7274):739-44. doi: 10.1038/nature08617.

DeBerardinis RJ, Lum JJ, Hatzivassiliou G, Thompson CB. The biology of cancer: metabolic reprogramming fuels cell growth and proliferation. Cell Metab. 2008 Jan;7(1):11-20. doi: 10.1016/j.cmet.2007.10.002.

DeBerardinis RJ, Mancuso A, Daikhin E, Nissim I, Yudkoff M, Wehrli S, Thompson CB. Beyond aerobic glycolysis: transformed cells can engage in glutamine metabolism that exceeds the requirement for protein and nucleotide synthesis. Proc Natl Acad Sci U S A. 2007 Dec 4;104(49):19345-50. doi: 10.1073/pnas.0709747104.

Efimova EV, Takahashi S, Shamsi NA, Wu D, Labay E, Ulanovskaya OA, Weichselbaum RR, Kozmin SA, Kron SJ. Linking Cancer Metabolism to DNA Repair and Accelerated Senescence. Mol Cancer Res. 2016 Feb;14(2):173-84. doi: 10.1158/1541-7786.MCR-15-0263.

Ellinghaus P, Heisler I, Unterschemmann K, Haerter M, Beck H, Greschat S, Ehrmann A, Summer H, Flamme I, Oehme F, Thierauch K, Michels M, Hess-Stumpp H, Ziegelbauer K. BAY 87-2243, a highly potent and selective inhibitor of hypoxia-induced gene activation has antitumor activities by inhibition of mitochondrial complex I. Cancer Med. 2013 Oct;2(5):611-24. doi: 10.1002/cam4.112.

Ema M, Taya S, Yokotani N, Sogawa K, Matsuda Y, Fujii-Kuriyama Y. A novel bHLH-PAS factor with close sequence similarity to hypoxia-inducible factor 1alpha regulates the VEGF

expression and is potentially involved in lung and vascular development. Proc Natl Acad Sci U S A. 1997 Apr 29;94(9):4273-8. doi: 10.1073/pnas.94.9.4273.

Epstein AC, Gleadle JM, McNeill LA, Hewitson KS, O'Rourke J, Mole DR, Mukherji M, Metzen E, Wilson MI, Dhanda A, Tian YM, Masson N, Hamilton DL, Jaakkola P, Barstead R, Hodgkin J, Maxwell PH, Pugh CW, Schofield CJ, Ratcliffe PJ. C. elegans EGL-9 and mammalian homologs define a family of dioxygenases that regulate HIF by prolyl hydroxylation. Cell. 2001 Oct 5;107(1):43-54. doi: 10.1016/s0092-8674(01)00507-4.

Erez N, Milyavsky M, Eilam R, Shats I, Goldfinger N, Rotter V. Expression of prolyl-hydroxylase-1 (PHD1/EGLN2) suppresses hypoxia inducible factor-1alpha activation and inhibits tumor growth. Cancer Res. 2003 Dec 15;63(24):8777-83.

Esteller M. Epigenetics in cancer. N Engl J Med. 2008 Mar 13;358(11):1148-59. doi: 10.1056/NEJMra072067. PMID: 18337604.

Fendt SM, Bell EL, Keibler MA, Davidson SM, Wirth GJ, Fiske B, Mayers JR, Schwab M, Bellinger G, Csibi A, Patnaik A, Blouin MJ, Cantley LC, Guarente L, Blenis J, Pollak MN, Olumi AF, Vander Heiden MG, Stephanopoulos G. Metformin decreases glucose oxidation and increases the dependency of prostate cancer cells on reductive glutamine metabolism. Cancer Res. 2013 Jul 15;73(14):4429-38. doi: 10.1158/0008-5472.CAN-13-0080.

Fendt SM, Bell EL, Keibler MA, Olenchock BA, Mayers JR, Wasylenko TM, Vokes NI, Guarente L, Vander Heiden MG, Stephanopoulos G. Reductive glutamine metabolism is a function of the α-ketoglutarate to citrate ratio in cells. Nat Commun. 2013;4:2236. doi: 10.1038/ncomms3236.

Figueroa ME, Abdel-Wahab O, Lu C, Ward PS, Patel J, Shih A, Li Y, Bhagwat N, Vasanthakumar A, Fernandez HF, Tallman MS, Sun Z, Wolniak K, Peeters JK, Liu W, Choe SE, Fantin VR, Paietta E, Löwenberg B, Licht JD, Godley LA, Delwel R, Valk PJ, Thompson CB, Levine RL, Melnick A. Leukemic IDH1 and IDH2 mutations result in a hypermethylation phenotype, disrupt TET2 function, and impair hematopoietic differentiation. Cancer Cell. 2010 Dec 14;18(6):553-67. doi: 10.1016/j.ccr.2010.11.015.

Fong GH, Takeda K. Role and regulation of prolyl hydroxylase domain proteins. Cell Death Differ. 2008 Apr;15(4):635-41. doi: 10.1038/cdd.2008.10.

Frey TG, Mannella CA. The internal structure of mitochondria. Trends Biochem Sci. 2000 Jul;25(7):319-24. doi: 10.1016/s0968-0004(00)01609-1.

Friedman JR, Nunnari J. Mitochondrial form and function. Nature. 2014 Jan 16;505(7483):335-43. doi: 10.1038/nature12985.

Gasparre G, Kurelac I, Capristo M, Iommarini L, Ghelli A, Ceccarelli C, Nicoletti G, Nanni P, De Giovanni C, Scotlandi K, Betts CM, Carelli V, Lollini PL, Romeo G, Rugolo M, Porcelli AM. A mutation threshold distinguishes the antitumorigenic effects of the mitochondrial gene MTND1, an oncojanus function. Cancer Res. 2011 Oct 1;71(19):6220-9. doi: 10.1158/0008-5472.CAN-11-1042.

Gasparre G, Porcelli AM, Bonora E, Pennisi LF, Toller M, Iommarini L, Ghelli A, Moretti M, Betts CM, Martinelli GN, Ceroni AR, Curcio F, Carelli V, Rugolo M, Tallini G, Romeo G. Disruptive mitochondrial DNA mutations in complex I subunits are markers of oncocytic phenotype in thyroid tumors. Proc Natl Acad Sci U S A. 2007 May 22;104(21):9001-6. doi: 10.1073/pnas.0703056104.

Girolimetti G, De Iaco P, Procaccini M, Panzacchi R, Kurelac I, Amato LB, Dondi G, Caprara G, Ceccarelli C, Santini D, Porcelli AM, Perrone AM, Gasparre G. Mitochondrial DNA sequencing demonstrates clonality of peritoneal implants of borderline ovarian tumors. Mol Cancer. 2017 Feb 27;16(1):47. doi: 10.1186/s12943-017-0614-y.

Gorres KL, Raines RT. Prolyl 4-hydroxylase. Crit Rev Biochem Mol Biol. 2010 Apr;45(2):106-24. doi: 10.3109/10409231003627991.

Grassian AR, Lin F, Barrett R, Liu Y, Jiang W, Korpal M, Astley H, Gitterman D, Henley T, Howes R, Levell J, Korn JM, Pagliarini R. Isocitrate dehydrogenase (IDH) mutations promote a reversible ZEB1/microRNA (miR)-200-dependent epithelial-mesenchymal transition (EMT). J Biol Chem. 2012 Dec 7;287(50):42180-94. doi: 10.1074/jbc.M112.417832.

Greenberger LM, Horak ID, Filpula D, Sapra P, Westergaard M, Frydenlund HF, Albaek C, Schrøder H, Ørum H. A RNA antagonist of hypoxia-inducible factor-1alpha, EZN-2968, inhibits tumor cell growth. Mol Cancer Ther. 2008 Nov;7(11):3598-608. doi: 10.1158/1535-7163.MCT-08-0510.

Guerra F, Perrone AM, Kurelac I, Santini D, Ceccarelli C, Cricca M, Zamagni C, De Iaco P, Gasparre G. Mitochondrial DNA mutation in serous ovarian cancer: implications for mitochondria-coded genes in chemoresistance. J Clin Oncol. 2012 Dec 20;30(36):e373-8. doi: 10.1200/JCO.2012.43.5933.

Guerrero-Castillo S, Baertling F, Kownatzki D, Wessels HJ, Arnold S, Brandt U, Nijtmans L. The Assembly Pathway of Mitochondrial Respiratory Chain Complex I. Cell Metab. 2017 Jan 10;25(1):128-139. doi: 10.1016/j.cmet.2016.09.002.

Hanahan D, Weinberg RA. Hallmarks of cancer: the next generation. Cell. 2011 Mar 4;144(5):646-74. doi: 10.1016/j.cell.2011.02.013.

Hanahan D, Weinberg RA. The hallmarks of cancer. Cell. 2000 Jan 7;100(1):57-70. doi: 10.1016/s0092-8674(00)81683-9. PMID: 10647931.

Harrison AP, Pierzynowski SG. Biological effects of 2-oxoglutarate with particular emphasis on the regulation of protein, mineral and lipid absorption/metabolism, muscle performance, kidney function, bone formation and cancerogenesis, all viewed from a healthy ageing perspective state of the art--review article. J Physiol Pharmacol. 2008 Aug;59 Suppl 1:91-106.

Haynes J, McKee TD, Haller A, Wang Y, Leung C, Gendoo DMA, Lima-Fernandes E, Kreso A, Wolman R, Szentgyorgyi E, Vines DC, Haibe-Kains B, Wouters BG, Metser U, Jaffray DA, Smith M, O'Brien CA. Administration of Hypoxia-Activated Prodrug Evofosfamide after Conventional Adjuvant Therapy Enhances Therapeutic Outcome and Targets Cancer-Initiating Cells in Preclinical Models of Colorectal Cancer. Clin Cancer Res. 2018 May 1;24(9):2116-2127. doi: 10.1158/1078-0432.CCR-17-1715.

He YF, Li BZ, Li Z, Liu P, Wang Y, Tang Q, Ding J, Jia Y, Chen Z, Li L, Sun Y, Li X, Dai Q, Song CX, Zhang K, He C, Xu GL. Tet-mediated formation of 5-carboxylcytosine and its excision by TDG in mammalian DNA. Science. 2011 Sep 2;333(6047):1303-7. doi: 10.1126/science.1210944.

Hegg EL, Que L Jr. The 2-His-1-carboxylate facial triad--an emerging structural motif in mononuclear non-heme iron(II) enzymes. Eur J Biochem. 1997 Dec 15;250(3):625-9. doi: 10.1111/j.1432-1033.1997.t01-1-00625.x.

Hewitson KS, McNeill LA, Riordan MV, Tian YM, Bullock AN, Welford RW, Elkins JM, Oldham NJ, Bhattacharya S, Gleadle JM, Ratcliffe PJ, Pugh CW, Schofield CJ. Hypoxia-inducible factor (HIF) asparagine hydroxylase is identical to factor inhibiting HIF (FIH) and is related to the cupin structural family. J Biol Chem. 2002 Jul 19;277(29):26351-5. doi: 10.1074/jbc.C200273200.

Intlekofer AM, Dematteo RG, Venneti S, Finley LW, Lu C, Judkins AR, Rustenburg AS, Grinaway PB, Chodera JD, Cross JR, Thompson CB. Hypoxia Induces Production of L-2-Hydroxyglutarate. Cell Metab. 2015 Aug 4;22(2):304-11. doi: 10.1016/j.cmet.2015.06.023.

Intlekofer AM, Wang B, Liu H, Shah H, Carmona-Fontaine C, Rustenburg AS, Salah S, Gunner MR, Chodera JD, Cross JR, Thompson CB. L-2-Hydroxyglutarate production arises from noncanonical enzyme function at acidic pH. Nat Chem Biol. 2017 May;13(5):494-500. doi: 10.1038/nchembio.2307.

Iommarini L, Calvaruso MA, Kurelac I, Gasparre G, Porcelli AM. Complex I impairment in mitochondrial diseases and cancer: parallel roads leading to different outcomes. Int J Biochem Cell Biol. 2013 Jan;45(1):47-63. doi: 10.1016/j.biocel.2012.05.016.

Iommarini L, Kurelac I, Capristo M, Calvaruso MA, Giorgio V, Bergamini C, Ghelli A, Nanni P, De Giovanni C, Carelli V, Fato R, Lollini PL, Rugolo M, Gasparre G, Porcelli AM. Different mtDNA mutations modify tumor progression in dependence of the degree of respiratory complex I impairment. Hum Mol Genet. 2014 Mar 15;23(6):1453-66. doi: 10.1093/hmg/ddt533.

Iommarini L, Porcelli AM, Gasparre G, Kurelac I. Non-Canonical Mechanisms Regulating Hypoxia-Inducible Factor 1 Alpha in Cancer. Front Oncol. 2017 Nov 27;7:286. doi: 10.3389/fonc.2017.00286.

Isaacs JS, Jung YJ, Mole DR, Lee S, Torres-Cabala C, Chung YL, Merino M, Trepel J, Zbar B, Toro J, Ratcliffe PJ, Linehan WM, Neckers L. HIF overexpression correlates with biallelic loss of fumarate hydratase in renal cancer: novel role of fumarate in regulation of HIF stability. Cancer Cell. 2005 Aug;8(2):143-53. doi: 10.1016/j.ccr.2005.06.017.

Ishikawa K, Takenaga K, Akimoto M, Koshikawa N, Yamaguchi A, Imanishi H, Nakada K, Honma Y, Hayashi J. ROS-generating mitochondrial DNA mutations can regulate tumor cell metastasis. Science. 2008 May 2;320(5876):661-4. doi: 10.1126/science.1156906.

Islam MS, Leissing TM, Chowdhury R, Hopkinson RJ, Schofield CJ. 2-Oxoglutarate-Dependent Oxygenases. Annu Rev Biochem. 2018 Jun 20;87:585-620. doi: 10.1146/annurev-biochem-061516-044724.

Ito S, Shen L, Dai Q, Wu SC, Collins LB, Swenberg JA, He C, Zhang Y. Tet proteins can convert 5-methylcytosine to 5-formylcytosine and 5-carboxylcytosine. Science. 2011 Sep 2;333(6047):1300-3. doi: 10.1126/science.1210597.

Ivan M, Haberberger T, Gervasi DC, Michelson KS, Günzler V, Kondo K, Yang H, Sorokina I, Conaway RC, Conaway JW, Kaelin WG Jr. Biochemical purification and pharmacological inhibition of a mammalian prolyl hydroxylase acting on hypoxia-inducible factor. Proc Natl Acad Sci U S A. 2002 Oct 15;99(21):13459-64. doi: 10.1073/pnas.192342099.

Ivan M, Kaelin WG Jr. The EGLN-HIF O_2-Sensing System: Multiple Inputs and Feedbacks. Mol Cell. 2017 Jun 15;66(6):772-779. doi: 10.1016/j.molcel.2017.06.002.

Ivan M, Kondo K, Yang H, Kim W, Valiando J, Ohh M, Salic A, Asara JM, Lane WS, Kaelin WG Jr. HIFalpha targeted for VHL-mediated destruction by proline hydroxylation: implications for O2 sensing. Science. 2001 Apr 20;292(5516):464-8. doi: 10.1126/science.1059817.

Jaakkola P, Mole DR, Tian YM, Wilson MI, Gielbert J, Gaskell SJ, von Kriegsheim A, Hebestreit HF, Mukherji M, Schofield CJ, Maxwell PH, Pugh CW, Ratcliffe PJ. Targeting of HIF-alpha to the von Hippel-Lindau ubiquitylation complex by O2-regulated prolyl hydroxylation. Science. 2001 Apr 20;292(5516):468-72. doi: 10.1126/science.1059796.

Jiang BH, Rue E, Wang GL, Roe R, Semenza GL. Dimerization, DNA binding, and transactivation properties of hypoxia-inducible factor 1. J Biol Chem. 1996 Jul 26;271(30):17771-8. doi: 10.1074/jbc.271.30.17771.

Jiang ZF, Wang M, Xu JL, Ning YJ. Hypoxia promotes mitochondrial glutamine metabolism through HIF1α-GDH pathway in human lung cancer cells. Biochem Biophys Res Commun. 2017 Jan 29;483(1):32-38. doi: 10.1016/j.bbrc.2017.01.015.

Kaelin WG Jr, Ratcliffe PJ. Oxygen sensing by metazoans: the central role of the HIF hydroxylase pathway. Mol Cell. 2008 May 23;30(4):393-402. doi: 10.1016/j.molcel.2008.04.009.

Kim JW, Tchernyshyov I, Semenza GL, Dang CV. HIF-1-mediated expression of pyruvate dehydrogenase kinase: a metabolic switch required for cellular adaptation to hypoxia. Cell Metab. 2006 Mar;3(3):177-85. doi: 10.1016/j.cmet.2006.02.002.

Koivunen P, Hirsilä M, Günzler V, Kivirikko KI, Myllyharju J. Catalytic properties of the asparaginyl hydroxylase (FIH) in the oxygen sensing pathway are distinct from those of its prolyl 4-hydroxylases. J Biol Chem. 2004 Mar 12;279(11):9899-904. doi: 10.1074/jbc.M312254200.

Koivunen P, Hirsilä M, Remes AM, Hassinen IE, Kivirikko KI, Myllyharju J. Inhibition of hypoxia-inducible factor (HIF) hydroxylases by citric acid cycle intermediates: possible links between cell metabolism and stabilization of HIF. J Biol Chem. 2007 Feb 16;282(7):4524-32. doi: 10.1074/jbc.M610415200.

Kühlbrandt W. Structure and function of mitochondrial membrane protein complexes. BMC Biol. 2015 Oct 29;13:89. doi: 10.1186/s12915-015-0201-x.

Kurelac I, Iommarini L, Vatrinet R, Amato LB, De Luise M, Leone G, Girolimetti G, Umesh Ganesh N, Bridgeman VL, Ombrato L, Columbaro M, Ragazzi M, Gibellini L, Sollazzo M, Feichtinger RG, Vidali S, Baldassarre M, Foriel S, Vidone M, Cossarizza A, Grifoni D, Kofler B, Malanchi I, Porcelli AM, Gasparre G. Inducing cancer indolence by targeting mitochondrial Complex I is potentiated by blocking macrophage-mediated adaptive responses. Nat Commun. 2019 Feb 22;10(1):903. doi: 10.1038/s41467-019-08839-1.

Lando D, Peet DJ, Gorman JJ, Whelan DA, Whitelaw ML, Bruick RK. FIH-1 is an asparaginyl hydroxylase enzyme that regulates the transcriptional activity of hypoxia-inducible factor. Genes Dev. 2002 Jun 15;16(12):1466-71. doi: 10.1101/gad.991402.

Lando D, Peet DJ, Whelan DA, Gorman JJ, Whitelaw ML. Asparagine hydroxylation of the HIF transactivation domain a hypoxic switch. Science. 2002 Feb 1;295(5556):858-61. doi: 10.1126/science.1068592.

Laukka T, Mariani CJ, Ihantola T, Cao JZ, Hokkanen J, Kaelin WG Jr, Godley LA, Koivunen P. Fumarate and Succinate Regulate Expression of Hypoxia-inducible Genes via TET Enzymes. J Biol Chem. 2016 Feb 19;291(8):4256-65. doi: 10.1074/jbc.M115.688762.

Lee K, Zhang H, Qian DZ, Rey S, Liu JO, Semenza GL. Acriflavine inhibits HIF-1 dimerization, tumor growth, and vascularization. Proc Natl Acad Sci U S A. 2009 Oct 20;106(42):17910-5. doi: 10.1073/pnas.0909353106.

Leone G, Abla H, Gasparre G, Porcelli AM, Iommarini L. The *Oncojanus* Paradigm of Respiratory Complex I. Genes (Basel). 2018 May 7;9(5):243. doi: 10.3390/genes9050243.

Letouzé E, Martinelli C, Loriot C, Burnichon N, Abermil N, Ottolenghi C, Janin M, Menara M, Nguyen AT, Benit P, Buffet A, Marcaillou C, Bertherat J, Amar L, Rustin P, De Reyniès A, Gimenez-Roqueplo AP, Favier J. SDH mutations establish a hypermethylator phenotype in paraganglioma. Cancer Cell. 2013 Jun 10;23(6):739-52. doi: 10.1016/j.ccr.2013.04.018.

Lim SC, Carey KT, McKenzie M. Anti-cancer analogues ME-143 and ME-344 exert toxicity by directly inhibiting mitochondrial NADH: ubiquinone oxidoreductase (Complex I). Am J Cancer Res. 2015 Jan 15;5(2):689-701.

Liu PS, Wang H, Li X, Chao T, Teav T, Christen S, Di Conza G, Cheng WC, Chou CH, Vavakova M, Muret C, Debackere K, Mazzone M, Huang HD, Fendt SM, Ivanisevic J, Ho PC. α-ketoglutarate orchestrates macrophage activation through metabolic and epigenetic reprogramming. Nat Immunol. 2017 Sep;18(9):985-994. doi: 10.1038/ni.3796.

Long LH, Halliwell B. Artefacts in cell culture: α-Ketoglutarate can scavenge hydrogen peroxide generated by ascorbate and epigallocatechin gallate in cell culture media. Biochem Biophys Res Commun. 2011 Mar 4;406(1):20-4. doi: 10.1016/j.bbrc.2011.01.091.

Loriot C, Domingues M, Berger A, Menara M, Ruel M, Morin A, Castro-Vega LJ, Letouzé É, Martinelli C, Bemelmans AP, Larue L, Gimenez-Roqueplo AP, Favier J. Deciphering the molecular basis of invasiveness in Sdhb-deficient cells. Oncotarget. 2015 Oct 20;6(32):32955-65. doi: 10.18632/oncotarget.5106.

Losman JA, Koivunen P, Kaelin WG Jr. 2-Oxoglutarate-dependent dioxygenases in cancer. Nat Rev Cancer. 2020 Dec;20(12):710-726. doi: 10.1038/s41568-020-00303-3.

Losman JA, Looper RE, Koivunen P, Lee S, Schneider RK, McMahon C, Cowley GS, Root DE, Ebert BL, Kaelin WG Jr. (R)-2-hydroxyglutarate is sufficient to promote leukemogenesis and its effects are reversible. Science. 2013 Mar 29;339(6127):1621-5. doi: 10.1126/science.1231677.

Lu C, Ward PS, Kapoor GS, Rohle D, Turcan S, Abdel-Wahab O, Edwards CR, Khanin R, Figueroa ME, Melnick A, Wellen KE, O'Rourke DM, Berger SL, Chan TA, Levine RL, Mellinghoff IK, Thompson CB. IDH mutation impairs histone demethylation and results in a block to cell differentiation. Nature. 2012 Feb 15;483(7390):474-8. doi: 10.1038/nature10860.

Lunt SY, Vander Heiden MG. Aerobic glycolysis: meeting the metabolic requirements of cell proliferation. Annu Rev Cell Dev Biol. 2011;27:441-64. doi: 10.1146/annurev-cellbio-092910-154237.

Mackay H, Hedley D, Major P, Townsley C, Mackenzie M, Vincent M, Degendorfer P, Tsao MS, Nicklee T, Birle D, Wright J, Siu L, Moore M, Oza A. A phase II trial with pharmacodynamic endpoints of the proteasome inhibitor bortezomib in patients with

metastatic colorectal cancer. Clin Cancer Res. 2005 Aug 1;11(15):5526-33. doi: 10.1158/1078-0432.CCR-05-0081.

MacKenzie ED, Selak MA, Tennant DA, Payne LJ, Crosby S, Frederiksen CM, Watson DG, Gottlieb E. Cell-permeating alpha-ketoglutarate derivatives alleviate pseudohypoxia in succinate dehydrogenase-deficient cells. Mol Cell Biol. 2007 May;27(9):3282-9. doi: 10.1128/MCB.01927-06. Epub 2007 Feb 26.

Mahon PC, Hirota K, Semenza GL. FIH-1: a novel protein that interacts with HIF-1alpha and VHL to mediate repression of HIF-1 transcriptional activity. Genes Dev. 2001 Oct 15;15(20):2675-86. doi: 10.1101/gad.924501..

Makino Y, Cao R, Svensson K, Bertilsson G, Asman M, Tanaka H, Cao Y, Berkenstam A, Poellinger L. Inhibitory PAS domain protein is a negative regulator of hypoxia-inducible gene expression. Nature. 2001 Nov 29;414(6863):550-4. doi: 10.1038/35107085.

Mardis ER, Ding L, Dooling DJ, Larson DE, McLellan MD, Chen K, Koboldt DC, Fulton RS, Delehaunty KD, McGrath SD, Fulton LA, Locke DP, Magrini VJ, Abbott RM, Vickery TL, Reed JS, Robinson JS, Wylie T, Smith SM, Carmichael L, Eldred JM, Harris CC, Walker J, Peck JB, Du F, Dukes AF, Sanderson GE, Brummett AM, Clark E, McMichael JF, Meyer RJ, Schindler JK, Pohl CS, Wallis JW, Shi X, Lin L, Schmidt H, Tang Y, Haipek C, Wiechert ME, Ivy JV, Kalicki J, Elliott G, Ries RE, Payton JE, Westervelt P, Tomasson MH, Watson MA, Baty J, Heath S, Shannon WD, Nagarajan R, Link DC, Walter MJ, Graubert TA, DiPersio JF, Wilson RK, Ley TJ. Recurring mutations found by sequencing an acute myeloid leukemia genome. N Engl J Med. 2009 Sep 10;361(11):1058-66. doi: 10.1056/NEJMoa0903840

Markolovic S, Wilkins SE, Schofield CJ. Protein Hydroxylation Catalyzed by 2-Oxoglutarate-dependent Oxygenases. J Biol Chem. 2015 Aug 21;290(34):20712-22. doi: 10.1074/jbc.R115.662627. Epub 2015 Jul 7.

Masoud GN, Li W. HIF-1α pathway: role, regulation and intervention for cancer therapy. Acta Pharm Sin B. 2015 Sep;5(5):378-89. doi: 10.1016/j.apsb.2015.05.007.

Masson N, Ratcliffe PJ. Hypoxia signaling pathways in cancer metabolism: the importance of co-selecting interconnected physiological pathways. Cancer Metab. 2014 Feb 4;2(1):3. doi: 10.1186/2049-3002-2-3.

Matsumoto K, Imagawa S, Obara N, Suzuki N, Takahashi S, Nagasawa T, Yamamoto M. 2-Oxoglutarate downregulates expression of vascular endothelial growth factor and erythropoietin through decreasing hypoxia-inducible factor-1alpha and inhibits angiogenesis. J Cell Physiol. 2006 Nov;209(2):333-40. doi: 10.1002/jcp.20733.

Matsumoto K, Obara N, Ema M, Horie M, Naka A, Takahashi S, Imagawa S. Antitumor effects of 2-oxoglutarate through inhibition of angiogenesis in a murine tumor model. Cancer Sci. 2009 Sep;100(9):1639-47. doi: 10.1111/j.1349-7006.2009.01249.x.

McNeill LA, Hewitson KS, Claridge TD, Seibel JF, Horsfall LE, Schofield CJ. Hypoxia-inducible factor asparaginyl hydroxylase (FIH-1) catalyses hydroxylation at the beta-carbon of asparagine-803. Biochem J. 2002 Nov 1;367(Pt 3):571-5. doi: 10.1042/BJ20021162.

Metallo CM, Gameiro PA, Bell EL, Mattaini KR, Yang J, Hiller K, Jewell CM, Johnson ZR, Irvine DJ, Guarente L, Kelleher JK, Vander Heiden MG, Iliopoulos O, Stephanopoulos G. Reductive glutamine metabolism by IDH1 mediates lipogenesis under hypoxia. Nature. 2011 Nov 20;481(7381):380-4. doi: 10.1038/nature10602.

Mirzoyan Z, Sollazzo M, Allocca M, Valenza AM, Grifoni D, Bellosta P. *Drosophila melanogaster*: A Model Organism to Study Cancer. Front Genet. 2019 Mar 1;10:51. doi: 10.3389/fgene.2019.00051.

Monné M, Miniero DV, Iacobazzi V, Bisaccia F, Fiermonte G. The mitochondrial oxoglutarate carrier: from identification to mechanism. J Bioenerg Biomembr. 2013 Feb;45(1-2):1-13. doi: 10.1007/s10863-012-9475-7. Erratum in: J Bioenerg Biomembr. 2013 Feb;45(1-2):175. Iacobazzi, Vito [added].

Morris JP 4th, Yashinskie JJ, Koche R, Chandwani R, Tian S, Chen CC, Baslan T, Marinkovic ZS, Sánchez-Rivera FJ, Leach SD, Carmona-Fontaine C, Thompson CB, Finley LWS, Lowe SW. α-Ketoglutarate links p53 to cell fate during tumour suppression. Nature. 2019 Sep;573(7775):595-599. doi: 10.1038/s41586-019-1577-5.

Mullen AR, Hu Z, Shi X, Jiang L, Boroughs LK, Kovacs Z, Boriack R, Rakheja D, Sullivan LB, Linehan WM, Chandel NS, DeBerardinis RJ. Oxidation of alpha-ketoglutarate is required for reductive carboxylation in cancer cells with mitochondrial defects. Cell Rep. 2014 Jun 12;7(5):1679-1690. doi: 10.1016/j.celrep.2014.04.037.

Mullen AR, Wheaton WW, Jin ES, Chen PH, Sullivan LB, Cheng T, Yang Y, Linehan WM, Chandel NS, DeBerardinis RJ. Reductive carboxylation supports growth in tumour cells with defective mitochondria. Nature. 2011 Nov 20;481(7381):385-8. doi: 10.1038/nature10642.

Niemann S, Müller U. Mutations in SDHC cause autosomal dominant paraganglioma, type 3. Nat Genet. 2000 Nov;26(3):268-70. doi: 10.1038/81551.

Norris RE, Shusterman S, Gore L, Muscal JA, Macy ME, Fox E, Berkowitz N, Buchbinder A, Bagatell R. Phase 1 evaluation of EZN-2208, a polyethylene glycol conjugate of SN38, in children adolescents and young adults with relapsed or refractory solid tumors. Pediatr Blood Cancer. 2014 Oct;61(10):1792-7. doi: 10.1002/pbc.25105.

Papandreou I, Cairns RA, Fontana L, Lim AL, Denko NC. HIF-1 mediates adaptation to hypoxia by actively downregulating mitochondrial oxygen consumption. Cell Metab. 2006 Mar;3(3):187-97. doi: 10.1016/j.cmet.2006.01.012.

Park JS, Sharma LK, Li H, Xiang R, Holstein D, Wu J, Lechleiter J, Naylor SL, Deng JJ, Lu J, Bai Y. A heteroplasmic, not homoplasmic, mitochondrial DNA mutation promotes tumorigenesis via alteration in reactive oxygen species generation and apoptosis. Hum Mol Genet. 2009 May 1;18(9):1578-89. doi: 10.1093/hmg/ddp069.

Pedersen MT, Helin K. Histone demethylases in development and disease. Trends Cell Biol. 2010 Nov;20(11):662-71. doi: 10.1016/j.tcb.2010.08.011.

Phillips RM. Targeting the hypoxic fraction of tumours using hypoxia-activated prodrugs. Cancer Chemother Pharmacol. 2016 Mar;77(3):441-57. doi: 10.1007/s00280-015-2920-7. Epub 2016 Jan 25.

Pollard PJ, Brière JJ, Alam NA, Barwell J, Barclay E, Wortham NC, Hunt T, Mitchell M, Olpin S, Moat SJ, Hargreaves IP, Heales SJ, Chung YL, Griffiths JR, Dalgleish A, McGrath JA, Gleeson MJ, Hodgson SV, Poulsom R, Rustin P, Tomlinson IP. Accumulation of Krebs cycle intermediates and over-expression of HIF1alpha in tumours which result from germline FH and SDH mutations. Hum Mol Genet. 2005 Aug 1;14(15):2231-9. doi: 10.1093/hmg/ddi227.

Porcelli AM, Ghelli A, Ceccarelli C, Lang M, Cenacchi G, Capristo M, Pennisi LF, Morra I, Ciccarelli E, Melcarne A, Bartoletti-Stella A, Salfi N, Tallini G, Martinuzzi A, Carelli V, Attimonelli M, Rugolo M, Romeo G, Gasparre G. The genetic and metabolic signature of oncocytic transformation implicates HIF1alpha destabilization. Hum Mol Genet. 2010 Mar 15;19(6):1019-32. doi: 10.1093/hmg/ddp566.

Porporato PE, Filigheddu N, Pedro JMB, Kroemer G, Galluzzi L. Mitochondrial metabolism and cancer. Cell Res. 2018 Mar;28(3):265-280. doi: 10.1038/cr.2017.155.

Rapisarda A, Hollingshead M, Uranchimeg B, Bonomi CA, Borgel SD, Carter JP, Gehrs B, Raffeld M, Kinders RJ, Parchment R, Anver MR, Shoemaker RH, Melillo G. Increased antitumor activity of bevacizumab in combination with hypoxia inducible factor-1 inhibition. Mol Cancer Ther. 2009 Jul;8(7):1867-77. doi: 10.1158/1535-7163.MCT-09-0274.

Ravaud A, Bernhard JC, Gross-Goupil M, Digue L, Ferriere JM. Inhibiteurs de mTOR : temsirolimus et évérolimus dans le traitement du cancer du rein [mTOR inhibitors: temsirolimus and everolimus in the treatment of renal cell carcinoma]. Bull Cancer. 2010;97:45-51. French. doi: 10.1684/bdc.2010.1069.

Ravenna L, Salvatori L, Russo MA. HIF3α: the little we know. FEBS J. 2016 Mar;283(6):993-1003. doi: 10.1111/febs.13572.

Rzeski W, Walczak K, Juszczak M, Langner E, Pożarowski P, Kandefer-Szerszeń M, Pierzynowski SG. Alpha-ketoglutarate (AKG) inhibits proliferation of colon adenocarcinoma cells in normoxic conditions. Scand J Gastroenterol. 2012 May;47(5):565-71. doi: 10.3109/00365521.2012.660539.

Saxton RA, Sabatini DM. mTOR Signaling in Growth, Metabolism, and Disease. Cell. 2017 Mar 9;168(6):960-976. doi: 10.1016/j.cell.2017.02.004. Erratum in: Cell. 2017 Apr 6;169(2):361-371.

Schöckel L, Glasauer A, Basit F, Bitschar K, Truong H, Erdmann G, Algire C, Hägebarth A, Willems PH, Kopitz C, Koopman WJ, Héroult M. Targeting mitochondrial complex I using BAY 87-2243 reduces melanoma tumor growth. Cancer Metab. 2015 Oct 20;3:11. doi: 10.1186/s40170-015-0138-0.

Schofield CJ, Ratcliffe PJ. Oxygen sensing by HIF hydroxylases. Nat Rev Mol Cell Biol. 2004 May;5(5):343-54. doi: 10.1038/nrm1366.

Sciacovelli M, Frezza C. Oncometabolites: Unconventional triggers of oncogenic signalling cascades. Free Radic Biol Med. 2016 Nov;100:175-181. doi: 10.1016/j.freeradbiomed.2016.04.025.

Sciacovelli M, Gonçalves E, Johnson TI, Zecchini VR, da Costa AS, Gaude E, Drubbel AV, Theobald SJ, Abbo SR, Tran MG, Rajeeve V, Cardaci S, Foster S, Yun H, Cutillas P, Warren A, Gnanapragasam V, Gottlieb E, Franze K, Huntly B, Maher ER, Maxwell PH, Saez-Rodriguez J, Frezza C. Fumarate is an epigenetic modifier that elicits epithelial-to-mesenchymal transition. Nature. 2016 Aug 31;537(7621):544-547. doi: 10.1038/nature19353. Erratum in: Nature. 2016 Dec 1;540(7631):150.

Selak MA, Armour SM, MacKenzie ED, Boulahbel H, Watson DG, Mansfield KD, Pan Y, Simon MC, Thompson CB, Gottlieb E. Succinate links TCA cycle dysfunction to oncogenesis by inhibiting HIF-alpha prolyl hydroxylase. Cancer Cell. 2005 Jan;7(1):77-85. doi: 10.1016/j.ccr.2004.11.022. PMID: 15652751.

Semenza GL. HIF-1 mediates metabolic responses to intratumoral hypoxia and oncogenic mutations. J Clin Invest. 2013 Sep;123(9):3664-71. doi: 10.1172/JCI67230.

Semenza GL. Hypoxia-inducible factors in physiology and medicine. Cell. 2012 Feb 3;148(3):399-408. doi: 10.1016/j.cell.2012.01.021.

Shim EH, Livi CB, Rakheja D, Tan J, Benson D, Parekh V, Kho EY, Ghosh AP, Kirkman R, Velu S, Dutta S, Chenna B, Rea SL, Mishur RJ, Li Q, Johnson-Pais TL, Guo L, Bae S, Wei S, Block K, Sudarshan S. L-2-Hydroxyglutarate: an epigenetic modifier and putative oncometabolite in renal cancer. Cancer Discov. 2014 Nov;4(11):1290-8. doi: 10.1158/2159-8290.CD-13-0696.

Sica V, Bravo-San Pedro JM, Izzo V, Pol J, Pierredon S, Enot D, Durand S, Bossut N, Chery A, Souquere S, Pierron G, Vartholomaiou E, Zamzami N, Soussi T, Sauvat A, Mondragón L, Kepp O, Galluzzi L, Martinou JC, Hess-Stumpp H, Ziegelbauer K, Kroemer G, Maiuri MC. Lethal Poisoning of Cancer Cells by Respiratory Chain Inhibition plus Dimethyl α-Ketoglutarate. Cell Rep. 2019 Apr 16;27(3):820-834.e9. doi: 10.1016/j.celrep.2019.03.058.

Shahmirzadi AA, Edgar D, Liao CY, Hsu YM, Lucanic M, Shahmirzadi AA, Wiley C, Riley R, Kaplowitz B, Gan G, Kuehnemann C, Bhaumik D, Campisi J, Kennedy BK, Lithgow GJ. Alpha-ketoglutarate, an endogenous metabolite, extends lifespan and compresses morbidity in aging mice. Cell Metabolism doi: 10.1016/j.cmet.2020.08.004

Smolková K, Plecitá-Hlavatá L, Bellance N, Benard G, Rossignol R, Ježek P. Waves of gene regulation suppress and then restore oxidative phosphorylation in cancer cells. Int J Biochem Cell Biol. 2011 Jul;43(7):950-68. doi: 10.1016/j.biocel.2010.05.003.
Sookoian S, Pirola CJ. Liver enzymes, metabolomics and genome-wide association studies: from systems biology to the personalized medicine. World J Gastroenterol. 2015 Jan 21;21(3):711-25. doi: 10.3748/wjg.v21.i3.711.

Spinelli JB, Haigis MC. The multifaceted contributions of mitochondria to cellular metabolism. Nat Cell Biol. 2018 Jul;20(7):745-754. doi: 10.1038/s41556-018-0124-1.

Stratakis CA, Carney JA. The triad of paragangliomas, gastric stromal tumours and pulmonary chondromas (Carney triad), and the dyad of paragangliomas and gastric stromal sarcomas (Carney-Stratakis syndrome): molecular genetics and clinical implications. J Intern Med. 2009 Jul;266(1):43-52. doi: 10.1111/j.1365-2796.2009.02110.x.

Su Y, Wang T, Wu N, et al. Alpha-ketoglutarate extends *Drosophila* lifespan by inhibiting mTOR and activating AMPK. *Aging (Albany NY)*. 2019;11(12):4183-4197. doi:10.18632/aging.102045

Tahiliani M, Koh KP, Shen Y, Pastor WA, Bandukwala H, Brudno Y, Agarwal S, Iyer LM, Liu DR, Aravind L, Rao A. Conversion of 5-methylcytosine to 5-hydroxymethylcytosine in mammalian DNA by MLL partner TET1. Science. 2009 May 15;324(5929):930-5. doi: 10.1126/science.1170116.

Tee AR, Proud CG. Staurosporine inhibits phosphorylation of translational regulators linked to mTOR. Cell Death Differ. 2001 Aug;8(8):841-9. doi: 10.1038/sj.cdd.4400876.

Tennant DA, Frezza C, MacKenzie ED, Nguyen QD, Zheng L, Selak MA, Roberts DL, Dive C, Watson DG, Aboagye EO, Gottlieb E. Reactivating HIF prolyl hydroxylases under hypoxia results in metabolic catastrophe and cell death. Oncogene. 2009 Nov 12;28(45):4009-21. doi: 10.1038/onc.2009.250.

Tennant DA, Gottlieb E. HIF prolyl hydroxylase-3 mediates alpha-ketoglutarate-induced apoptosis and tumor suppression. J Mol Med (Berl). 2010 Aug;88(8):839-49. doi: 10.1007/s00109-010-0627-0.

Tomlinson IP, Alam NA, Rowan AJ, Barclay E, Jaeger EE, Kelsell D, Leigh I, Gorman P, Lamlum H, Rahman S, Roylance RR, Olpin S, Bevan S, Barker K, Hearle N, Houlston RS, Kiuru M, Lehtonen R, Karhu A, Vilkki S, Laiho P, Eklund C, Vierimaa O, Aittomäki K, Hietala M, Sistonen P, Paetau A, Salovaara R, Herva R, Launonen V, Aaltonen LA; Multiple Leiomyoma Consortium. Germline mutations in FH predispose to dominantly inherited uterine fibroids, skin leiomyomata and papillary renal cell cancer. Nat Genet. 2002 Apr;30(4):406-10. doi: 10.1038/ng849.

Tran TQ, Hanse EA, Habowski AN, Li H, Gabra MBI, Yang Y, Lowman XH, Ooi AM, Liao SY, Edwards RA, Waterman ML, Kong M. α-Ketoglutarate attenuates Wnt signaling and drives differentiation in colorectal cancer. Nat Cancer. 2020 Mar;1(3):345-358. doi: 10.1038/s43018-020-0035-5.

Tseng CW, Kuo WH, Chan SH, Chan HL, Chang KJ, Wang LH. Transketolase Regulates the Metabolic Switch to Control Breast Cancer Cell Metastasis via the α-Ketoglutarate Signaling Pathway. Cancer Res. 2018 Jun 1;78(11):2799-2812. doi: 10.1158/0008-5472.CAN-17-2906.

Tsukada Y, Fang J, Erdjument-Bromage H, Warren ME, Borchers CH, Tempst P, Zhang Y. Histone demethylation by a family of JmjC domain-containing proteins. Nature. 2006 Feb 16;439(7078):811-6. doi: 10.1038/nature04433.

Turcan S, Rohle D, Goenka A, Walsh LA, Fang F, Yilmaz E, Campos C, Fabius AW, Lu C, Ward PS, Thompson CB, Kaufman A, Guryanova O, Levine R, Heguy A, Viale A, Morris LG, Huse JT, Mellinghoff IK, Chan TA. IDH1 mutation is sufficient to establish the glioma hypermethylator phenotype. Nature. 2012 Feb 15;483(7390):479-83. doi: 10.1038/nature10866.

Unwith S, Zhao H, Hennah L, Ma D. The potential role of HIF on tumour progression and dissemination. Int J Cancer. 2015 Jun 1;136(11):2491-503. doi: 10.1002/ijc.28889.

Vanharanta S, Buchta M, McWhinney SR, Virta SK, Peçzkowska M, Morrison CD, Lehtonen R, Januszewicz A, Järvinen H, Juhola M, Mecklin JP, Pukkala E, Herva R, Kiuru M, Nupponen NN, Aaltonen LA, Neumann HP, Eng C. Early-onset renal cell carcinoma as a novel extraparaganglial component of SDHB-associated heritable paraganglioma. Am J Hum Genet. 2004 Jan;74(1):153-9. doi: 10.1086/381054.

Vatrinet R, Leone G, De Luise M, Girolimetti G, Vidone M, Gasparre G, Porcelli AM. The α-ketoglutarate dehydrogenase complex in cancer metabolic plasticity. Cancer Metab. 2017 Feb 2;5:3. doi: 10.1186/s40170-017-0165-0.

Vaupel P, Thews O, Hoeckel M. Treatment resistance of solid tumors: role of hypoxia and anemia. Med Oncol. 2001;18(4):243-59. doi: 10.1385/MO:18:4:243.

Vaz FM, Wanders RJ. Carnitine biosynthesis in mammals. Biochem J. 2002 Feb 1;361(Pt 3):417-29. doi: 10.1042/0264-6021:3610417.

Vichai V, Kirtikara K. Sulforhodamine B colorimetric assay for cytotoxicity screening. Nat Protoc. 2006;1(3):1112-6. doi: 10.1038/nprot.2006.179.

Villani LA, Smith BK, Marcinko K, Ford RJ, Broadfield LA, Green AE, Houde VP, Muti P, Tsakiridis T, Steinberg GR. The diabetes medication Canagliflozin reduces cancer cell

proliferation by inhibiting mitochondrial complex-I supported respiration. Mol Metab. 2016 Aug 26;5(10):1048-1056. doi: 10.1016/j.molmet.2016.08.014.

Wang GL, Jiang BH, Rue EA, Semenza GL. Hypoxia-inducible factor 1 is a basic-helix-loop-helix-PAS heterodimer regulated by cellular O2 tension. Proc Natl Acad Sci U S A. 1995 Jun 6;92(12):5510-4. doi: 10.1073/pnas.92.12.5510.

Ward PS, Patel J, Wise DR, Abdel-Wahab O, Bennett BD, Coller HA, Cross JR, Fantin VR, Hedvat CV, Perl AE, Rabinowitz JD, Carroll M, Su SM, Sharp KA, Levine RL, Thompson CB. The common feature of leukemia-associated IDH1 and IDH2 mutations is a neomorphic enzyme activity converting alpha-ketoglutarate to 2-hydroxyglutarate. Cancer Cell. 2010 Mar 16;17(3):225-34. doi: 10.1016/j.ccr.2010.01.020.

Wheaton WW, Weinberg SE, Hamanaka RB, Soberanes S, Sullivan LB, Anso E, Glasauer A, Dufour E, Mutlu GM, Budigner GS, Chandel NS. Metformin inhibits mitochondrial complex I of cancer cells to reduce tumorigenesis. Elife. 2014 May 13;3:e02242. doi: 10.7554/eLife.02242.

Wigerup C, Påhlman S, Bexell D. Therapeutic targeting of hypoxia and hypoxia-inducible factors in cancer. Pharmacol Ther. 2016 Aug;164:152-69. doi: 10.1016/j.pharmthera.2016.04.009.

Wise DR, Ward PS, Shay JE, Cross JR, Gruber JJ, Sachdeva UM, Platt JM, DeMatteo RG, Simon MC, Thompson CB. Hypoxia promotes isocitrate dehydrogenase-dependent carboxylation of α-ketoglutarate to citrate to support cell growth and viability. Proc Natl Acad Sci U S A. 2011 Dec 6;108(49):19611-6. doi: 10.1073/pnas.1117773108.

Wodarz A, Näthke I. Cell polarity in development and cancer. Nat Cell Biol. 2007 Sep;9(9):1016-24. doi: 10.1038/ncb433.

Wu X, Zhang Y. TET-mediated active DNA demethylation: mechanism, function and beyond. Nat Rev Genet. 2017 Sep;18(9):517-534. doi: 10.1038/nrg.2017.33.

Xiao D, Zeng L, Yao K, Kong X, Wu G, Yin Y. The glutamine-alpha-ketoglutarate (AKG) metabolism and its nutritional implications. Amino Acids. 2016 Sep;48(9):2067-80. doi: 10.1007/s00726-016-2254-8.

Xiao M, Yang H, Xu W, Ma S, Lin H, Zhu H, Liu L, Liu Y, Yang C, Xu Y, Zhao S, Ye D, Xiong Y, Guan KL. Inhibition of α-KG-dependent histone and DNA demethylases by fumarate and succinate that are accumulated in mutations of FH and SDH tumor suppressors. Genes Dev. 2012 Jun 15;26(12):1326-38. doi: 10.1101/gad.191056.112.

Xu W, Yang H, Liu Y, Yang Y, Wang P, Kim SH, Ito S, Yang C, Wang P, Xiao MT, Liu LX, Jiang WQ, Liu J, Zhang JY, Wang B, Frye S, Zhang Y, Xu YH, Lei QY, Guan KL, Zhao SM, Xiong Y. Oncometabolite 2-hydroxyglutarate is a competitive inhibitor of α-ketoglutarate-dependent dioxygenases. Cancer Cell. 2011 Jan 18;19(1):17-30. doi: 10.1016/j.ccr.2010.12.014.

Yan H, Parsons DW, Jin G, McLendon R, Rasheed BA, Yuan W, Kos I, Batinic-Haberle I, Jones S, Riggins GJ, Friedman H, Friedman A, Reardon D, Herndon J, Kinzler KW, Velculescu VE, Vogelstein B, Bigner DD. IDH1 and IDH2 mutations in gliomas. N Engl J Med. 2009 Feb 19;360(8):765-73. doi: 10.1056/NEJMoa0808710.

Yang B, Zhong C, Peng Y, Lai Z, Ding J. Molecular mechanisms of "off-on switch" of activities of human IDH1 by tumor-associated mutation R132H. Cell Res. 2010 Nov;20(11):1188-200. doi: 10.1038/cr.2010.145.

Yang SL, Wu C, Xiong ZF, Fang X. Progress on hypoxia-inducible factor-3: Its structure, gene regulation and biological function (Review). Mol Med Rep. 2015 Aug;12(2):2411-6. doi: 10.3892/mmr.2015.3689.

Yang Y, Padilla-Nash HM, Vira MA, Abu-Asab MS, Val D, Worrell R, Tsokos M, Merino MJ, Pavlovich CP, Ried T, Linehan WM, Vocke CD. The UOK 257 cell line: a novel model for studies of the human Birt-Hogg-Dubé gene pathway. Cancer Genet Cytogenet. 2008 Jan 15;180(2):100-9. doi: 10.1016/j.cancergencyto.2007.10.010.

Yu F, White SB, Zhao Q, Lee FS. HIF-1alpha binding to VHL is regulated by stimulus-sensitive proline hydroxylation. Proc Natl Acad Sci U S A. 2001 Aug 14;98(17):9630-5. doi: 10.1073/pnas.181341498. Erratum in: Proc Natl Acad Sci U S A 2001 Dec 4;98(25):14744.

Zdzisińska B, Żurek A, Kandefer-Szerszeń M. Alpha-Ketoglutarate as a Molecule with Pleiotropic Activity: Well-Known and Novel Possibilities of Therapeutic Use. Arch Immunol Ther Exp (Warsz). 2017 Feb;65(1):21-36. doi: 10.1007/s00005-016-0406-x.

Zhao S, Lin Y, Xu W, Jiang W, Zha Z, Wang P, Yu W, Li Z, Gong L, Peng Y, Ding J, Lei Q, Guan KL, Xiong Y. Glioma-derived mutations in IDH1 dominantly inhibit IDH1 catalytic activity and induce HIF-1alpha. Science. 2009 Apr 10;324(5924):261-5. doi: 10.1126/science.1170944.

Zheng J. Energy metabolism of cancer: Glycolysis versus oxidative phosphorylation (Review). Oncol Lett. 2012 Dec;4(6):1151-1157. doi: 10.3892/ol.2012.928.

Acknowledgments

This work was supported by H2020-MSCA-ITN-2016 TRANSMIT-TRANSlating the role of Mitochondria In Tumorigenesis project (G.A. 722605)

Anna Maria Porcelli, Department of Pharmacy and Biotechnology, University of Bologna, Italy

Luisa Iommarini, Department of Pharmacy and Biotechnology, University of Bologna, Italy

Stefano Miglietta, Department of Pharmacy and Biotechnology, University of Bologna, Italy

Manuela Sollazzo, Department of Pharmacy and Biotechnology, University of Bologna, Italy

Giulia Leone, Department of Pharmacy and Biotechnology, University of Bologna, Italy

Alessandra Locatelli, Department of Pharmacy and Biotechnology, University of Bologna, Italy

Rita Morigi, Department of Pharmacy and Biotechnology, University of Bologna, Italy

Monica De Luise, Department of Surgical and Medical Sciences, University of Bologna, Italy

Ivana Kurelac, Department of Surgical and Medical Sciences, University of Bologna, Italy

Giuseppe Gasparre, Department of Surgical and Medical Sciences, University of Bologna, Italy

Giuseppe De Bonis, Department of Interpreting and Translation, University of Bologna, Italy

Serena Paterlini, Istituto O. Spaventa, Italy

Cristian Frezza, Medical Research Council, Cancer Unit, Cambridge, UK

Christina Schmidt, Medical Research Council, Cancer Unit, Cambridge, UK

Marco Sciacovelli, Medical Research Council, Cancer Unit, Cambridge, UK

Laura Tronci, Medical Research Council, Cancer Unit, Cambridge, UK

Efterpi Nikitopoulou, Medical Research Council, Cancer Unit, Cambridge, UK

Tim Young, Medical Research Council, Cancer Unit, Cambridge, UK

Lucas Maddelna, Medical Research Council, Cancer Unit, Cambridge, UK

Vincent Zucchini, Medical Research Council, Cancer Unit, Cambridge, UK

Lorea Valcarcel, Medical Research Council, Cancer Unit, Cambridge, UK

Cissy Yong, Medical Research Council, Cancer Unit, Cambridge, UK

Elfi Topfer, microfluidic ChipShop GmbH, Germany

Serena Jasmine Aleo, Department of Pharmacy and Biotechnology, University of Bologna, Italy

Anna Maria Ghelli, Department of Pharmacy and Biotechnology, University of Bologna, Italy

Claudia Zanna, Department of Pharmacy and Biotechnology, University of Bologna, Italy

Daniela Grifoni, Department of Pharmacy and Biotechnology, University of Bologna, Italy

Roberto Ciaccio, Department of Pharmacy and Biotechnology, University of Bologna, Italy

Giorgio Milazzo, Department of Pharmacy and Biotechnology, University of Bologna, Italy

A special thought to my fellow TRANSMITers for all the moments shared together: Saharnaz Sarlak, Ana Carolina Bastos Sant'Anna Silva, Floriana Di Paola, Christina Schmidt, Nikkitha Umesh Ganesh, Nicole Bezuidenhout, Maheshwor Thapa, Ana Catarina Da Silva Almeida, Luca Zampieri and Daniela Weber, and with whom this adventure was even more special.

To the sweet and crazy girls: Monica De Luise, Nikkitha Umesh Ganesh, Camelia Coada, Lorena Marchio, Maria Iorio, Greta Tedesco and Licia Bressi.

Above all, to my family: mum, dad for always believing in me. To my brother and to you Renaud.